LUND UNIVERSITY

Data-Rich Multivariable Control of Heavy-Duty Engines

Henningsson, Maria

2012

[Link to publication](#)

Total number of authors:
1

Data-Rich Multivariable Control of
Heavy-Duty Engines

Data-Rich Multivariable Control of Heavy-Duty Engines

Maria Henningsson

To Toivo, Arthur, and Alice

Contents

Contents

Abstract

The combustion engine is today the dominant technology for transportation of goods and people world-wide. Concerns for global warming, toxic exhaust emissions, as well as cost and availability of fuel have in recent years created incentives for technological evolution of combustion engines. More sophisticated engine instrumentation with additional degrees of freedom has been added to the engine design to reduce emissions and fuel consumption. But, as engines become more complex, the task of calibration and control becomes more challenging.

This thesis investigates approaches to utilize rich sensor information for multivariable engine control. Different combustion modes, and different combinations of sensors and actuators have been studied and evaluated experimentally on a full-scale six-cylinder heavy-duty engine. The work is divided into four areas: virtual emissions sensing, dynamic emissions models, optimal engine control, and control of sensitive combustion modes. The theme of the thesis is to show how feedback control based on rich sensor information can be exploited to improve the engine operation and reduce the off-line calibration effort.

The virtual sensing work presents a data-mining method for predicting exhaust emissions from cylinder pressure data. Principal component analysis was used to reduce the dimensionality of the high-resolution data, and a neural network model was trained to predict emissions on a cycle-to-cycle, cylinder-individual basis.

The work on dynamic models investigates how system identification can be used to find multivariable dynamic models from a set of engine actuators to a set of variables related to high-level engine specifications, namely emissions, work output, combustion phasing, and peak pressure derivative. It was shown how fairly simple Wiener models can capture the main dynamics of the engine at a grid of operating points.

One of the identified multivariable models was used for optimal control of the engine. In contrast to most previous work in the field, integration of fuel- and gas-path control into a single framework was pursued. A model predictive

controller was designed based on a cost function expressed in terms of high-level engine control objectives, and feedback was based on measured emissions as well as cylinder pressure data.

The final part of the thesis presents work on two sensitive combustion modes, HCCI and dual-fuel operation. Here, feedback control is necessary to achieve robust operation. For both types of combustion, it was shown how a combination of two actuators can be used to successfully control the combustion process.

Acknowledgements

During the last few years, I have had the privilege to work in an exciting research field, at an amazing department, and with some truly great people. First, I would like to acknowledge my main supervisor, Rolf Johansson, for his impressive knowledge in a wide range of fields, for setting high research standards, and for always taking the time to discuss and review my work.

Per Tunestål has been a great co-supervisor by sharing his expert knowledge on combustion engines. Bo Bernhardsson joined as a co-supervisor for the final part of the project. I am very impressed by his ability to instantly grasp the essence of a research topic, and to immediately spot any error in a mathematical text. I am especially grateful for the support from Rolf, Per, and Bo during a particularly difficult time.

I would also like to acknowledge Per Hagander for being a supportive co-supervisor during my first years as a Ph.D. student, and Bengt Johansson for his dynamic leadership of the Combustion Engine Research Lab.

Much of the work in the thesis was performed in close collaboration with fellow Ph.D. student Kent Ekholm. He has contributed a lot of practical knowledge and skills towards the research project, and has been very patient with my own limited practical experience. It has been great to share the challenges and rewards of experimental research with Kent.

I would like to thank Volvo Powertrain for the fruitful collaboration throughout the project. Particularly, I would like to thank Petter Strandh and Johan Dahl for taking the time for discussions and advice, and supporting me to pursue my ideas. Petter has somehow always managed to find creative solutions for all issues that have arised in our experimental setup.

Financial support from Vinnova through the grant PFF 2005-00180, *Diesel-HCCI in Multi-Cylinder Engines*, and from the Swedish Energy Agency through the grant FFI P32067-1, *Diesel Combustion with Low Environmental Impact*, is gratefully acknowledged.

I would like to thank everyone at the Department of Automatic Control

for the nice atmosphere, the moral support, and the interesting lunch- and coffee time discussions. Especially, I want to thank Leif Andersson and Anders Blomdell who have gone out of their way to help me with Linux issues and hardware drivers to keep the engine control system running. I would also like to thank Anders Widd for sharing the interest in combustion engine control.

I have also enjoyed the time at the Combustion Engine Research Lab. There, I would like to thank all past and present Ph.D. students, technicians, and faculty for the very creative, helpful, and friendly atmosphere.

During the last year, two courses have been a great source of inspiration and motivation in my research and the writing of this thesis. I would like to thank Thomas Schön for his course on Machine Learning, and Karl Johan Åström for his course on History of Control. I would also like to thank Karl Johan for contacting John Cassidy who provided an interesting perspective on the historical development of engine control in industry, and generously allowed me to include it in the thesis.

I would also like to thank Magnus Karlsson and Nils-Gustaf Nilsson, my high school teachers of mathematics, physics, chemistry, and biology, for their inspiring teaching that contributed to my decision to study engineering.

Outside the world of studies and research, I would like to thank my parents, sisters, and friends for supporting me in my work, as well as distracting me from it at times.

Finally, I want to thank my husband Toivo and my wonderful children Arthur and Alice. Toivo, I could not have done this without your encouragement and support that has strengthened my confidence in both my research and myself. Also, you have been amazing in allowing me the time to focus on this thesis, and I promise to make it up to you. To all of you, I apologize for the nights and weekends I spent on the thesis instead of being with you. At last, mom's book is finished!

Maria

Publications

The thesis is based on the following publications. Note that the author's previous surname was Karlsson.

Henningsson, M., P. Tunestål, and R. Johansson (2012): "A Virtual Sensor for Predicting Diesel Engine Emissions from Cylinder Pressure Data" *Submitted to the 2012 IFAC Workshop on Engine and Powertrain Control, Simulation and Modeling (E-COSM'12).*

Henningsson, M., B. Bernhardsson, P. Tunestål, and R. Johansson (2012): "A Machine-Learning Approach to Information Extraction from Cylinder Pressure Sensors" SAE Technical Paper 2012-01-0440.

Karlsson, M., K. Ekholm, P. Strandh, R. Johansson, P. Tunestål (2010): "Multiple-Input Multiple-Output Model Predictive Control of a Diesel Engine." In *Proc. for the Sixth IFAC Symposium on Advances in Automotive Control (AAC 2010) Jul 12–14.* Munich, Germany.

Karlsson, M., K. Ekholm, P. Strandh, R. Johansson, and P. Tunestål (2010): "Dynamic Mapping of Diesel Engine through System Identification." In *Proc. of the 2010 American Control Conference (ACC 2010) Jun 30–Jul 2.* Baltimore, MD, USA.

Karlsson, M., P. Strandh, K. Ekholm, R. Johansson, and P. Tunestål (2008): "LQG Control for Minimization of Emissions in a Diesel Engine". In *IEEE Multi-conference on Systems and Control (MSC 2008) Sep 3–5.* San Antonio, TX, USA.

Ekholm, K., M. Karlsson, P. Tunestål, R. Johansson, B. Johansson, and P. Strandh (2008): "Ethanol-Diesel Fumigation in a Multi-Cylinder Engine". SAE Technical Paper 2008-01-0033.

Karlsson, M., K. Ekholm, P. Strandh, R. Johansson, P. Tunestål, and B. Johansson (2007): "Closed-loop Control of Combustion Phasing in an HCCI Engine Using VVA and Variable EGR". In *Proc. for the Fifth IFAC Symposium on Advances in Automotive Control (AAC 2007) Aug 20–22*, pp. 517–524. Aptos, CA, USA.

The author was a principal contributor to all these publications. All authors jointly determined the general direction of the research, for example the combustion mode that was studied at each stage of the research projects. Planning, execution, and evaluation of experiments was performed together with K. Ekholm. K. Ekholm and the author wrote the first two papers together. The author wrote the other papers herself with input from the co-authors. The author was the main contributor to the work related to modeling and control in the publications. This includes problem formulation, as well as developing, implementing, testing, and evaluating control designs.

Other Publications by the Author

Karlsson, M. (2008): "Control Structures for Low-Emission Combustion in Multi-Cylinder Engines." Department of Automatic Control, Lund University, Licentiate Thesis TFRT--3243--SE.

Blom, D., M. Karlsson, K. Ekholm, P. Tunestål, and R. Johansson (2008): "HCCI Engine Modeling and Control using Conservation Principles." In SAE Technical Paper 2008-01-0789.

Haugwitz, S., M. Karlsson, S. Velut, and P. Hagander (2005): "Anti-Windup in Mid-Ranging Control." In Proceedings of the 44th IEEE Conference on Decision and Control and European Control Conference (CDC-ECC 2005) Dec 12–15. Seville, Spain.

Karlsson, M. (2005): "Control of Bacillus Subtilis Cultivations—Feeding Strategies and the Role of Anti-Windup in Mid-Ranging Control." Department of Automatic Control, Lund University, Master's Thesis TFRT--5745--SE.

1

Introduction

Combustion engines have been the dominant technology for vehicle propulsion for over a century. They have revolutionized transportation, and have been a key enabler for our modern, global civilization. Over 47 million cars and 17 million commercial road vehicles were manufactured in 2009 [International Organization of Motor Vehicle Manufacturers, 2011], the overwhelming majority powered by combustion engines.

1.1 Context

In the last decades, the reliance upon combustion engine technology has become increasingly problematic. Three concerns can be raised:

- Green-house gas emissions contributing to global warming.

- Reliance on fossil fuel which is a finite natural resource.

- Emissions of other substances that are harmful to humans or the environment, such as soot particles or nitrogen oxides.

Despite enormous financial incentives to develop an alternative mode of propulsion that can address these issues, results have so far been scarce. Electric vehicles are sometimes mentioned as the solution, but have yet to show feasibility outside niche markets. In order to address all three concerns through electric vehicles, the task of generating green electricity must also be solved. Important reasons for the enormous success of the combustion engine for vehicle propulsion are high power-to-weight ratio for both the engine itself and the fuel, relatively low cost, and versatility. Batteries used for electric vehicles today need to be substantially heavier in order to carry the same energy. So far, battery lifetime has also been unreliable. Gas turbine engines have an even higher power-to-weight ratio than combustion engines, but higher cost and poorer transient and part-load capability. Fuel cells is another potential future technology that has

not yet left the concept stage despite large research investments [Andress et al., 2012]. It is thus likely that the combustion engine will remain a mass-market product for quite some time, despite the three concerns mentioned.

Greenhouse gas emissions from transportation are often at the heart of the global warming discussion. The reason could be that the general public can easily relate to CO_2 emissions from car engines. Emissions become tangible when you see the exhaust pipe of a truck, or when you need to fill up the tank of your car. However, transportation only accounts for one fourth to one third of total greenhouse gas emissions. In a U.S. Environmental Protection Agency study, 33% of U.S. CO_2 emissions in 2009 were attributed to transportation [U.S. Environmental Protection Agency, 2011b], worldwide it was estimated that 25% of CO_2 emissions in 2005 came from transportation [Vinot and Coussy, 2009]. Considering the growing demand for energy globally, targets for greenhouse gas emissions would be hard to reach even if greenhouse gas emissions from vehicles were completely eliminated.

Other main contributors to greenhouse emissions are electric power and heat generation, manufacturing, deforestation, agriculture, and buildings. A McKinsey report [Enkvist et al., 2007] analyzed the abatement potential and associated cost for different means to reduce greenhouse gas emissions. Among the abatement options that were estimated to cost less than EUR 40 per ton of CO_2, transportation (fuel-efficient vehicles and bio-fuels) accounted for 11% whereas power generation (renewable power sources, nuclear power, and carbon capture and storage) accounted for 22%. The report advocates that the greatest potential in greenhouse gas emissions lies in the appropriate use of mature technology, and the number one recommendation in a list of cost-conscious regulatory measures is to ensure strict technical standards and rules for the energy efficiency of buildings and vehicles.

It can be concluded that replacing the combustion engine with a yet-to-be-invented technology is not an easy fix to the global warming challenge. Many different measures must be taken, such as better building insulation, carbon capture from power plants, reforestation, exploitation of renewable energy sources, and changes in life-style to reduce energy consumption. However, advanced technological solutions for increasing energy efficiency in combustion engines could be a cost-efficient short-term measure towards reducing greenhouse gas emissions.

The reliance on fossil crude oil is perhaps a more pressing concern for the future of the combustion engine. Even though transportation only accounts for 25% of greenhouse gas emissions, it is responsible for 51% of the worldwide liquid fuel consumption [Energy Information Administration, U.S. Department of Energy, 2009]. Moreover, this number can be expected to increase since it is easier to find alternative energy sources for other sectors such as electricity

generation. As mentioned, liquid fuels have excellent energy efficiency in terms of weight and volume, which makes them hard to replace for mobile applications. As the supplies of crude oil drain, possible alternatives may be found in biofuels or synthetic fuels.

The third concern regarding emissions of other substances, such as nitrogen oxides and soot particles (PM), has to a large extent been solved. Through the force of legislation, dramatic reductions of harmful combustion byproducts have been possible. As an example, the first European emissions legislation for heavy-duty vehicles came in 1992, limiting NO_x emissions to 8 g/kWh and PM emissions to 0.36 g/kWh. The forthcoming legislation, Euro VI, will be enforced from 2013 limiting NO_x emissions to 0.4 g/kWh and PM emissions to 0.01 g/kWh [European Union, 2007]. Emissions of these two substances, toxic to both human health and the environment, have thus been reduced by 95% or more over two decades through legislation and technological development.

1.2 The Combustion Engine Control Problem

Control is the engineering discipline that studies how to make decisions. Informed decisions can be based on a model that predicts the effect of various potential decisions, and on data that tell the outcome of past decisions. Combustion engines are challenging to control because there are many conflicting objectives to fulfill when making the decisions, it is hard to find good models that will predict the result of a given decision, and it is hard to directly measure the effect of the decisions taken.

An engine is a torque-generating machine. Air and fuel are supplied to the cylinder, and combustion produces heat that is transformed to work performed on the crankshaft, as well as exhaust gases that are discharged into the surroundings.

To optimize engine performance, many factors must be considered. On one hand, society imposes constraints in terms of regulated levels of harmful exhaust emissions, and regulated levels of audible noise from the engine. On the other hand, the engine has to fulfill market demands on cost, reliability, and durability.

These societal and market constraints lead to challenging technical constraints on engine control:

- The engine is a multiple-input multiple-output (MIMO) system. The number of degrees of freedom of the engine increases all the time as new actuators and sensors are added to it to make the system more flexible.

- The dynamics are fast. One hundred combustion events may occur every second, which means that the time to make computations and change

actuator settings is very short.

- The dynamics are nonlinear. Very small changes of operating conditions can move the engine from an optimal sweet spot to an operating point where emissions exceed the legal constraints, or where cycle-to-cycle variability in combustion is too high.

- Engine operation is highly dynamical; to respond to the driver's requests and to road conditions, the engine must traverse a large part of its operating range in a matter of seconds.

- The engine is difficult to model. Combustion varies both spatially over the cylinder, and temporally over the course of operation. Mechanical, chemical, as well as thermodynamical processes interact.

- The engine is a mass-produced consumer product. Thus, cost is a major issue. This means that sensing and computing capabilities are severly restricted.

- Engine operation needs to be extremely reliable. Combustion engines are a mature technology, where customers expect flawless operation. Malfunction could in the worst case cause accidents, and in mild cases disrupt people's life by requiring to take the car for maintenance.

Mathematically, we can formulate the control design objective as an optimal control problem

$$\min_{u \in \mathcal{U}(y, d_m)} V(x, u, \dot{u}, d_m, d_u)$$
$$\text{s.t.} \quad x \in \mathcal{X}(u, d_m, d_u) \tag{1.1}$$
$$y = h(x, u, d_m, d_u)$$

Here, the cost function $V(\cdot)$ is typically a time integral that penalizes emissions, fuel consumption, and audible noise, which all would be included in the state vector x. It may also give higher cost to some values of the control variable u, or penalize changes in actuator positions $\dot{u}$, and may also include measured and unmeasured disturbances d_m and d_u. The set of admissible control laws $\mathcal{U}(y, d_m)$ is a function of the measured outputs y and measured disturbances d_m, and is further constrained by control variable saturation and rate constraints. The state inclusion $\mathcal{X}$ contains constraints on the state imposed by system dynamics, state constraints, or state- or output references constraints for example that the torque should follow driver requests.

1.3 Current Trends in Combustion Engine Design

Major trends in engine development at the moment are increased performance requirements, increased engine flexibility, and as a result increased complexity. Concerns for environmental impact as well as cost and availability of fuel create incentives for optimizing performance of combustion engines. To respond to demands from market and legislators, engines are becoming more complex with an increasing number of degrees of freedom. New actuation options are added to adapt performance at each operating point, for example variable valve timings, multiple injections, dual-stage turbocharging, or complex after-treatment systems.

  Proper calibration and control design is required to make optimal use of a complex and expensive set of actuators. The traditional method of engine control design, dominated by precalibrated feedforward maps, here poses a problem. Calibration effort increases exponentially in the number of variables. Clever schemes for design of experiments (DoE), and the use of domain knowledge to separate the calibration task into subsystems is necessary, but may not be enough. The calibration time may still be prohibitive, and most importantly, precalibrated maps cannot adapt to equipment that degrades with time.

  These shortcomings may have consequences for the engine control design process. A possible future trend is that the increased number of actuators will be accompanied by an increased number of sensors. If so, the fundamentals of engine calibration and control design will need to be rethought. Focus may be moved from off-line calibration to on-line control. Potentially, the calibration effort can be substantially reduced, and less precise actuators can be used since the controller can compensate for unit-to-unit variations.

  This possible future scenario sets the stage for the research presented in this thesis. Much of the current published research on engine control focuses on finding solutions aligned with the current topology of engine sensors and computational resources in the ECU. By contrast, in this work makes generous use of sensors and computing power that are normally used only in laboratory settings. For example, cylinder pressure sensor data are used throughout the thesis, and soot measurement from an opacimeter is used for feedback.

1.4 Outline of the Thesis

The work presented in the thesis investigates some ideas for efficient use of on-line information to optimize performance in heavy-duty engines. Different combustion modes have been investigated, with different aims for the control design.

  Background material on combustion engines and systems and control meth-

ods that relate to the work presented in the thesis is presented in Chapters 2 and 3. The experimental facilities are described in Chapter 4.

The core of the thesis consists of Chapters 5 to 8, where the research contributions are presented. The work is divided into four areas:

- virtual emissions sensing (Chapter 5)

- dynamic emissions models (Chapter 6)

- optimal emissions control (Chapter 7)

- control of sensitive combustion modes (Chapter 8)

Chapter 5 presents a method to extract information from cylinder pressure data using machine-learning techniques. It is shown how information processing methods allow the pressure sensor to be used as a virtual sensor for NO_x and soot emissions.

Chapter 6 presents a study on dynamic mapping of the engine, where dynamic multiple-input multiple-output models are found through system identification. Input to the models are fuel injection and gas flow control variables, and outputs are combustion diagnosis variables such as emissions and combustion phasing. It is shown how local linear black-box models at each operating point can be combined into a dynamic model over a larger operating range that still has quite low complexity.

Chapter 7 presents methods for joint control of fuel injection and gas exchange in order to optimize emissions. Fuel control and gas exchange control are usually seen as two separate tasks, but in terms of effects on combustion, there are strong interconnections.

Chapter 8 treats stabilization of the combustion process in combustion modes that are very sensitive to operating conditions, namely HCCI combustion and dual-fuel combustion. Here, cylinder-pressure based control allow to use combustion modes that otherwise would not be feasible.

A theme of the thesis is on-line optimization of the combustion process in heavy-duty engines based on feedback control. However, it is not claimed that the proposed solutions can outperform map-based open-loop control. First, the work here is limited to single operating points to show proof of concept, no claims are made for a full solution over the entire operating range. Second, the purpose of feedback is to handle uncertainty [Åström, 2006]. Conventional diesel combustion is robust and stable. If all uncertainty originating from disturbances and different operating conditions has been mapped, and actuators of highest quality and precision are employed, optimal feedback control cannot outperform an optimized open-loop map.

The benefits of feedback control can only be fully realized by exploiting the increased tolerance for uncertainty. This requires rethinking the engine develop-

ment and calibration process. Ways to gain from increased allowed uncertainty include:

- Enabling combustion concepts that are more sensitive to operating conditions, such as HCCI, PPC, or dual-fuel.

- Allowing more actuators to be incorporated into the engine without prohibitive calibration requirements.

- Reducing calibration time.

- Better long-term performance as the feedback controller adapts to degrading equipment.

- Using less precise actuators and letting the feedback controller compensate for the reduced accuracy.

To succeed in one or more of these respects, proper integration of information from off-line calibration and on-line sensor data is important.

Information processing is currently a fast-growing industry, providing tools to make sense of systems that are complex and difficult to model [Hardy, 2011; Naone, 2011]. Examples of application areas include financial statistics, bioinformatics, natural language processing, computer vision, and business intelligence. The common characteristics of these areas is to make use of abundant data from systems that are complex and hard to model. This trend has not yet gained momentum in the combustion engine field, but it is not far fetched to claim that on-line optimization based on rich sensor information will play an important part in future engine development.

2

Engine Fundamentals

Two different engine types are widely used in automotive vehicles today. In popular language, they are referred to as diesel engines and gasoline engines. In the technical and scientific community, the diesel engine is known as *compression ignition* (CI) engine and the gasoline engine as *spark ignition* (SI) engine [Heywood, 1988].

Compression ignition engines dominate the market for heavy-duty commercial vehicles such as trucks and buses. The characteristics of CI engines are that the fuel is injected directly into the cylinder where it is ignited by compression alone, i.e., no spark plug is used. The popular term *diesel engine* refers to the engine's inventor Rudolf Diesel [Diesel, 1895], and does not imply that it must operate on diesel fuel. Thus, a CI (or diesel) engine may operate on a wide range of fuels, of which diesel is the most common choice.

The advantage of CI engines compared to SI engines is that the over-all fuel efficiency is superior. Therefore, they are more cost efficient for long-term commercial use and produce less CO_2 emissions. It is difficult to quantify the difference in CO_2 emissions as this depends on the vehicle and driving pattern, but it is generally estimated that the well-to-wheel CO_2 emissions are in the order of 15-30% lower for CI engines [Sullivan et al., 2004]. In the past, the disadvantage of the CI engine was high levels of emissions of nitrogen oxides, NO_x and soot particles, PM. These emissions are linked to a broad range of environmental and human health effects including eutrophication of water bodies, acid rain, smog, and increased frequency of diseases such as asthma and lung cancer [U.S. Environmental Protection Agency, 2001].

As a response to the findings of the effects of NO_x and PM emissions, legislators have imposed increasingly stringent emissions standards over the past 20 years. Figure 2.1 shows European and American legislated NO_x and PM emissions levels for heavy-duty engines from 1990 to 2015 [U.S. Environmental Protection Agency, 2011a; European Union, 2007]. The exact levels should not be directly compared over region and year because the certification procedures

differ in terms of driving cycle, operating points, and policies for deterioration during long-term use. It is clear, however, that emissions legislation has provided the incentive to develop and introduce new technology to significantly reduce emissions from vehicles.
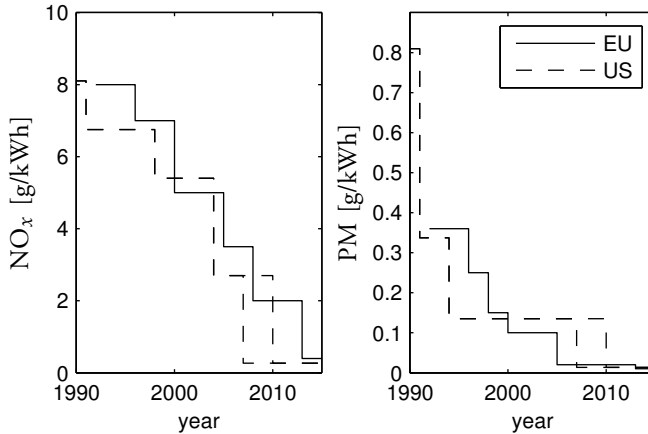
Figure 2.1   Legislated emission levels for heavy-duty vehicles in the European Union and the United States. New U.S. standards were introduced on a 50% of sales basis in 2007 and took full effect in 2010. [U.S. Environmental Protection Agency, 2011a; European Union, 2007]

To comply with the stringent legislation, a shift in technology has been necessary. One major development has been to add exhaust after-treatment systems to the engine. That way, undesired emissions are removed from the exhaust gases after leaving the combustion chamber. Another major development has been to modify the combustion process such that the engine-out emissions are reduced, thus eliminating or reducing the need for after-treatment.

2.1 Low-Emission Engine Concepts

Engine Emission Characteristics

Regulated emissions for automotive engines are hydrocarbons (HC), carbon monoxide (CO), oxides of nitrogen NO_x, and particulate matter (PM). Forthcoming legislation is expected to also include standards for greenhouse gas emissions [U.S. Environmental Protection Agency, 2011c]. In diesel engines, CO emissions are low because the engine is always operated lean, i.e., with excess of oxygen, and HC emissions are low except for low-load and cold-start conditions

when the fuel-air mixture in the cylinder may locally be too lean or too cold for the fuel to ignite [Tschöke et al., 2010].

Diesel engine emissions of NO_x and PM are however significant. NO_x is a common notation for NO and NO_2, but under normal engine conditions, formation of NO dominates over NO_2. The main part of NO is formed as so called thermal NO, where formation can be modeled by the extended Zeldovich mechanism consisting of three chain reactions [Heywood, 1988, pp. 572-575]

$$O + N_2 \leftrightharpoons NO + N$$
$$N + O_2 \leftrightharpoons NO + O \qquad (2.1)$$
$$N + OH \leftrightharpoons NO + H$$
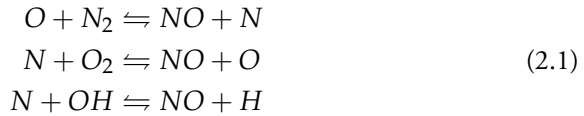
Taking into account the chemical kinetics rate constants, the kinetics can be simplified by assuming equilibrium concentrations of certain species which yields an expression for the initial NO formation rate given in mol/(cm^3s)

$$\frac{d[\text{NO}]}{dt} = \frac{k_1}{T^{1/2}} \exp(\frac{-k_2}{T})[O_2]_e^{1/2}[N_2]_e \qquad (2.2)$$

where $k_1 = 6 \cdot 10^{16}$ s(Kmol/cm^3)$^{1/2}$, $k_2 = 69,090$ K, and $[O_2]_e$ and $[N_2]_e$ denote equilibrium concentrations. Formation rate is strongly dependent upon temperature, as can be seen in Fig. 2.2 where the formation rate is plotted normalized by the species concentration expression $[O_2]_e^{1/2}[N_2]_e$.

From Eq. (2.2), it can be deduced that three factors are required for any significant NO formation to occur: high temperature, air, and sufficient time for

Figure 2.2 Initial formation rate of NO from Zeldovich mechanism, normalized by species concentration expression $[O_2]_e^{1/2}[N_2]_e$.
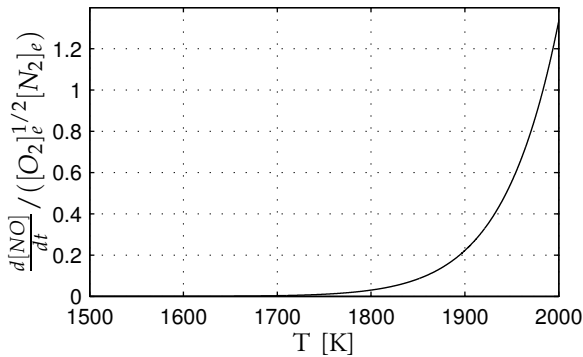
the reaction to proceed. In [Dec, 1997], a number of studies on diesel combustion using different optical techniques were condensed into a phenomenological model of the diesel engine combustion process. The studies indicate that NO is mainly formed in the diffusion flame around the fuel jet periphery and in the hot gas regions that remain at the end of combustion. At these locations, all three conditions for NO formation are fulfilled.

Particulate matter from diesel engines consists mainly of soot which is carbonaceous particles that may absorb organic liquid compounds. Soot formation is governed by the processes of particle formation, where small nuclei of hydrocarbons with a low H/C ratio are formed where combustion is locally very rich, and particle growth where these nuclei aggregate and adsorb smaller particles to the surfaces. When the soot particles come in contact with oxygen at sufficiently high temperature (above 1000 K), they oxidize to form CO_2 or CO [Tschöke et al., 2010]. Conditions required for PM emissions are thus combustion with a locally rich mixture, sufficient time for particle growth, and for the particles to avoid entering zones where they may be oxidized.

In [Dec, 1997], it was concluded that soot is formed throughout the fuel jet cross section but the major part of soot formed is oxidized within the cylinder. Soot that does not oxidize and ends up as PM emissions is thought to be formed mainly during the end of fuel injection and after injection stops. Injection pressure drops towards the end of injection, resulting in poorer atomization of fuel and thus poorer mixing of fuel and air which means that more fuel is burnt in rich zones. Additionally, the soot particles formed from the last fuel injected during the cycle will have less time to oxidize within the cylinder, and the cylinder temperature late during the expansion stroke may be too low for oxidation to occur.

The NO_x-soot trade-off is a well-known fact in combustion engine research and development. It states that most engine design parameters and control variables will have opposite effects on NO_x and PM emissions [Tschöke et al., 2010]. To avoid NO_x emissions, the local combustion temperature and oxygen concentration should be low. To avoid PM emissions, the local combustion temperature and oxygen concentration should be high.

The HCCI Engine

A way to simultaneously reduce NO_x and PM emissions is to replace the inhomogeneous diffusion combustion of the diesel fuel jet with combustion of a homogeneous, lean mixture of fuel and air. With homogeneous combustion of a homogeneous mixture, temperature is approximately homogeneous over the cylinder. With a homogeneous temperature, zones with very high temperature are eliminated so that the maximum temperature is reduced to a value below which no significant NO_x formation occurs. Also, with a lean homogeneous

mixture there are no locally rich zones that contribute to PM formation.

Homogeneous charge compression ignition (HCCI) was first studied in the '70s [Onishi et al., 1979; Noguchi et al., 1979] for two-stroke engines where the combustion concept was shown to reduce emissions, improve fuel economy and reduce cyclic variability. The concept was later transferred to four-stroke engines [Najt and Foster, 1983; Thring, 1989]. These early four-stroke papers advocated the HCCI engine for its potential to combine CI efficiencies with SI power densities. With the increased focus on emissions in the '90s, publications a decade later focus heavily on the potential excellent emission characteristics of the HCCI concept [Ryan and Callahan, 1996; Aoyama et al., 1996; Christensen et al., 1997].

The HCCI concept is based on auto-ignition of a homogeneous fuel-air mixture. For the mixture to be homogeneous at the time of ignition, there must be sufficient time available for the fuel and air to mix. This can be accomplished either by injecting the fuel into the inlet port and thus let air and fuel mix before entering the cylinder, called port fuel injection (PFI), or injecting it directly into the cylinder early enough to allow for mixing before autoignition.

In order for the lean mixture to auto-ignite, temperature must be sufficiently high. Depending on the fuel, the temperature requirements are different. With high octane-number fuels that do not auto-ignite easily, such as gasoline or ethanol, preheating of the mixture in the intake or high levels of internal residuals (hot gases retained in cylinder from one cycle to next) is required. With low octane-number fuels, such as diesel, sufficient temperature for auto-ignition may not be an issue but the temperature must still be high enough for the fuel to vaporize. For maximum efficiency, the mixture should auto-ignite close to top dead center (TDC).

Another key aspect in making HCCI combustion feasible is to limit the heat release rate once combustion has started. Very rapid heat release causes high in-cylinder pressures and rapid pressure changes that may damage the engine and lead to unacceptable levels of audible noise [Heywood, 1988, p. 450]. The heat release rate depends on combustion phasing, i.e., the time during the engine cycle where combustion occurs, and the dilution of the mixture. There are two principal ways of diluting the mixture, either by making the mixture leaner through excess air, or by using exhaust gas recirculation (EGR).

The two requirements on ensuring that the mixture auto-ignite, and on limiting the heat release rate are to a large extent conflicting [Zhao and Asmus, 2003]. With higher temperatures, the mixture will auto-ignite more easily but also demonstrate a more rapid combustion. High dilution may limit the heat release rate to acceptable levels, but also requires higher temperatures for auto-ignition [Olsson et al., 2003]. A major current limitation of the HCCI concept is that the operating range is restricted to medium load, limited by temperature

requirements to avoid misfire at low load and dilution capacity at high load. To put the HCCI concept into production, it is essential that the engine can operate in dual-mode, i.e., switch to conventional SI or diesel engine operation at low and/or high loads [Zhao and Asmus, 2003].

Low-Temperature Combustion Diesel Engines

HCCI research using diesel fuel has mainly focused on direct injection of fuel into the cylinder [Zhao and Asmus, 2003]. The basic engine setup is then in principle identical to a conventional diesel engine which facilitates mode switching at high or low loads. In pure HCCI operation, the fuel-air mixture should be completely premixed at the time of auto-ignition whereas in conventional diesel combustion, the grand majority of the fuel burns in a diffusion flame [Dec, 1997]. Between these two extremes, there is a range of combustion modes varying with respect to the homogeneity of fuel and air both spatially throughout the cylinder and temporally throughout the combustion process.

Because the difference between premixed and diffusion flame combustion is not sharp for such engine setups, nomenclature is somewhat unclear. Depending on the setup and the degree of homogeneity, the combustion mode has been referred to by different names, e.g., PREDIC (premixed lean diesel combustion) [Takeda et al., 1996], PCI (premixed compression ignited) [Iwabuchi et al., 1999], MK (modulated kinetics) [Kimura et al., 1999], and PPC (partially premixed combustion) [Noehre et al., 2006; Lewander et al., 2008; Manente et al., 2009]. The setups differ in terms of injection strategy (injection timings, injection pressure, multiple injections), injector design, EGR rate, combustion chamber geometry, compression ratio, etc. Common issues in these setups are to avoid over-penetration of liquid fuel causing wall wetting and high HC emissions, to balance NO_x and soot emissions, and to retain diesel-like efficiencies.

Musculus [2006] performed a similar study to [Dec, 1997] for early-injection, high-EGR, low-temperature diesel combustion. The optical studies show that compared to conventional diesel combustion, liquid fuel penetrates further into the combustion chamber. Also, combustion occurs throughout the fuel jet cross section indicating a premixed combustion process of a locally lean mixture. Soot is formed further downstream compared to conventional diesel combustion, at the head of the fuel jet.

For conventional diesel combustion, there is a clear NO_x-soot trade-off [Heywood, 1988]. High levels of EGR or late combustion phasing reduces in-cylinder temperature which leads to reduced NO_x formation according to Fig. 2.2, but at the same time, reduced temperature inhibits oxidation of soot. Though, for very high EGR rates, temperature drops below a threshold under which no soot is formed so that simultaneous reduction of NO_x and soot is possible [Akihama et al., 2001; Noehre et al., 2006]. Figure 2.3 shows how NO_x, soot measured by
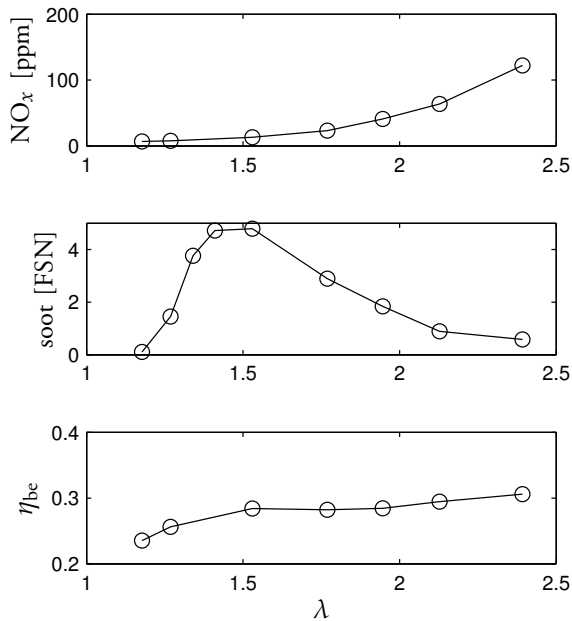
Figure 2.3 NO_x, soot, and brake efficiency η_{be} at engine speed N_{engine} = 1200 rpm, $IMEP_n$ = 5 bar. The inlet manifold pressure was kept constant and λ was varied by adjusting the EGR flow. Data from the Volvo D13 engine, see Chapter 4.

an AVL 415 filter smoke meter, and brake efficiency (over-all engine efficiency from fuel energy to crankshaft torque) vary with λ for constant load, speed, injection timing, and inlet manifold pressure. The definition of λ is the ratio of actual air-fuel ratio to stoichiometric air-fuel ratio for complete combustion. Thus, $\lambda = 1$ implies that exactly enough oxygen is available during combustion to burn all fuel. In the experiments in Fig. 2.3, the inlet manifold pressure was kept constant which means that the gas flow into the engine was approximately the same for all the data points. For high EGR rate (low λ), both NO_x and soot emissions are low, as is unfortunately also brake efficiency. For low EGR rate (high λ), there is a clear NO_x-soot trade-off.

After-Treatment Systems

After-treatment systems are added to the engine to remove undesired chemical compounds from the exhaust gases after they leave the engine. Three-way catalysts that can simultaneously oxidize CO and hydrocarbons and reduce NO_x have been standard in SI engines for many years. The three-way catalyst has

been an enormous success in terms of reducing emissions from vehicles, but it requires stoichiometric operation (no excess air in the exhausts) and can therefore not be used for diesel engines. In recent years, other types of catalytic conversion technology for lean combustion have been developed and put into production vehicles to comply with more stringent emissions standards.
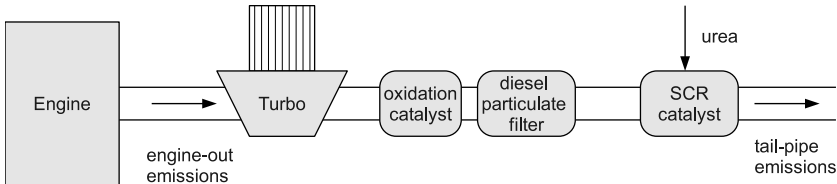
Figure 2.4   After-treatment system for a heavy-duty engine [Heck et al., 2009].

The standard after-treatment system configuration for modern heavy-duty vehicles is shown in Fig. 2.4 [Heck et al., 2009]. The exhausts are passed through an oxidation catalyst to oxidize unburned hydrocarbons and the soluble part of the particulate matter. The oxidation catalyst is followed by a diesel particulate filter that captures and stores solid soot particles. When the pressure drop over the particulate filter exceeds a threshold, active regeneration is started which means that additional fuel is injected to burn in the oxidation catalyst thus raising the temperature in the particulate trap so that the deposited soot is ignited and removed.

Finally, a selective catalytic reduction (SCR) catalyst reduces NO_x to N_2 and H_2O with the aid of ammonia. Urea must be carried on-board the vehicle to continuously supply ammonia to the SCR catalyst. It is estimated that the required amount of urea is around 1% of the fuel consumption, so an infrastructure for urea distribution is required.

The conversion efficiency and long-term performance of these after-treatment devices depend on driving pattern, fuel properties (particularly sulfur content), and ambient conditions. Under favorable conditions, top conversion efficiencies can be expected to be around 95% for both NO_x [Helden et al., 2004] and PM [Walker, 2004].

2.2 Engine Instrumentation

A facilitator in moving towards cleaner combustion has been an increased number of degrees of freedom in the engine. New hardware allows the engine to better adapt to different operating conditions to improve performance in the

whole operating range. In engine research and development, a plethora of actuation and sensing options are actively explored, and a few of these have found their way to production engines. This section presents various different actuation and sensing options of modern diesel engines.

In a production engine, control algorithms that tie actuator commands to sensor input are implemented in the engine electronic control unit (ECU) which is the microprocessor used for engine management.

Actuators

Fuel injection actuation   Fuel may be injected into the engine at two different locations. Direct injection is normally used for diesel engines and modern SI engines, and implies that fuel is injected directly into the cylinder at a high pressure. With port injection, commonly used for SI engines, fuel is injected into the intake port and mixes with air before entering the cylinder. Operating strategies that combine the two injection systems have also been the subject of research studies [Alger et al., 2005; Ekholm et al., 2008; Curran et al., 2010]. Such operation is sometimes referred to as fumigation, dual-fuel, or RCCI (reactivity controlled compression ignition) and will be further discussed in Chapter 8.

For direct-injection engine operation, the injection profile is one of the most important characteristics for the combustion process. Fuel should be injected at the right time during the engine cycle, and at a high pressure. The high pressure is necessary for the fuel to atomize, and for fuel and air to mix well. High injection pressure significantly reduces soot formation because there are less fuel-rich zones, and it may slightly increase NO_x formation because more oxygen is available during combustion. Two opposite effects influence fuel consumption. Higher injection pressure allows more fuel to be injected near TDC, which may give better efficiency, but there is also a cost associated with generating the high rail pressure [Tschöke et al., 2010].

There are two main technologies for generating high injection pressure: unit injectors and common-rail injection [Egler et al., 2010]. In unit injection, a low-pressure pump supplies fuel to the injectors where it is compressed by the camshaft movement and then injected through the nozzle. Electronic solenoid valves control the injection timing and injection duration.

The other technology, common-rail injection, has gained wide-spread use in recent years. As the name suggests, a common high-pressure rail supplies fuel to all cylinders. The rail pressure must be very high, up to 2000 bar. The fuel is injected from the high-pressure rail into the cylinders through individual solenoid or piezo-electric valves [Mock and Lubitz, 2008].

An advantage of common-rail injection is that it can easily accomodate

multiple fuel injections per cycle. There are several potential benefits of multiple injections [Projahn et al., 2010]. A pilot injection, i.e., injecting a small amount of fuel before the main injection, is commonly used to reduce audible noise. A post-injection, i.e., injecting a small amount of fuel late during the expansion stroke can improve soot oxidation or help increase exhaust temperature to match the requirements of after-treatment systems.

Gas flow actuation   Beside fuel, fresh air and EGR are supplied to the engine cylinders. Appropriate pressure and temperature at different parts of the engine ensure the right gas flows into the cylinder.

Turbocharging is used to increase the pressure in the inlet manifold so that more air, and thus more fuel, can be supplied to an engine of a given volume. This allows the engine to be smaller and more fuel efficient than a naturally aspirated engine [Steinparzer et al., 2010]. Energy from the hot exhaust gases is converted to work in the turbine, and the work is transferred to a compressor which increases the pressure in the inlet manifold. A fixed turbine geometry has to be designed for maximum gas flow at high load and speed. To get appropriate boost at different operating conditions, a variable geometry turbocharger (VGT) is used [Hiereth and Prenninger, 2007]. The VGT has an actuator which changes the angle of the turbine vanes to adapt to the exhaust gas flow.

According to the ideal gas law, density ρ is inversely proportional to absolute temperature T,

$$\rho = \frac{pM}{RT} \qquad (2.3)$$

The compressor increases the temperature of the gas flow, both by heat transfer from the warm exhaust gases, and through compression. A heat exchanger, called intercooler, is therefore used for turbocharged engines to reduce the temperature of the gas after the compressor.

There are two different configurations that allow EGR to circle from the exhaust manifold into the inlet manifold. In a high-pressure (also known as short-route) EGR loop, exhaust gas passes from the exhaust manifold before the turbine to the inlet manifold after the compressors as shown in Fig. 2.5. In a low-pressure (also known as long-route) EGR loop, exhausts are taken after the turbine and mixed with the fresh air before the compressor as shown in Fig. 2.6. A heat exchanger is normally used in both configuration to cool the EGR flow to increase density.

High-pressure EGR has a faster dynamical reponse, but is more limited in the amount of EGR it can deliver. The amount of EGR is controlled by an actuated valve in the EGR pipe. Low-pressure EGR has a longer response time but can deliver very high EGR ratios. The amount of EGR is here controlled by two actuated valves. An EGR valve in the EGR pipe allows the EGR flow to
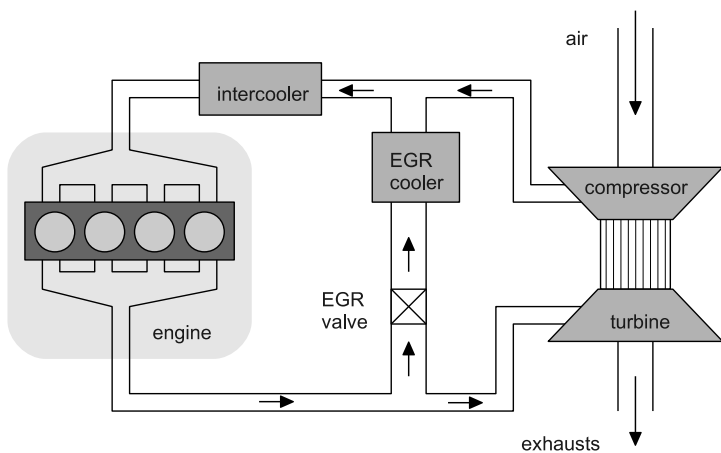
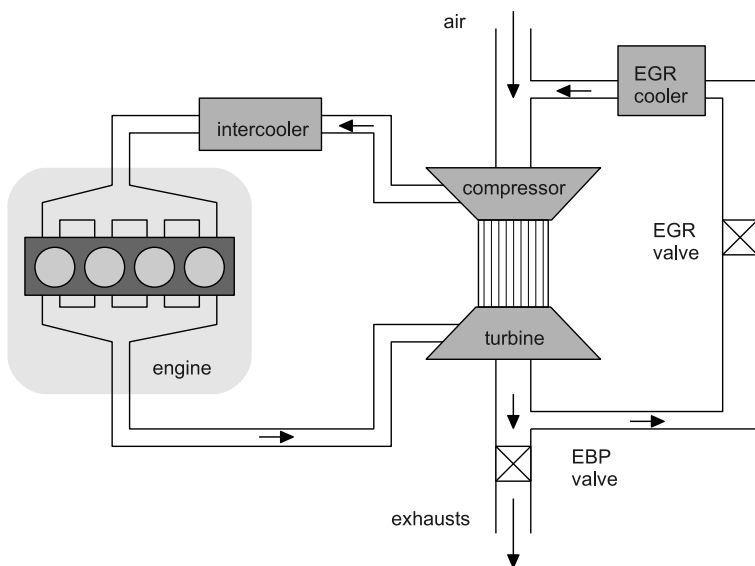**Figure 2.5**   Gas flow in engine equipped with VGT and high-pressure EGR.

Figure 2.6   Gas flow in engine equipped with VGT and low-pressure EGR.

be completely cut off. An exhaust back pressure (EBP) valve in the exhaust pipe increases the pressure such that exhausts are pressed through the EGR pipe.

In HCCI engines, the temperature of the gas entering the cylinder must be high enough to allow the fuel to completely vaporize and mix with air, and high enough for the lean mixture to auto-ignite. One way to accomplish such fuel vaporization is to pass the air and EGR through an electric heater instead of an intercooler. The power of the electric heater can be used as an actuator for intake temperature.

Valve timing actuation   Variable valve actuation (VVA), also known as variable valve timing (VVT), refers to technologies that allow the opening and closing timings of the intake and exhaust valves to change during operation. Normally, valve timings are fixed and determined by the mechanical design of the cam shaft. When the exhaust valve opens, exhaust gases exit the cylinder, and when the intake valve opens, fresh air and EGR enters the cylinder. There is normally a valve overlap, during which both valves are open simultaneously to improve gas exchange. At high engine speeds it is an advantage to let the valves be open a larger part of the cycle to exchange enough gas. At low speed, the torque and efficiency may suffer if the valves are open for too long. Therefore, the choice of valve timings in a conventional engine is a trade-off in terms of performance at different operating points [Pucher, 2010].

With variable valve timings, the valve overlap can be optimized for each operating point individually. It also opens for other possibilities to influence engine operation. The effective compression ratio can be reduced by retarding inlet valve closing after bottom dead center. This approach is exploited in Chapter 8. Another option is negative valve operlap (NVO) where the exhaust valves close before bottom dead center so that some hot residuals are trapped in the cylinder. This can be seen as a form of internal EGR, and is one option that has been suggested for obtaining sufficiently high temperatures for HCCI combustion. Yet another option is rebreathing, where valve timings are chosen such that exhaust gases first leave the cylinder and then flow back through the exhaust valve and mix with the fresh intake gas [Trajkovic et al., 2006].

Actuation of after-treatment systems   With advanced after-treatment using a diesel oxidation catalyst, a diesel particulate filter, and an SCR catalyst, new actuation capabilities are introduced. Particle filters with active regeneration require that the temperature of the exhaust be raised intermittently to burn off soot deposits. Exhaust temperature above 540 °C are required [Heck et al., 2009], which can be achieved by injecting additional fuel to burn in the oxidation catalyst. Appropriate conditions are required to initiate regeneration [Swift et al., 2008]. For SCR control, dosage of urea is an important control variable to

obtain high conversion efficiency of NO_x while avoiding ammonia slip [Hsieh and Wang, 2011].

Sensors

Many different types of sensors are relevant for combustion engine development and operation. The simplest forms are low-cost, low-complexity sensors that are used for monitoring purposes in production engines, such as an on-off indicator for oil level. The most advanced forms are extraordinarily complex and expensive laboratory setups, such as systems for optical combustion diagnostics.

Sensors can be categorized in different ways: by the physical quantities that are measured, by the time-scale on which they operate, or by the application domain (laboratory or production). This section will give a brief description of different sensors used in combustion engine research and development. The focus is placed on their current or potential impact on diesel engine feedback control. This potential is determined by time-scale, cost, robustness, and durability.

Mechanical position, rotation, and vibration   Position sensors are used to measure position of mechanical components, such as the accelerator pedal or the EGR valve. They rely on simple techniques, for example potentiometry, and are common-place in both laboratory and production engines [Fleming, 2008].

To synchronize fuel injection with piston and valve motion, crank shaft or cam shaft sensors are used. These sensors emit one pulse each revolution (crank shaft) or cycle (cam shaft), which are used to determine the next firing cylinder. The pulse train is also used to estimate engine speed. If the sensor is designed to register several pulses per revolution, angular speed may estimated with high resolution [Robert Bosch GmbH, 2011].

All SI engines use knock sensors to detect knock and subsequently retard combustion timing [Ribbens et al., 2003]. Knock sensors are vibration sensors that capture acoustic oscillations generated from knocking combustion.

Temperature, pressure, and mass flow outside the cylinder   Proper flow of air, fuel, and EGR into the cylinders is required for engine performance. Therefore, thermodynamic properties such as temperature, pressure, and mass flows are measured in both production and laboratory settings.

Pressure sensors with a response time of a few milliseconds are standard equipment in combustion engines. Sensors aimed for low pressure applications (up to a few bars), are used at various locations outside of the cylinder such as the intake or exhaust manifold or to measure ambient pressure. They are used for feedback control of EGR flow and boosting, or to sense differential pressure for estimation of mass flow. Pressure sensors for high pressure applications are

used for fuel-pressure monitoring in common-rail engines [Robert Bosch GmbH, 2011].

Commonly used temperature sensors (thermocouples) have a longer response time, in the order of seconds, and are used for on-line adaptation to properties that change slowly such as temperature of fuel or ambient air, or for monitoring of e.g. oil or coolant temperature [Fleming, 2008].

Chemical composition of exhausts   The exhaust gases contain a large number of different chemical compounds. The main species are nitrogen N_2, oxygen O_2, carbon dioxide CO_2, water H_2O, argon Ar, carbon monoxide CO, unburned hydrocarbons HC, and nitrogen oxides NO and NO_2.

The most recent versions of emissions legislation require that emission control systems be monitored and malfunction be detected and reported to the driver [U.S. Environmental Protection Agency, 2008]. This feature, known as on-board diagnostics (OBD), requires sensors that can diagnose emissions levels that exceed legislated limits by a certain factor. Incentives are thus imposed for additional on-board sensors that can detect such malfunction.

The most widespread sensor for measuring gas composition is the lambda sensor that measures the exhaust oxygen concentration. Lambda sensors have been used in SI engines since three-way catalysts were introduced in the late '70s [Heck et al., 2009]. Originally, lambda sensors were of narrow-band type, which essentially means they give an on-off signal indicating whether engine operation is rich or lean, i.e., with excess of fuel (rich) or excess of oxygen (lean). Later, wide-band lambda sensors have become available, thus making them suitable for heavy-duty applications where operation is always lean. Wide-band lambda sensors are used in both production and laboratory engines, and have response times in the order of 0.05–1 s [Swingler, 2009].

Lambda sensors were for long the only sensors measuring chemical composition in exhausts of production vehicles. Since the advent of complex after-treatment and OBD requirements, sensors measuring other exhaust species are emerging. Siemens VDO / NGK produce the Smart NOx Sensor [Siemens VDO, 2005], which is widely used to control urea dosage in SCR catalysts. This sensor also measures λ, and has a response time of 750 ms for NO_x and 550 ms for wide-band λ. Delphi has announced that they will put an ammonia sensor for SCR control on the market from 2012 [Delphi, 2010; Wang et al., 2008]. The sensor is reported to have a response time of 3–5 s. Particulate matter sensors have also been announced by Delphi [Delphi, 2011] and Bosch [Bosch GmbH, 2011a], targeted at OBD monitoring of the diesel particulate filter performance.

In laboratory studies of engine combustion, it is common to measure O_2, CO_2, CO, NO, and hydrocarbons in the exhausts [Martyr and Plint, 2007].

Together with measurements of fuel consumption and CO_2 in intake, it is possible to do a fairly detailed analysis of the combustion process, the engine efficiency, and the mass flows in the engine. However, measurement systems for such analyses are large, expensive, and require substantial maintenance. The response times of the systems are also normally at least a few seconds. Such measurements are mostly useful for steady-state experimentation and calibration in laboratory settings.

Diesel exhaust particulate matter (PM) is a mixture of different chemical compounds of varying composition and molecular structure. Different metrics are used to quantify the particulate matter content in the exhausts, e.g., the total mass of particles, the number of particles, the size distribution of particles, or the light-absorbing properties of the particles [Swingler, 2009]. For steady-state measurements, filter smoke number is commonly used. Here, the exhausts are passed through a fine filter for a period of time, in the order of 30 s. After that period, the filter is analyzed either optically to measure the blackening, or by measuring the change of mass. The filter method is not applicable to transients.

For transient measurements, an opacimeter is used both in certification processes and in research and development. The opacimeter passes light through the exhaust gas flow, and measures the amount of light absorbed. It is less precise than the filter method, and is biased towards particle shapes and sizes that absorb the most light.

High-resolution combustion sensing   None of the sensors described so far detect the combustion process for individual cycles separately for each cylinder. They measure the mean-value effect of several cycles, and generally only the average over the cylinders. Sensors that measure the combustion process inside the cylinder are with few exceptions only used in laboratory settings.

The technical requirements for combustion sensing are high. The dynamic response must be fast, to allow sampling frequencies in the order of 10–100 kHz. The sensor must be able to withstand high pressure, up to 200 bar, and high temperatures, up to 650 °C [Eastwood, 2009]. Sufficient computing power must also be available to handle the large amounts of data. Another concern is to fit the sensor into the mechanical design of the cylinder head.

Cylinder pressure sensing is by far the most widely used technology for evaluating the in-cylinder combustion process in engine research, development, and calibration. These sensors provide data with high temporal resolution of the combustion process for an individual cylinder. By thermodynamic laws, the heat release rate can be computed from the cylinder pressure, see [Gatowski et al., 1984] and Chapter 4. The heat release rate and cylinder pressure provide many of the standard parameters used for combustion evaluation and calibration, such as start of combustion, ignition delay, and combustion phasing. From cylinder

pressure data, it is also possible to detect incomplete combustion and combustion that may damage the engine where the peak pressure or the pressure derivative is too high. Methods to predict emissions based on pressure data have also been suggested [Traver et al., 1999; Wilhelmsson et al., 2009; Çebi et al., 2011].

Because of the high technical demands and associated cost, the technology has not yet reached widespread use in production vehicles. For large marine engines, cylinder pressure sensors are currently employed in production engines to monitor and control the combustion process [Rolle and Wiesmann, 2011]. However, the market profile as well as the operating pattern are very different in this case compared to road vehicle engines. Some announcements still indicate that cylinder pressure sensing is starting to emerge in production also for on-road vehicles [Birch, 2008; Pudenz, 2007; General Motors, 2007; Shahroudi, 2008].

Shahroudi [2008] presented a survey of technological evolution and market potential of high-resolution sensors for combustion control. He listed some key benefits of closed-loop combustion control, suggested in interviews with industry experts:

- Better cylinder-to-cylinder balancing

- Reducing cycle-to-cycle variations in combustion

- Reducing emissions

- Detection and avoidance of misfires

- Detection and avoidance of engine knock

- Improving efficiency

- Faster time-to-market

- Reducing engine noise

- Easier calibration

Shahroudi argued that introducing cylinder pressure sensors in production engines would be an example of *architectural innovation*. That is, the sensors would change the architecture of the engine development and calibration process. Reaping benefits of directly sensing the combustion process requires rethinking the configuration of other sensors, the control design, and the calibration process:

> ICPS [in-cylinder pressure sensors] enables closing the loop around the combustion process to improve the trade-off of complexity versus robustness for the engine system as a whole, thereby helping the engine developers maintain bottom line robustness as they add complexity to meet the tighter requirements. But to be part of the solution and not the problem, the ICPS component itself has

to have an excellent robust performance at a reasonable cost and size [Shahroudi, 2008].

Water-cooled piezo-electrical pressure transducers are the state-of-the-art in terms of cylinder pressure sensing in laboratory setups. They have excellent dynamic properties, but are not applicable to production vehicles due to high cost, insufficient robustness and durability, and the need for continuous water cooling. A number of technical solutions to produce cylinder pressure sensors viable for production have been presented by automotive industry suppliers. BERU [Beru AG, 2008] produces piezo-resistive sensors where the sensing element is integrated into a diesel engine glow plug. Both Siemens [Siemens VDO Automotive, 2006] and Bosch [Bosch GmbH, 2011b] produce piezo-electric sensors integrated with the glow plug. Optrand [Optrand, 2011] produces fibre-optic pressure sensors that may be integrated into the spark plug of SI engines, or the glow plug of light-duty diesel engines [Wlodarczyk, 2006].

Another technology to gain information on the in-cylinder process is ion-current. Ion-current sensing exploits the conductivity of intermediate products of the combustion process. High-resolution data that may be used to estimate for example start of combustion is provided. In SI engines, the spark plug can be used as an ion-current sensing element during combustion. Delphi have developed a combustion monitoring technology for diesel engines based on ion-current sensing integrated with the glow plug [Delphi Technologies, Inc., 2011], but this technology has not yet resulted in a product. There are many research publications related to ion-current feedback control of the combustion process, e.g., [Glavmo et al., 1999; Malaczynski and Baker, 2003; Strandh et al., 2003; Larsson, 2009].

Heavy-duty diesel engines are normally neither equipped with spark plugs nor glow plugs, so other means of combustion sensing that do not require separate access to the cylinder are actively explored. Integrating a sensing element into the fuel injector is one approach that has been suggested [S. Simon, 2001; Zöls et al., 2010]. Other options include using high-resolution sensing of angular speed [Citron and O'Higgins, 1989], crankshaft torque [McKelvey et al., 2007], or engine block vibration [Grondin et al., 2008] to infer information on combustion in individual cylinders.

2.3 Models

Modeling of complex systems is an art. What constitutes a good model depends on the application, the available data for calibration, and the available computational resources. A very brief overview of modeling approaches of different

complexity for combustion engines is presented here, with a few references to relevant texts where the corresponding approach is applied. The list is ordered according to complexity, with the most detailed and complex models first.

Computational fluid dynamics models   Computational fluid dynamics (CFD) uses numerical algorithms for simulation and analysis of partial differential equations describing dynamical fluid flow. Chemical reactions in the fluid can also be modeled, which means that CFD is appropriate for detailed simulation of the combustion process. The combustion chamber is discretized in a large finite number of points, which gives models with high resolution both temporally and spatially.

Shi et al. [2011] present a good overview of CFD models for engine optimization. Applications include optimization of hardware such as piston bowl geometry or injectors, and studies of the effect of fuel properties on the combustion process. The computational effort, where several hours or even days are typically required for simulation of a single engine cycle, is prohibitive for using such models for design or evaluation of control algorithms.

Low-dimensional crank angle-resolved models   The next class of models have high temporal but low spatial resolution. A single state represents the mean value of a variable over a larger space such as the entire cylinder volume (one-zone model), the burned or unburned zone (two-zone model), or the cylinder walls. The models are built from low-order ordinary differential equations or differential-algebraic equations. State variables could for example represent cylinder wall temperature, pressure in unburned gas, flame front radius, or concentration of a chemical species in the cylinder. The models are often based on first principles with compensation for unmodeled phenomena by means of empirical coefficients or maps.

Some examples of such models:

- Convective heat transfer between the cylinder and cylinder wall [Heywood, 1988, p. 670],

$$\frac{dQ}{dt} = h_c A_w (T_{\text{cyl}} - T_{\text{wall}}) \tag{2.4}$$

  where h_c is the heat transfer coefficient and A_w the cylinder wall temperature.

- Heat release rate from combustion related to cylinder pressure and volume [Gatowski et al., 1984]

$$\frac{dQ}{d\alpha} = \frac{\gamma}{\gamma - 1} p \frac{dV}{d\alpha} + \frac{1}{\gamma - 1} V \frac{dp}{d\alpha} \tag{2.5}$$

- Auto-ignition models for HCCI combustion [Bengtsson et al., 2004] such as the integrated Arrhenius rate threshold

$$K_{\text{th}} = \frac{1}{N} \int_{u_{\text{IVC}}}^{\alpha_{\text{ign}}} 1/\tau \, d\alpha$$
$$1/\tau = A \exp(E_a/(R_u T))[\text{Fuel}]^a [\text{O}_2]^b$$

(2.6)

- Wiebe function for fraction of burned fuel mass [Wiebe, 1970],

$$x_b = 1 - \exp\left(-a\left(\frac{\alpha - \alpha_0}{\Delta\alpha}\right)^{m+1}\right)$$

(2.7)

- Pollutant formation, e.g., the formation rate of NO in the Zeldovich mechanism (2.2).

Cycle-to-cycle models   The crank-angle resolved models are not directly applicable to control design since actuation of e.g. valve events and fuel injection only has cycle-to-cycle resolution. Many approaches to simplifying crank-angle resolved models into discrete-time models with sampling based on engine cycle have been suggested. Examples of such models are presented in [Widd et al., 2008; Ravi et al., 2010; Hillion et al., 2011].

Mean-value models   Mean-value models are often used to describe the engine processes outside the combustion chamber. Such processes include flow of air and EGR, turbocharger dynamics, fuel vaporization in PFI engines, and temperature of oil and coolant. In this modeling framework, the engine cylinders are modeled as a continuous process, i.e., individual cycle events such as opening and closing the valves are not included. Mean-value models are low-dimensional ordinary differential equations, with states representing for example pressure and temperature in the intake and exhaust manifolds, turbocharger rotational speed, or actuator and sensor dynamics. A good overview of mean-value models is given in [Guzzella and Onder, 2004]. Mean-value models are widely used for model-based gas flow control design, as will be presented in Section 2.4.

Empirical models   Empirical models are built from experimental data by fitting the data to some generic model structure. The model structure can take many forms, e.g. linear regression models, splines, wavelets, or neural networks [Hastie et al., 2009]. General dynamic models on e.g. state-space or polynomial form can be found using system identification techniques [Johansson, 1993] on dynamic input-output data. Sometimes first principles may be used to suggest a model structure where parameters are then fitted to data, so called grey-box modeling.

Empirical models are widely used by industry for engine control design, where open-loop optimal maps for actuator settings are determined from experimental calibration, as will be described in the next section. Dynamical empirical models are also used in a number of closed-loop control designs presented in research papers.

The disadvantage of empirical models is that they rely heavily on the data used for calibration. The extrapolation performance is often poor, and the models cannot easily be adapted when the physical design of the engine changes. On the other hand, any physical model relies on simplifications, approximations, and assumptions that may not be appropriate for a given situation. Data-based models are not prejudiced against such assumptions.

2.4 Diesel Engine Control

Electronic engine control has been used since the 1970's, where it was first applied to spark-ignition engines. A historical perspective on the early development of engine control in industry is given in Appendix A by John Cassidy, a pioneer of engine control at GM. Today, electronic control is universally applied for both SI and diesel engines.

Production Setups

The engine management system in the ECU is responsible for ensuring that the right amounts of fuel, air, and EGR are delivered to the engine. The standard practice in control design is to separate the fuel path control design and the gas path (air and EGR) control design [Guzzella and Onder, 2004]. The fuel path controller determines fuel injection duration and injection pressure based on accelerator pedal position and measured engine speed. A map is used to limit the amount of fuel injected during transients until the air flow has become sufficiently high.

The gas path controller determines EGR valve and VGT vane positions to get the desired air- and EGR flows to the cylinders. This control path uses feedback from pressure, temperature, and/or mass flow sensors to estimate the gas flows. The estimated air flow is passed to the fuel path controller. Setpoints for engine speed, injection timing, air flow and EGR flow according to operating conditions are given by maps that are pre-calibrated for optimal efficiency and emissions. An illustration of the scheme, adapted from [Guzzella and Onder, 2004; Alberer, 2009], is shown in Fig. 2.7.

In practice, the scheme implies that only static interactions between the gas path and fuel path are considered. For conventional diesel combustion, it is reasonable to assume that the gas path dynamics is significantly slower
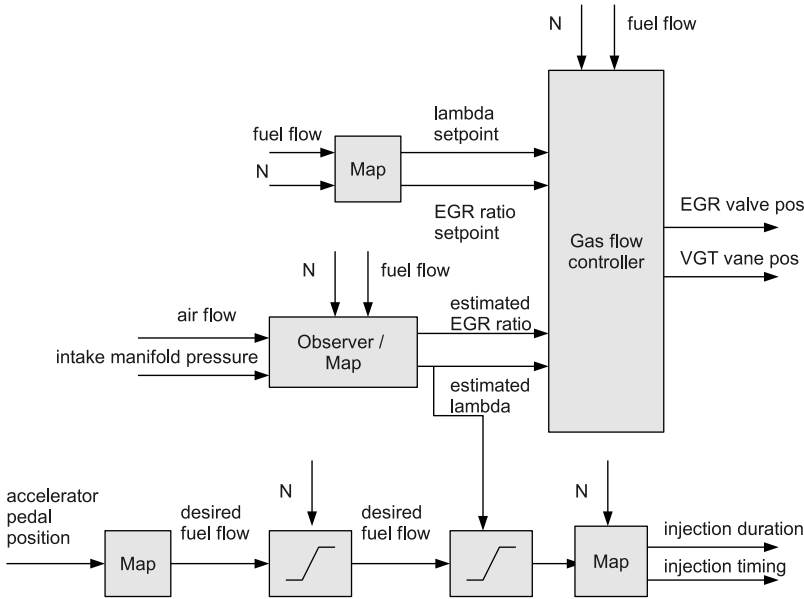
Figure 2.7   Schematic drawing of the standard structure for the most important control loops in production diesel engines, adapted from [Guzzella and Onder, 2004; Alberer, 2009]. *N* = engine speed.

than the dynamics related to in-cylinder combustion. It is then possible to neglect dynamic interactions between the two systems. For sensitive combustion modes, such as low temperature combustion or HCCI, it may be necessary to consider the dynamic interactions to achieve optimal performance. With a more premixed combustion, the combustion process becomes more sensitive to in-cylinder conditions such as cylinder wall temperature and temperature and composition of residual gases.

With more actuators added to the engine, such as variable valve timings and multiple injections, it also becomes harder to separate the control design task into subsystems while preserving optimality. Full calibration becomes exponentially more difficult with increasing dimensionality of the design space. After-treatment systems impose additional complexity [Westerlund et al., 2010]. They add both new actuator variables, such as urea dosage, and new optimization criteria, such as requiring sufficiently high exhaust temperatures.

Published Research

Diesel engine control is a vast research field [Guzzella and Onder, 2004]. The published contributions address different engine subsystems, use different actuators and sensors, base the designs of different models, and vary greatly in terms of computational complexity of the proposed algorithms. The common challenge is to convert high-level objectives of efficiency and emissions to low-level specifications on individual control loops.

The published literature can be divided into two classes depending on the relation between the high- and low-level specifications. In *indirect* approaches, optimal setpoint trajectories for measurable intermediate quantities are determined off-line. The control design task is then limited to tracking these setpoint trajectories. In *direct* approaches, one or more of the high-level specification variables are measured or estimated on-line, and directly optimized by the controller.

This section will attempt to give an overview of state-of-the art published research relevant for the thesis.

Gas path control   Much of the published diesel engine control research focuses on gas path control. Because the combustion process is highly dependent on the properties of the gas flow into the cylinder, the general approach is to specify desired trajectories for air and EGR flow and design controllers for EGR valve position and VGT vane position to follow these trajectories. A high-level controller would then be used to generate setpoint trajectories for air and EGR flow to optimize emissions and efficiency.

Time constants in gas path dynamics are relatively long, associated with mass flows, heat transfer, and mechanical inertia in the turbo. The gas exchange system is a bottleneck for fast torque tracking; fuel flow can be increased immediately as a response to the driver's command, but to avoid very large peaks in emissions, the fuel injection must be rate limited until the air and EGR flows have caught up.

Various different control design methods have been suggested for control of air and EGR flow in turbocharged diesel engines, mostly based on mean-value models. Jankovic et al. [2000] used an approach based on a control Lyapunov function. Stefanopoulou and Kolmanovsky [2000] used nonlinear feedforward control combined with gain-scheduled linear H_∞ control. Jung and Glover [2006] expressed the nonlinear mean-value model of the engine on LPV form and designed an H_∞ controller. Wei and del Re [2007] used a semi-empirical LPV model of the engine with data-based identification of the coefficients to design a gain-scheduled H_∞ controller. Ortner and del Re [2007] used data-based models and explicit model predictive control (MPC). Wang [2008] studied the problem of boost/EGR control for mode switching between low temperature combustion at low load and diesel combustion at medium load. A physical mean-

value-model was here used to design a sliding mode controller. García-Nieto et al. [2008] performed a simulation study where a nonlinear mean-value model was linearized at a grid of operating point and an explicit MPC was designed for each operating point. Wahlström et al. [2010] presented a control strategy based on PID controllers and switching logic to satisfy physical constraints and optimize performance. Wang et al. [2011] identified linear systems at a grid of operating points and used static decoupling and two single-input-single-output PID controllers tuned using quantitative feedback design.

Other publications focus on either a reduced or extended set of actuators for gas path control. One direction is control of λ using the EGR actuator, as in [Amstutz and del Re, 1995] where an LQG design was used, and [Alfieri et al., 2009] where a gain-scheduled H_∞ controller was designed. More advanced configurations, such as double EGR loops [Grondin et al., 2009], and dual-stage turbocharging [Moulin et al., 2009] have also been studied.

This wide selection of publications are all based on some common principles and assumptions. The gas path controller is not coordinated with the fuel path controller; fuel injection is modeled as a disturbance to the gas exchange system. No cylinder-individual sensing or actuation is used, only the mean-value properties of all cylinders is controlled. The relation to the high-level specifications is indirect. The control objective is in most cases formulated as tracking of setpoints for compressor mass flow and inlet manifold pressure. Determining optimal setpoint trajectories is usually not addressed in the publications, but is rather seen as an independent calibration task.

Cylinder-individual combustion control   The trend towards more sensitive combustion modes, with HCCI combustion being the most extreme case, has brought an increased interest in direct cylinder-individual feedback control of the combustion process. For such operating conditions, small differences in ambient conditions, such as air temperature, engine temperature, coolant temperature, ambient pressure etc., can lead to knocking or misfiring combustion.

The combustion conditions may vary between cylinders in a multi-cylinder engine for a number of reasons, including:

- Difference in fuel flow due to unit-to-unit variations for injectors.

- Difference in flows of air and EGR due to pressure variations in the inlet manifold.

- Difference in the amount of residual gases retained in the cylinder from the previous cycle, due to pressure variations in the exhaust manifold.

- Difference in temperature of air, EGR, residual gases, and cylinder walls due to heat transfer effects; the first and last cylinders in a row will tend to be cooler.

Such differences exist for all types of engine combustion, but they have a larger influence on the combustion process for sensitive combustion modes such as HCCI and low-temperature diesel combustion.

Many different actuation options and control strategies have been explored for feedback control of combustion phasing in HCCI engines, see for example [Olsson et al., 2001; Martinez-Frias et al., 2001; Agrell et al., 2003; Strandh et al., 2004; Shaver et al., 2004; Bengtsson et al., 2006].

Cylinder-individual direct control of the combustion process (keeping a desired combustion phasing or balancing the power generation in each cylinder) can also be applied for conventional diesel and SI combustion if an appropriate sensor is available. Examples include Larsson and Andersson [2008] (combustion phasing in SI engine estimated from crankshaft torque sensor, controlled by spark advance), Willems et al. [2010] (combustion phasing and $IMEP_n$ estimated from cylinder pressure sensors, controlled by injection timing and injection duration), Östman and Toivonen [2011] (high-resolution crankshaft angular speed sensor estimates cylinder-to-cylinder imbalances in torque, controlled by injection duration), and Lewander et al. [2012] (cylinder pressure sensors estimate combustion phasing, controlled by injection timing).

Analogous to gas path control, the control task of tracking a combustion timing setpoint and the calibration task of determining the optimal setpoint are usually separated.

Integrated control of fuel- and gas path   Few publications address coordination of the fuel- and gas path controllers. Hillion et al. [2011] presented an open-loop strategy for maintaining a desired combustion phasing during sharp transients when air and EGR flow deviate from their setpoints. Knock integral models were used to predict the end of the cool flame combustion, and the injection timing was adjusted accordingly.

Alfieri [2009] used start of injection and EGR valve as actuators to control a light-duty diesel engine by feedback from NO_x and λ-sensors. A nonlinear physical mean-value model was used, and control design was based on static feedforward, decoupling of the plant, and two SISO gain-scheduled IMC controllers.

Meyer [2011] proposed a strategy to determine optimal maps for a set of five fuel injection parameters (pilot injection timing and quantity, main injection timing, post-injection timing and quantity) based on engine speed, load, and cylinder oxygen concentration. The purpose was to optimize fuel consumption and NO_x during transients when air and EGR flows deviate from setpoints. Benefits were shown in simulation.

Work by the author in [Karlsson et al., 2008] and [Karlsson et al., 2010b] on coordinated fuel- and gas path control will be presented in Chapter 8.

High-level specifications   While most engine control publications follow the indirect approach in relation to the high-level specifications, and consider optimization of setpoint trajectories as a separate task, a few explicitly position their results in a high-level specifications framework.

A number of papers on optimal engine control were published in the late 1970's and early 1980's, see for example [Tennant et al., 1979; Cassidy et al., 1980; Dohner, 1981] and references therein. In these publications, the optimal control problem of minimizing fuel consumption and maximizing driveability subject to constraints on emissions was considered explicitly. Optimal control concepts such as LQG and dynamic programming were suggested and applied to find optimal control strategies in simulations or experimentally on laboratory setups. Because of the limited computational capabilities available at the time, the focus was to use the model and optimal controllers in a calibration process, to extract open-loop optimal maps, or indirect closed-loop optimal control strategies.

To provide a comtemporary perspective on the work in the thesis, a number of relevant publications from 2000 and onward on control related to high-level specifications are presented in some detail:

- Stefanopoulou et al. [2000]: Diesel engine; EGR + VGT actuation. Stationary data are used to determine setpoints for inlet manifold pressure and air flow such that the EGR rate is maximized subject to an upper constraint on inlet pressure and a lower constraint on λ. The scheme would implicitly minimize NO_x and limit PM.

- Hafner et al. [2000]: Diesel engine; EGR + VGT + injection duration + injection timing actuation. Dynamic neural networks are trained to predict emissions from actuator settings. A cost function is specified in terms of emissions and fuel consumption. It is shown in experiments how different optimal trajectories for start of injection result from different weights in the cost function.

- Ouladsine et al. [2004]: Diesel engine; fuel injection duration actuation. Dynamic neural networks are trained to predict engine speed and opacity. Based on the neural-network model, a neural-network controller is designed to track engine speed while limiting opacity. Only simulations results are shown.

- Ferreau et al. [2006]: SI engine; EGR + throttle actuation. A cost function in terms of NO_x emissions and torque tracking is defined. Nonlinear model predictive control is applied to a nonlinear mean-value model of the engine. Only simulations results are shown.

- Darlington et al. [2006]: Diesel engine; EGR + VGT + injection duration actuation. Physical mean-value model for in-cylinder air-fuel ratio and burned-gas ratio. The model was validated using fast emissions analyzers. Based on the model, a controller that limits NO_x and PM emissions spikes during load transients was developed. The controller limits NO_x by introducing a lower limit on the burned-gas ratio which is controlled by the EGR valve, and PM by introducing a lower limit on the air-fuel ratio which is kept by limiting the fuel injection duration.

- Larsson and Andersson [2008]: SI engine; spark advance actuation. Fuel consumption is estimated from a high-resolution crankshaft torque sensor and optimized by an extremum-seeking controller.

- Atkinson et al. [2008]: Diesel engine; EGR + injection duration + injection timing + pilot injection + injection pressure actuation. Transient optimal calibration of a diesel engine with respect to emissions and fuel consumption based on an initial transient experimental campaign, a dynamic neural network model trained from the initial data, optimization of this model, and finally tests of the optimal dynamic calibration. In [Atkinson et al., 2009], it was suggested that the model inverse may be used for optimal control in a mainly open-loop fashion.

- Alfieri [2009]: Diesel engine; EGR + injection timing actuation. Optimal setpoints for λ and NO_x are determined in stationarity by optimizing fuel consumption subject to constraint on NO_x. Optimizing fuel consumption implicitly implies that PM emissions are limited.

- Omran et al. [2009]: Diesel engine; VGT actuation. A cost function is chosen as a weighted sum of fuel consumption and opacity. The engine is modeled using a combination of a physical mean-value model and maps, and a neural network is trained to determine optimal VGT trajectories as functions of load and speed. No experimental verification of the controller is presented.

- Killingsworth et al. [2009]: HCCI engine; fast thermal management. On-line optimization of fuel consumption. Fuel consumption measured on fuel scale, and combustion phasing is optimized by an extremum-seeking controller.

- Alberer [2009]: Diesel engine; EGR + VGT actuation. Several aspects of engine control formulated as an optimal control problem are presented. One study shows that oxygen concentration before and after combustion are better suited as setpoints for gas flow control than the commonly used air mass flow and inlet manifold pressure. A linear model predictive

controller is then presented for gas flow control based on a physical mean-value model. Experimental results on a light-duty engine show that the controller can achieve significantly better transient emissions compared to the standard ECU controller. Nonlinear extensions of the controller are discussed but not tested experimentally due to computational complexity.

- Wahlström et al. [2010]: Diesel engine; EGR + VGT actuation. When λ is above a pre-specified limit, the spare degree of freedom is used to minimize the pumping work, which is formulated as minimizing the difference between the exhaust manifold and inlet manifold pressures, and constraints are specified for λ and turbo speed. Setpoints are defined for EGR rate and torque.

- Willems et al. [2010]: Diesel engine; EGR + VGT + injection duration + injection timing actuation. In an *Outlook* section, it is discussed how cylinder pressure sensors may be used as virtual sensors for NO_x and PM for on-line feedback control of these quantities. No results of such scheme are presented, however.

- Vermillion et al. [2010]: SI engine; throttle + fuel injection duration + VVT + spark advance actuation. A high-level cost function including emissions, fuel consumption, and torque tracking is introduced. The cost on emissions is reformulated as a stoichiometric setpoint, $\lambda^{\text{ref}} = 1$, and a model predictive controller is designed for a full nonlinear model of the engine, driveline, and vehicle. Only simulation results are shown.

- Lewander et al. [2012]: Diesel engine; injection timing actuation. An approach to on-line optimization of fuel consumption is presented. Fuel consumption is estimated from cylinder pressure sensors and an extremum-seeking controller finds the fuel-optimal combustion phasing.

3

Systems and Control Fundamentals

A short overview of systems and control concepts and methods that will be applied in the thesis is given in this chapter.

3.1 Dynamic Models

Dynamic models are used to describe systems that evolve with time. Three simple forms of dynamic systems are the linear state-space innovations model, the Hammerstein model, and the Wiener model.

Linear Models

A linear discrete-time dynamic model with Gaussian measurement- and process noise is given by the innovations model

$$\begin{aligned} x_{k+1} &= Ax_k + Bu_k + Kw_k \\ y_k &= Cx_k + Du_k + w_k \end{aligned} \tag{3.1}$$

Here, u_k denotes the input, y_k the measured output, and w_k a zero-mean white Gaussian noise process with

$$E(w_k w_k^T) = Q_w \tag{3.2}$$

Hammerstein Models

A Hammerstein model [Narendra and Gallman, 1966] is a linear dynamic model $H(z)$ with a static nonlinear transformation $f(\cdot)$ on the input, as illustrated in Fig. 3.1.

$$\begin{aligned} x_{k+1} &= Ax_k + Bf(u_k) \\ y_k &= Cx_k + Du_k \end{aligned}$$
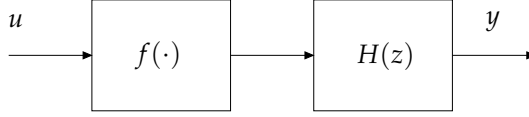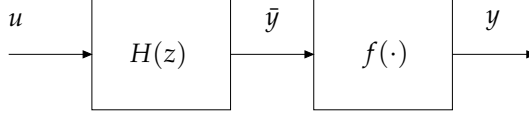
Figure 3.1   Hammerstein model.

Figure 3.2   Wiener model.

Wiener Models

A Wiener model [Billings, 1980] is a linear dynamic model $H(z)$ with a non-linear transformation $f(\cdot)$ on the output, as shown in Fig. 3.2.

$$
\begin{aligned}
x_{k+1} &= Ax_k + Bu_k \\
\bar{y}_k &= Cx_k + Du_k \\
y_k &= f(\bar{y}_k)
\end{aligned}
\tag{3.3}
$$

3.2 Data-Based Modeling

Data-based, or empirical, modeling is the process of using observed data from a system to find a model that can be used for prediction. Two types of empirical models that are used in the thesis are static neural networks and dynamic black-box state-space models. A short introduction to the structure and inference of these model types are given here.

Neural Networks

A neural network is a nonlinear approximation $\hat{f}_{\text{NN}} : x \to y$ of a function $f(\cdot)$ mapping a set of inputs $x \in \mathbb{R}^L$ into a set of outputs $y \in \mathbb{R}^K$ [Bishop, 2006]. The approximation is based on a set of basis functions and a parameter set θ. The term *training* of a neural network refers to estimating θ from a set of input-output data $\{x_n, y_n\}_{n=1}^N$.

A common parameterization of $f_{\text{NN}}(\cdot)$ is the feed-forward network with a single hidden layer and sigmoidal basis functions, illustrated in Fig. 3.3. The
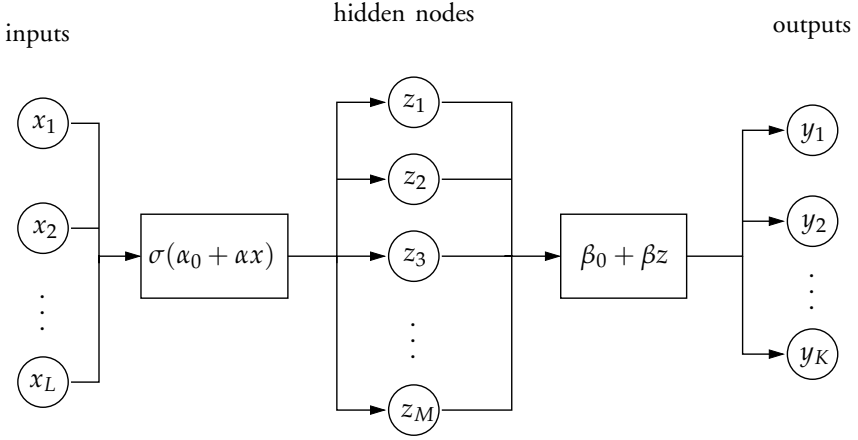
inputs

hidden nodes

outputs

Figure 3.3 Structure of a feedforward neural network with a single hidden layer and sigmoidal basis functions.

hidden layer consists of intermediate variables z_m, also known as hidden variables or hidden nodes. The nonlinearities of $f_{\text{NN}}(\cdot)$ are parameterized by the sigmoid function

$$\sigma(a) = \frac{1}{1 + \exp(-a)} \tag{3.4}$$

The hidden variables $z \in \mathbb{R}^M$ are obtained by passing affine combinations of the inputs x through the sigmoid function

$$z_m = \sigma(\alpha_{0m} + \alpha_m^T x), \quad m = 1, \ldots, M \tag{3.5}$$

The output y is then modeled as an affine combination of the hidden variables z

$$\hat{y}_k = \beta_{0k} + \beta_k^T z, \quad k = 1, \ldots, K \tag{3.6}$$

The parameters to be estimated are $\theta = \{\alpha_0, \alpha, \beta_0, \beta\}$. With $\alpha_0 \in \mathbb{R}^M$, $\alpha \in \mathbb{R}^{M \times L}$, $\beta_0 \in \mathbb{R}^K$, $\beta \in \mathbb{R}^{K \times M}$, the total number of parameters ν for the model is

$$\nu = (K + L + 1)M + K \tag{3.7}$$

scaling linearly with the number of hidden nodes M.

The parameters are estimated by numerical optimization of the squared error cost function

$$J = \sum_{n=1}^{N} ||y_n - \hat{y}_n||^2 \tag{3.8}$$

from a training data set $\{x_n, y_n\}_{n=1}^{N}$ of N samples. Closed-form algebraic expressions of the derivative of J with respect to the parameters can be derived. Optimization algorithms based on gradient descent are therefore attractive for network training [Hastie et al., 2009]. However, the optimization problem is non-convex which means that there are no guarantees for convergence to a global optimum. More details on optimization for network training will be presented in Chapter 5, where the model is extended and applied to estimation of emissions for individual cylinders.

System Identification of State-Space Models

System identification is the art of finding dynamic models of a system from data observed from the system [Johansson, 1993; Ljung, 1999]. Two main directions in system identification are black-box identification and grey-box identification. In grey-box identification, the structure of the model is determined by a-priori knowledge of the system, often from first principles. The identification task consists of determining a few unknown parameters in the model such as mass, inertia, heat transfer coefficient etc. In black-box identification, very general model structures are used. Examples include polynomial linear models (AR, ARX, MA, ARMAX) and state-space models. Model order selection is generally part of the identification task.

In the work presented in this thesis, identification of black-box state-space models was used. State-space models are convenient for multivariable systems, both in terms of numerical stability of the identification algorithms and in terms of notational convenience. They are therefore the natural modeling framework for the control algorithms used in the thesis.

Subspace identification of linear state-space models   Subspace identification algorithms make use of advanced linear algebra to find linear dynamic state-space models from input-output data. A brief overview of the fundamental principles of subspace identification is given here. For details, see [van Overschee and de Moor, 1996; Katayama, 2005]. The general idea behind subspace identification is that the system state lies in a subspace spanned by matrices compiled from the input- and output sequences. By first estimating the extended observability matrix of the system, the state sequence can be constructed. When the state sequence is known, the system matrices can be computed.

For illustration, we consider the special case of identification of a deterministic linear discrete-time single-input single-output system

$$
\begin{aligned}
x_{k+1} &= Ax_k + Bu_k \\
y_k &= Cx_k + Du_k
\end{aligned}
\tag{3.9}
$$

Input-output data from the system $\{u_k, y_k\}_{k=0}^{N}$ is given, and the task is to identify the system matrices A, B, C, D, and the order n of the system. For the general case of identification of the model in Eq. (3.1), refer to the references above.

The first step of the algorithm is to define block-Hankel matrices, which are obtained by stacking shifted input and output data. Define

$$
U_{a|b} = \begin{pmatrix}
u_a & u_{a+1} & \cdots & u_{M-b} \\
u_{a+1} & u_{a+2} & \cdots & u_{M-b+1} \\
\vdots & \vdots & \ddots & \vdots \\
u_b & u_{b+1} & \cdots & u_M
\end{pmatrix} \tag{3.10}
$$

where $M < N$ is the last sample of the input-output sequence to be included. Analogously, $Y_{a|b}$ can be defined. By partioning the block-Hankel matrices, we see that

$$
U_{0|2i-1} = \begin{pmatrix} U_{0|i-1} \\ U_{i|2i-1} \end{pmatrix} \overset{\text{def}}{=} \begin{pmatrix} U_p \\ U_f \end{pmatrix} = \begin{pmatrix} U_{0|i} \\ U_{i+1|2i-1} \end{pmatrix} \overset{\text{def}}{=} \begin{pmatrix} U_p^+ \\ U_f^+ \end{pmatrix} \tag{3.11}
$$

Here, the index p denotes past inputs and outputs at time i, and f denotes future inputs and outputs. We introduce the notation X_i for the (unknown) state sequence

$$
X_i = \begin{pmatrix} x_i & x_{i+1} & \cdots x_{M-i} \end{pmatrix} \tag{3.12}
$$

where each column x_k represents the state at time k.

From the system dynamics and the definitions above, the relationship between the inputs, outputs, and states is now given by

$$
\begin{aligned}
Y_p &= \Gamma_i X_p + H_i U_p \\
Y_f &= \Gamma_i X_f + H_i U_f \\
X_f &= A^i X_p + \Delta_i U_p
\end{aligned} \tag{3.13}
$$

where

$$
\Gamma_i = \begin{pmatrix} C \\ CA \\ \vdots \\ CA^{i-1} \end{pmatrix} \tag{3.14}
$$

$$
\Delta_i = \begin{pmatrix} A^{i-1}B & A^{i-2}B & \cdots & AB & B \end{pmatrix} \tag{3.15}
$$

$$H_i = \begin{pmatrix} D & 0 & 0 & \cdots & 0 \\ CB & D & 0 & \cdots & 0 \\ CAB & CB & D & \cdots & 0 \\ \vdots & \vdots & \vdots & \ddots & \vdots \\ CA^{i-2}B & CA^{i-3}B & CA^{i-4}B & \cdots & B \end{pmatrix} \tag{3.16}$$

Here, U_p, U_f, Y_p, Y_f are known, and the other matrices are constrained by the subspaces spanned by the block-Hankel input and output matrices. The unknown matrices can be obtained by first computing oblique projections of the future output onto the past inputs and outputs [van Overschee and de Moor, 1996]

$$\mathcal{O}_i = Y_f /_{U_f} \begin{pmatrix} U_p \\ Y_p \end{pmatrix} \tag{3.17}$$

Through the singular value decomposition of the (possibly weighted) oblique projection

$$W_1 \mathcal{O}_i W_2 = U\Sigma V^T \tag{3.18}$$

we learn the system order n from the number of non-zero singular values in Σ. Let

$$\Sigma_n = \text{diag}(\sigma_1, \sigma_2, \cdots, \sigma_n) \tag{3.19}$$

and let U_n be the first n rows of U. Now, Γ_i can be taken as by

$$\Gamma_i = W_1^{-1} U_n \Sigma_n^{1/2} \tag{3.20}$$

and the state sequence X_i can be obtained from the pseudo-inverse of Γ_i

$$X_i = \Gamma_i^\dagger \mathcal{O}_i \tag{3.21}$$

Finally, the system matrices are obtained from the equation

$$\begin{pmatrix} X_{i+1} \\ Y_{i|i} \end{pmatrix} = \begin{pmatrix} A & B \\ C & D \end{pmatrix} \begin{pmatrix} X_i \\ U_{i|i} \end{pmatrix} \tag{3.22}$$

The extension to multivariable stochastic systems is based on the same principles, but involves more notation, concepts, and details, and was not included here.

Early papers on subspace identification introduce the CVA algorithm [Larimore, 1990], the MOESP algorithm [Verhaegen, 1994], and the N4SID algorithm [van Overschee and de Moor, 1994]. The algorithms have been shown to all be special cases of the algorithm presented above, with different weighting matrices W_1 and W_2.

In the thesis, the `n4sid` implementation of subspace identification in the Matlab System Identification Toolbox [Mathworks, 2008] was used. Despite the name, this implementation makes an automatic choice between the MOESP or the CVA weighting matrices.

Identification based on prediction error   The subspace algorithms are elegant in the sense that they are not iterative, and therefore very efficient for large data sets. To further improve the fit between model and data, iterative methods based on numerical optimization can be used.

The Matlab function `pem` [Mathworks, 2008] starts by an initial model (e.g., obtained through subspace identification) and adjusts the system matrices through numerical optimization to minimize the prediction error of the model. Because this optimization problem is non-convex, there is no guarantee that it will converge to a globally optimal solution, and the computational effort may be significant when the model order is high or the identification data set is large.

Model Validation

To evaluate and compare different data-based models, a common statistic is the coefficient of determination R^2 [Casella and Berger, 2002], defined as

$$R^2 = 1 - \frac{SS_{\text{err}}}{SS_{\text{tot}}} \tag{3.23}$$

where SS_{err} is the sum-of-squares of the model residuals

$$SS_{\text{err}} = \sum_{i=1}^{N} (y_i - \hat{y}_i)^2 \tag{3.24}$$

and SS_{tot} the total sum-of-squares of the sample

$$SS_{\text{tot}} = \sum_{i=1}^{N} (y_i - \bar{y})^2 \tag{3.25}$$

where $\bar{y}$ is the sample mean. For a perfect model, we have $R^2 = 1$.

The statistic R^2 is sometimes denoted VAF (variance accounted for) in the system identification literature [Johansson, 1993], and is normally given as a percentage,

$$\text{VAF} = 100 \cdot R^2 \tag{3.26}$$

The VAF describes the percentage of variance in the data that is explained by the model.

Another metric for model evaluation is the root-mean-square-error (RMSE) given by

$$\text{RMSE} = \sqrt{\frac{1}{N} \sum_{i=1}^{N} (y_i - \hat{y}_i)^2} \tag{3.27}$$

The RMSE has the same unit as the data, and may be interpreted as the standard deviation of the prediction error.

3.3 Multivariable Control

LQG Control

Linear quadratic Gaussian (LQG) control is one of the simplest approaches to optimal control. The LQG controller solves the general optimal control problem from Eq. (1.1) under the rather restrictive assumptions of

- Linear process model.

- Cost function V which is quadratic positive (semi-)definite in u and x.

- Additive white Gaussian noise w.

- No constraints on inputs u, outputs y, or state x.

Let the linear system be given by (3.1) and let the cost function be given by

$$J(\mathcal{U}) = \lim_{N \to \infty} E \left(\frac{1}{N} \sum_{k=0}^{N} x_k^T Q_x x_k + u_k^T Q_u u_k \right) \tag{3.28}$$

It can be shown [Åström and Wittenmark, 1997] that, under mild assumptions, the optimal controller is given by

$$u_k = -L\hat{x}_k \tag{3.29}$$

where $\hat{x}_k$ is the state estimate obtained from an optimal Kalman filter of the same order as the process model, and the optimal feedback gain L is obtained by solving a Riccati equation.

Though restrictive compared to (1.1), the LQG formulation can incorporate some useful features. By extending the state dimension of the process model, it is possible to include a colored noise model, to add integral action to the controller, or to put a quadratic penalty on changes in the control signal Δu in the cost function.

An important property of the infinite-horizon LQG controller 3.28 is that the resulting controller is a linear time-invariant dynamic system. Thus, all optimization can be done off-line, so that the real-time complexity of the controller is very low.

Model Predictive Control

Model predictive control (MPC) is a discrete-time optimal control formulation that has reached widespread industrial use, particularly in the process industry [Maciejowski, 2002].

MPC is based on the idea of receding horizon control. At each sample instant k, the optimal future control sequence,

$$\mathcal{U}^*(k) = \{u(k), u(k+1), \ldots, u(k + H_c - 1)\} \tag{3.30}$$
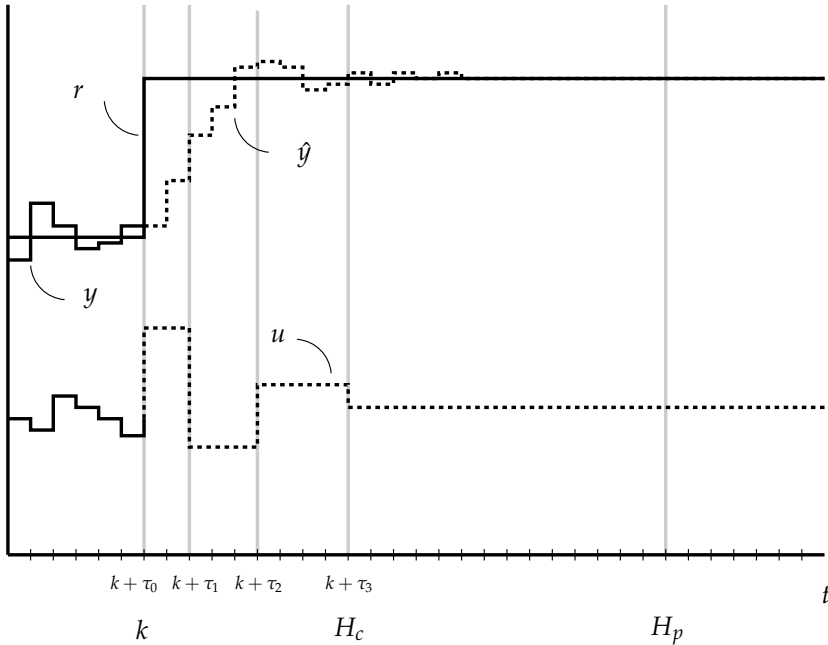

Figure 3.4 Illustration of model predictive control. A cost function is specified in terms of reference tracking of y and rate of change of the control variable u. The future trajectory of u is parameterized by a set of control moves, here $\mathcal{T}_u = \{0, 2, 5, 9\}$, and the cost function is optimized over this trajectory using a Kalman filter to predict $\hat{y}$ for any given control variable trajectory. The first element in the optimal sequence $u(k)$ is applied to the process. At the next sample, a new optimal trajectory is computed.

is considered over a finite horizon H_c. This control sequence is parameterized into a finite number of control moves $\mathcal{T}_u = \{\tau_0, \tau_1, \ldots, \tau_L\}$ where u is kept constant over each interval $\tau_i \leq k < \tau_{i+1}$. This optimization problem is solved, and the first element of the optimal control sequence is applied to the process. At the next sample, the procedure is repeated.

The cost function to be minimized reflects the behavior of the system over a finite prediction horizon H_p

$$J(k) = \sum_{i=1}^{H_p} \mathcal{Y}(k+i|k) + \sum_{i=1}^{H_p} \mathcal{U}(k+i|k) + \rho_\epsilon \epsilon^2 \qquad (3.31)$$

Here, $\mathcal{Y}(k+i|k)$ is the cost associated with the system outputs at time $k+i$ given information available at time k, and $\mathcal{U}(k+i|k)$ is the cost associated with the control variables at time $k+i$ given information available at time k. The cost may be formulated in terms of setpoint tracking of the outputs, target values for the control variables, or penalty on rate changes of the control variables. The prediction horizon H_p is typically longer than the control horizon H_c, and it is assumed that $u(k+i) = u(k+H_c-1)$ for $i \geq H_c$. The scheme is illustrated in Fig. 3.4. Note that the cost function (3.31) is similar to the LQG control cost function (3.28). The difference is that it is restricted to a finite horizon which allows the optimization to be performed on-line with constraints included.

In the most commonly used MPC formulation [Maciejowski, 2002], the cost function and system model is restricted such that the resulting optimization problem can be formulated as a quadratic program (QP). Efficient solvers for QPs exist, so that on-line optimization is feasible [Boyd and Vandenberghe, 2004]. The QP formulation includes

- Linear plant model (3.1) including both measured and unmeasured disturbances.

- Quadratic cost function in u and y.

- Maximum and minimum constraints on control variables u and outputs y.

- Rate constraints on control variables u.

- Soft constraints, i.e., a way to trade off small violations of one or more constraints for a decrease in cost V.

With this formulation, the output cost $\mathcal{Y}(k+i|k)$ in (3.31) is defined as

$$\mathcal{Y}(k+i|k) = \sum_{j=1}^{p} w_j^y (r_j^y(k) - \hat{y}_j(k+i|k))^2 \qquad (3.32)$$

where p is the number of outputs, r_j^y is the setpoint for output y_j, w_j is the weight associated with setpoint tracking of output y_j, and $\hat{y}_j(k+i|k)$ is the prediction of the output y_j at time $k+i$ given measurements up to time k. The prediction may be computed by an optimal Kalman filter [Kalman, 1960].

The control variable cost $\mathcal{U}(k+i|k)$ is defined as

$$\mathcal{U}(k+i|k) = \sum_{j=1}^{m} w_j^u (r_j^u(k) - u_j(k+i|k))^2 + \sum_{j=1}^{m} w_j^{\Delta u} \Delta u_j(k+i|k)^2 \quad (3.33)$$

where m is the number of control variables, r_j^u is the setpoint for output u_j, w_j is the weight associated with keeping u_j at its setpoint, $u(k+i|k)$ are the optimization variables, $\Delta u_j(k+i|k) = u_j(k+i|k) - u_j(k+i-1|k)$ is the rate of change of the control variable, and $w_j^{\Delta u}$ specifies the cost associated with this rate of change.

Upper and lower constraints may be specified for the output y, the control variable u, and the rate of change of the control variable Δu,

$$
\begin{aligned}
y_{\min} - \epsilon \eta_{\min}^y &\leq y(k) \leq y_{\max} + \epsilon \eta_{\max}^y \\
u_{\min} - \epsilon \eta_{\min}^u &\leq u(k) \leq u_{\max} + \epsilon \eta_{\max}^u \\
\Delta u_{\min} - \epsilon \eta_{\min}^{\Delta u} &\leq \Delta u(k) \leq \Delta u_{\max} + \epsilon \eta_{\max}^{\Delta u} \\
0 &\leq \epsilon
\end{aligned}
\quad (3.34)
$$

Here, η are positive vectors that specify the concern for violating each of the constraints. For $\eta = 0$, the corresponding constraint is hard. The optimization variable ϵ is included into the cost function (3.31) and manages the trade-off between violating the constraints and minimizing the output and control variable cost.

Mid-Ranging Control

Mid-ranging control is a control structure that is useful for processes with two control variables and only one process variable to control [Allison and Isaksson, 1998]. The key idea is to combine a fast, accurate control variable that has a small operating range with a slow, less accurate control variable to extend the operating range. Mid-ranging control was introduced in process control for the problem of controlling a flow using a small, fast, and accurate valve, and a large slower valve [Allison and Isaksson, 1998]. Later, it has been applied in different contexts where a combination of two control variables with different dynamic properties are used to control a single process variable [Haugwitz et al., 2005; Solyom and Eriksson, 2006].
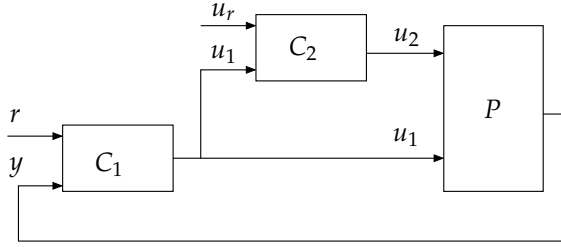
Figure 3.5   The basic mid-ranging control structure.

The structure of a basic mid-ranging controller is shown in Fig. 3.5. In a first controller C_1, the fast input u_1 is used to control the process output y to its setpoint r. A second controller C_2 controls u_1 to a sepoint u_r. The setup ensures fast and accurate control of y through u_1, and prevents u_1 from loosing control authority through saturation by adjusting u_2. The controllers C_1 and C_2 should be tuned according to the dynamics of the corresponding control variables u_1 and u_2, which typically means that C_2 should have a lower bandwidth than C_1.

In principle, any type of controller could be used for C_1 and C_2. The most straight-forward choice would be PID controllers due to their ease of implementation and wide-spread use in industry. In [Allison and Isaksson, 1998], the mid-ranging control structure with PID controllers is compared to model predictive control (MPC). The desired mid-ranging effect can be obtained by a suitably defined optimization criterion for the MPC controller. MPC has the advantage of handling constraints explicitly , but the disadvantage of greater complexity in terms of implementation and on-line computation.

4

Experimental Setup

4.1 The Volvo D12 and Volvo D13 Engines

All experiments were performed in the combustion engine research lab at Lund University. Two similar six-cylinder Volvo heavy-duty engines were used during the course of the project. Both engines were originally standard production engines, but adaptations were made both in hardware and instrumentation to conform to the project's research objectives. Engine specifications are given in Table 4.1.

The first engine, a Volvo D12 engine shown in Fig. 4.1, was previously used for heavy-duty HCCI research [Strandh, 2006; Bengtsson, 2004]. The compression ratio was $r_c = 18.5$ at the early stage of the project, and was later reduced to $r_c = 14.1$ by exchanging the pistons in order to facilitate low-temperature combustion.

The second engine, a Volvo D13 engine, replaced the D12 engine in the final year of the project.

4.2 Instrumentation

Most of the instrumentation was the same in both the D12 and the D13 engines.

Actuation

Port fuel injection Part of the experiments presented in the thesis used port fuel injection, or a combination of port fuel injection and direct injection. Two injectors were mounted upstream the inlet port of each cylinder. The injectors
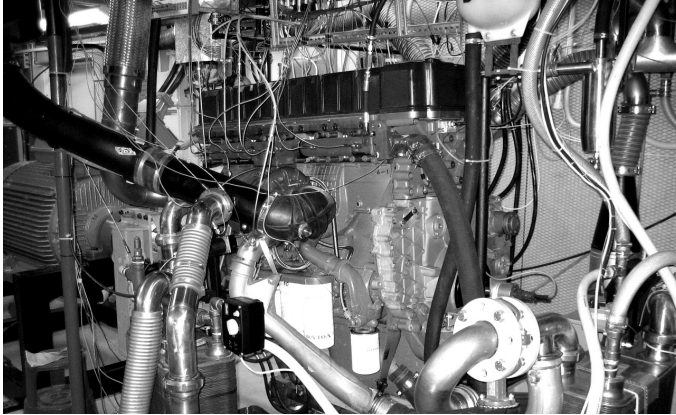
Figure 4.1   Volvo D12 engine.

were standard production-type SAAB gasoline injectors. One set of injectors were used for ethanol, and the other for n-heptane. The injectors opened once every engine cycle, and the amount of fuel injected was controlled by varying the injection duration. The twelve injectors were controlled from the computer using fiber-optic cables to one PIC (peripheral interface controller) processor for each injector.

Direct fuel injection   Delphi E3 unit injectors were used for direct injection. Only one injection event for each cylinder and cycle was possible. A modified ECU interface allowed start of injection, injection duration, and fuel injection pressure to be set from the computer using CAN communication.

Table 4.1   Engine specifications for the Volvo D12 and D13 engines.

	D12	D13
Operated cylinders	6	6
Total displaced volume	12.2 dm^3	13 dm^3
Bore	131 mm	131 mm
Stroke	150 mm	158 mm
Connecting rod length	260 mm	267.6 mm
Valves per cylinder	4	4
Compression ratio	18.5 and 14.1	16

Gas flow management   Both engines were equipped with a long-route (low-pressure) EGR system, and a variable geometry turbo-charger (VGT). Two valves, the EGR and the EBP valves, were used to control the EGR rate in the engine, see Fig. 4.2. Servo motors from JVL Industri Elektronik A/S of type MAC 140-A1 were used to actuate the valves. The servo motors were controlled from the computer using serial communication.

The Volvo D12 engine was equipped with a prototype VGT from Holset, designed for the large flows necessary in high-load HCCI operation. The VGT vanes were actuated using the same type of servo motor as the EGR and the EBP valves.

The Volvo D13 engine was equipped with the standard production-type turbocharger, where the actuator was controlled using a CAN interface to the main computer.

Variable valve actuation   The Volvo D12 engine was equipped with a a commercial research-type electro-hydraulic variable valve actuation (VVA) system. The system was driven by the cam shaft and allowed for valve closings ahead of the cam curve, a so-called *lost motion system*. A hydraulic cylinder was used to move the inlet valve. Oil was transferred to this cylinder from another hydraulic cylinder either by an electronically controlled valve or by the cam shaft pushing on the second cylinder. Hence, valve closings ahead of the cam curve, but not after was possible. PIC processors were used, analogously to the port fuel injection system. Only inlet valve closing (IVC) actuation was used in the experiments, the other valve timings were fixed.

The Volvo D13 engine was not equipped with the variable valve actuation system.

Inlet air heating   A Leister Typ 40'000 electrical air heater with a capacity of 35 kW was used to control the temperature of the inlet air in the HCCI experiments on the Volvo D12 engine. A PI controller was used to set the heater power from an inlet temperature setpoint and the measured inlet temperature.

The inlet air heater was only used in the port-fuel injection experiments. When inlet air heating was not needed, two valves were manually shifted such that air instead passed through an intercooler.

Engine speed control   The engine speed was governed by an ABB M2BA 355 electrical motor with a rated power of 355 kW. The reference speed was adjusted manually, which meant that fast, preprogrammed changes of speed were not possible.

Sensing

A schematic drawing of the engine with sensor locations marked out is found in Fig. 4.2.

Synchronization of sampling   Crank angle based sampling was enabled through a Leine & Linde encoder attached to the engine crankshaft. The encoder emits 5 pulses every crank angle degree that trigger sampling of cylinder pressure with a resolution of 0.2 CAD. Synchronization with engine events was performed through an optical cam shaft sensor.

In-cylinder pressure sensors   Piezo-electrical, water-cooled pressure transducers of type Kistler 7061B were used to measure the cylinder pressure. The transducers had a calibrated pressure range of 0–250 bar.

Fuel pressure sensor   Diesel injection pressure was measured for Cylinder 1 with a resolution of 0.2 CAD. The sensor was a strain gauge mounted on the rocker arm.

Pressure and temperature monitoring   Pressures and temperatures were measured at various locations outside of the cylinders. These sensors were mostly used for monitoring and steady-state calibration.

Pressure transducers for measuring pressure outside the cylinder were used for

- pressure after compressor
- inlet manifold pressure
- outlet pressure for cylinders 1,2,3
- outlet pressure for cylinders 4,5,6
- pressure after turbine
- oil pressure
- fuel pressure for port-injected fuels
- diesel pressure

The sensors were of type Keller PAA-21S, and had measurement ranges of either 0–5 bar or 0–10 bar.

Temperature sensors were used for

- temperature after compressor
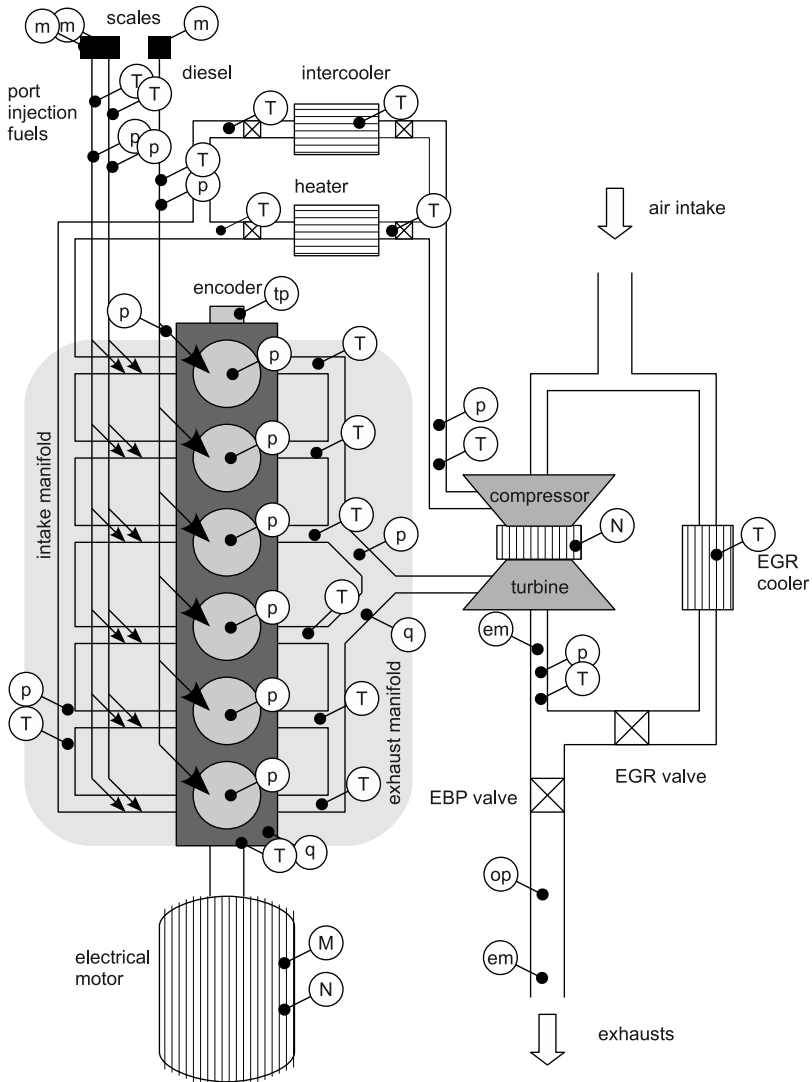- temperature before heater

Figure 4.2   Schematic drawing of laboratory engine configuration with sensor locations. The scale is not correct. Sensor abbreviations: tp = trigger pulses, p = pressure, T = temperature, M = torque, N = rotational speed, m = mass, em = emissions, op = opacity.

- intercooler temperature

- temperature after intercooler

- temperature after heater

- inlet manifold temperature

- individual exhaust temperatures from the six cylinders

- temperature after turbine

- EGR cooler temperature

- temperature after EGR cooler

- cooling water temperature

- oil temperature

- fuel temperature for port-injected fuels

- diesel temperature

Thermocouples of type K from Pentronic were used as temperature sensors.

Torque sensor   A force sensor integrated in the electrical motor was used to estimate engine torque.

Rotational Speed Sensing   Engine speed was obtained both through the internal speed measurement of the electrical motor (slow and accurate), and by from the engine crank shaft high-resolution encoder (fast but noisy).

An optical sensor was used to measure the rotational frequency of the turbocharger shaft.

Fuel Flow   Fuel flow was computed from measurements from fuel scales. An AVL 7131-09E fuel balance was used for diesel weight measurements, and Sartorius BP8100 scales for measurements of the port injected fuels.

Fast NO$_x$ / lambda sensor   A Siemens VDO/NGK Smart NOx sensor was used for measuring NO$_x$ concentration and λ in the exhausts.

Opacimeter   Soot was measured using an opacimeter from SwRI.

Exhaust emissions analysis   The emission measurement equipment for CO, CO_2, O_2, hydrocarbon and high-precision NO_x had a long response time, and was only appropriate for steady-state evaluation.

In the first years of the project, emissions measurement instrumentation compiled by Boo Instrument AB was used. Hydrocarbons were measured using a flame ionization detector from JUM Engineering. NO_x concentration were measured using a chemiluminescence detector from Eco Physics. CO and CO_2 were measured using a non-dispersive infrared detector, and oxygen concentration was measured using an oxygen paramagnetic attraction device, both from SICK-MAIHAK.

In the last part of the project, a Horiba Mexa 9200 system was used to measure exhaust emissions.

4.3 Control System Architecture

The control system, dapmeas, was originally developed by P. Strandh for his thesis work [Strandh, 2006]. Within the scope of the present thesis, the system was substantially extended by adding new features and improving the user interaction. The system has grown into a rather capable tool for multi-cylinder engine research, particularly it handles cycle-to-cycle cylinder-individual feedback control very well. Today the system is built from a few thousand lines of codes.

Hardware

The main program runs on a standard Linux PC with a 2.4 GHz Pentium 4 processor. The interface between the computer and the engine is illustrated in Fig. 4.3.

A Microstar DAP 5400a/627 PCI data acquisition board was used for the high-frequency sampling. The board has 16 analog input channels with eight 1.25 MHz AD-converters with 14 bits resolution, and was used for cylinder pressures and fast sampling of engine speed, inlet temperature, inlet pressure, and opacity. Sampling was triggered by pulses from the crank shaft encoder, yielding 5 samples per crank angle degree. Data was transferred to the main program in batches, six times per engine cycle.

A National Instruments NI6014 PCI card was used to actuate the voltage level for the electrical air heater through an analog output.

A PCIcanX II card from Kvaser was used for communication with the diesel injectors through the engine ECU, with the Siemens NGK Smart NOx sensors, and with the VGT actuator on the Volvo D13 engine.

The variable valve actuators and port fuel injectors were actuated through fiber optic cables from peripheral interface controllers (PIC) that received timing
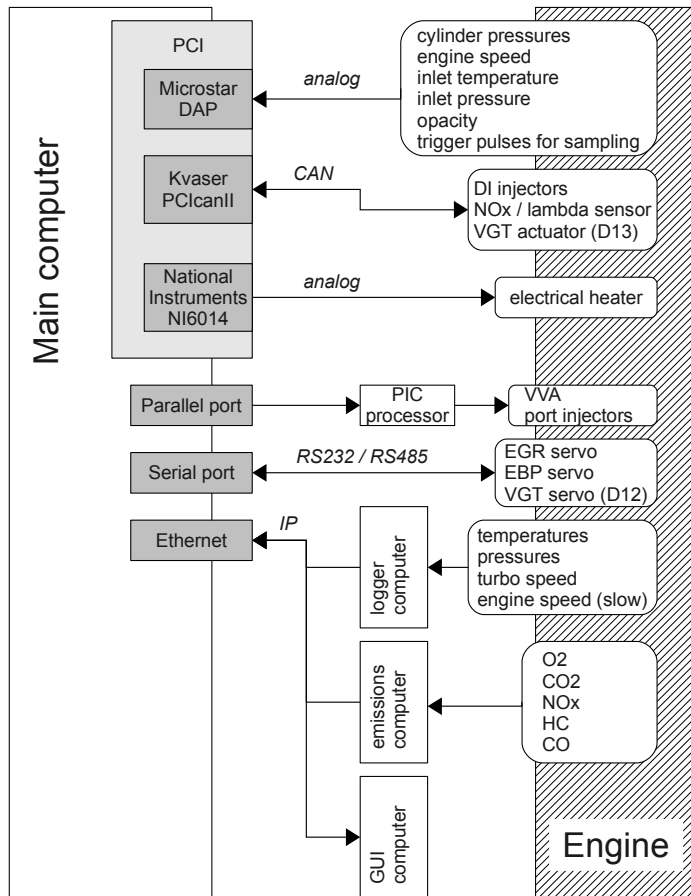
PCI

Microstar
DAP

analog

cylinder pressures
engine speed
inlet temperature
inlet pressure
opacity
trigger pulses for sampling

Kvaser
PCIcanII

CAN

DI injectors
NOx / lambda sensor
VGT actuator (D13)

National
Instruments
NI6014

analog

electrical heater

Main computer

Parallel port

PIC
processor

VVA
port injectors

Serial port

RS232 / RS485

EGR servo
EBP servo
VGT servo (D12)

Ethernet

IP

logger computer

temperatures
pressures
turbo speed
engine speed (slow)

emissions computer

O2
CO2
NOx
HC
CO

GUI computer

Engine

Figure 4.3   The interface between the main computer and the engine.

settings from the main computer through the parallel port.

Communication with electrical servos used for EGR, EBP, and VGT actu-
ation were handled through the serial port of the main computer. To reduce
the influence of noise, a RS232 to RS485 converter was installed after the serial
port.

A HP 2852A data logger was used to sample temperatures, pressures, fuel
scale weights, engine torque, and turbo and engine speed with a frequency of

0.4 Hz. The logger was connected to a second computer and communicated with the main computer over ethernet.

A separate computer was used for managing the emission measurement systems, and transferred data to the main computer through ethernet.

In the later part of the project, another separate computer was introduced to run the user interface, again communicating with the main computer through ethernet.

Software

The control system was developed in C/C++ and is responsible for handling communication with sensors and actuators, processing data, logging data, interacting with the graphical user interface and controllers. Feedback controllers and the graphical user interface were executed as separate programs.

Feedback controllers were designed using Matlab / Simulink, and converted to C-code using the automatic code generation tool Real-Time Workshop. The C-code was compiled into executable programs that communicated with the main program through named pipes.

The graphical user interface was designed using the tool glade which automatically generates codes for the visual elements in the interface. The back-end application was written in C++ in the early version, and was later transferred to Python. A screenshot of the user interace is shown in Fig. 4.4.
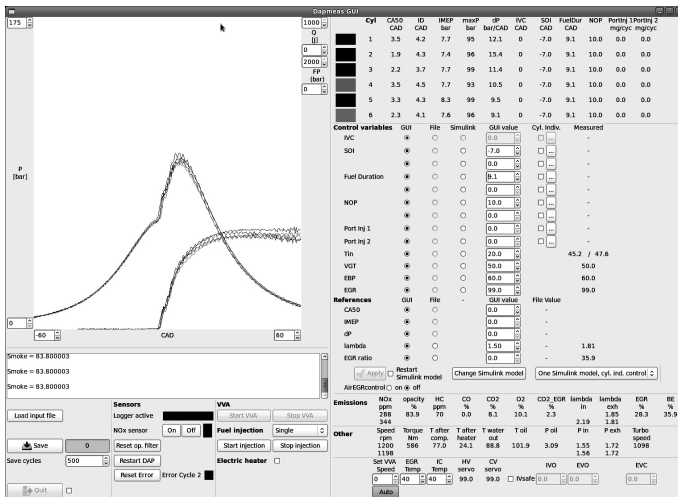

Figure 4.4   The graphical user interface.

Heat-Release Computation

Heat-release analysis was integrated in the control system, and performed in real-time. A standard procedure was used to compute the heat-release and associated parameters such as combustion phasing. The steps of the algorithm (described in detail below) were

- Estimating the pressure sensor offset
- Computing the heat-release rate
- Computing and storing key combustion parameters from the pressure signal and the heat-release rate

Pressure sensor offset   Piezo-electrical pressure sensor have significant steady-state drift, implying that the measured cylinder pressure p_m is perturbed by an offset Δp from the true pressure p

$$p_m = p + \Delta p \qquad (4.1)$$

Different methods of estimating the offset Δp have been suggested, see [Tunestål, 2009] and references therein. The method used in the thesis is based on the assumption of isentropic compression during the compression stroke,

$$pV^\kappa = C \qquad (4.2)$$

where V is the cylinder volume, κ is the polytropic exponent which is determined by γ (ratio of specific heats) and heat transfer losses, and C is an unknown constant. Combining (4.1) and (4.2), a linear model for the unknown parameters Δp and C is obtained

$$p_m = \begin{pmatrix} 1 & V^{-\kappa} \end{pmatrix} \theta \qquad (4.3)$$

where

$$\theta = \begin{pmatrix} \Delta p \\ C \end{pmatrix} \qquad (4.4)$$

The offset Δp was estimated using a least-squares fit from the measured pressure and known volume in a crank angle range during the compression stroke before injection.

Heat-release rate   The heat released dQ was computed according to the commonly used model for apparent heat release with a fixed γ [Heywood, 1988]

$$dQ = \frac{\gamma}{\gamma - 1} p\, dV + \frac{1}{\gamma - 1} V\, dp \qquad (4.5)$$

The differentials are taken with respect to crank angle. In the ideal case with no heat transfer, the polytropic exponent γ is given by the ratio of specific heats

$$\gamma = \frac{c_p}{c_v} \tag{4.6}$$

A detailed heat-release analysis would include a model for heat transfer to and from cylinder walls, and temperature-dependent γ [Gatowski et al., 1984; Heywood, 1988]. Such a model requires additional calibration constants, and often the simple model (4.5) of apparent rate of heat release with a fixed γ is used. Heat transfer can to some extent be accounted for by selecting an adjusted polytropic exponent $\kappa < \gamma$.

Tunestål [2009] presents a method where the pressure sensor offset Δp and the polytropic exponent κ are estimated jointly before and after combustion in each cycle. For analysis during combustion, interpolated values are used. This method was used for the work presented in Chapter 5. For the rest of the thesis, a fixed value of $\kappa = 1.3$ was used.

Fig. 4.5 shows the measured pressure at one cycle and one cylinder in the upper plot. The lower plots show the cumulative heat released, and the instantaneous heat release rate computed from (4.5), respectively. The instantaneous heat release rate $dQ/d\alpha$ is generally heavily corrupted by noise if computed directly from (4.5). Heat release rates that are shown in this thesis are therefore low-pass filtered using a Hamming window [Hamming, 1998] of width ± 1 CAD, see the lower plot in Fig. 4.5.

Combustion parameters   From the pressure trace and the heat release rate, important parameters of the combustion process were computed.

The maximum pressure derivative d_p, an important indicator of audible noise from the engine, was computed as

$$d_p = \max_\alpha \frac{dp}{d\alpha} \tag{4.7}$$

The parameters α_{10} and α_{50}, representing crank angle degrees of 10% and 50% fuel burnt were computed from the heat release rate. In general, α_x is defined by

$$100 \cdot \frac{Q(\alpha_x)}{\max_\alpha Q(\alpha)} = x \tag{4.8}$$

The ignition delay was defined as

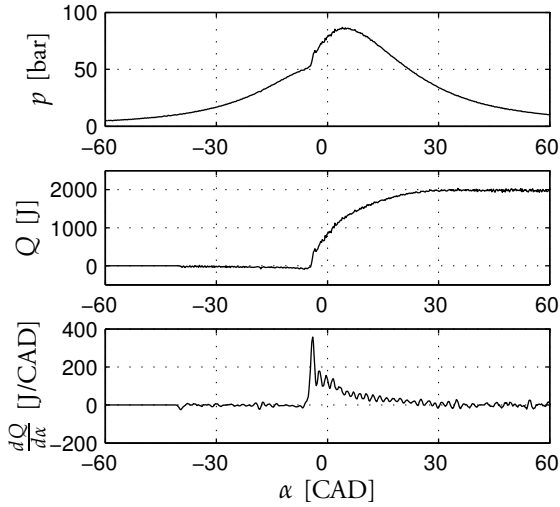$$\alpha_{\mathrm{ID}} = \alpha_{10} - u_{\mathrm{SOI}} \tag{4.9}$$

Figure 4.5 Cylinder pressure measurement for one cycle (top), cumulative heat released (middle), and low-pass filtered instantaneous heat release rate (bottom).

where u_{SOI} is the start-of-injection crank angle degree.

The net indicated mean effective pressure IMEP_n is defined as

$$\mathrm{IMEP}_n = \frac{1}{V_D} \int p \, dV \tag{4.10}$$

where the integral is computed over an entire engine cycle. IMEP_n is a commonly used measure of work produced during an engine cycle, normalized by the displaced volume.

5

Virtual Emissions Sensing

Target variables for engine control ζ, such as emissions, are often not measured on-line. Feedback is instead based on measured variables y such as air mass flow $\dot{m}_{\text{air}}$ and inlet manifold pressure p_{in}. Availability of low-cost, durable sensors determine the choice of feedback variables. As described in Chapter 2, the calibration task of determining optimal setpoints y^{ref} for the measured variables, and the control design task of designing a controller to let y track y^{ref} are normally separated. This separation is used both for production engine control design, and in a large number of research papers, as presented in Chapter 2.

A few concerns can be raised regarding this setup. For this discussion, let

$$y = \begin{pmatrix} \dot{m}_{\text{air}} \\ p_{\text{in}} \end{pmatrix} \tag{5.1}$$

$$\zeta = \begin{pmatrix} \chi_{\text{NOx}} \\ X_{\text{op}} \end{pmatrix} \tag{5.2}$$

The measured feedback variables y, and target variables ζ are related through a series of physical processes, illustrated in Fig. 5.1. This path consists of phenomena that are notoriously hard to model: combustion, volumetric efficiency, and mass flow sensor drift. Modeling errors in the path may arise, either from incorrect or incomplete original calibration, or from equipment that deteriorates
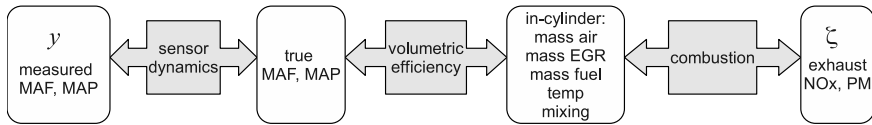

Figure 5.1 Illustration of the processes that relate exhaust emissions ζ to commonly used measured feedback variables $\dot{m}_{\text{air}}$ (MAF) and p_{in} (MAP).

with time. If the setpoints y^{ref} that optimize ζ are calibrated in steady-state, performance may be lost in transients. Performance metrics is another issue. A standard optimization criterion for tuning the controller for y, such as quadratic cost for $e = y^{\mathrm{ref}} - y$, may not transfer well to the target variable coordinates ζ due to the nonlinear relation between y and ζ. Also, there is no cylinder-individual feedback even though cylinder-individual fuel actuation is possible. This implies that the actuator system is not optimally used.

Cylinder-pressure feedback is one option of moving the feedback variables y closer to the target variables ζ, providing detailed information on the in-cylinder process on a cylinder-individual, cycle-to-cycle basis.

The idea of using cylinder pressure to predict other engine outputs such as emissions has been exploited in many contexts before, both using empirical data-based models, and physical models. For example, Seykens et al. [2009] proposed a physical model for predicting NO_x and soot where cylinder pressure was used as one out of several inputs. Wilhelmsson et al. [2009] proposed a physical two-zone model for NO_x prediction based on cylinder pressure data. Traver et al. [1999] defined a set of physical quantities extracted from the cylinder pressure trace (such as ignition delay, combustion duration, peak pressure) and trained a neural network to predict HC, CO, CO_2 and NO_x emissions from these physical quantities. Çebi et al. [2011] also used a set of physical quantities extracted from the cylinder pressure trace, and a parametric empirical model to predict PM emissions.

A common issue in all approaches that use crank-angle-resolved sensor data for control is to find smart ways to reduce the dimensionality of the data. Cylinder pressure sensors typically operate at a resolution in the order of 0.1– 0.2 CAD, thus providing a large amount of data that cannot directly be used for feedback control. In order to use the data for control and diagnostics, the dimension of the data needs to be reduced.

Two approaches to relate cylinder pressure data to emissions for feedback control are presented in this chapter. The first part of this chapter presents a method published in [Karlsson et al., 2008], where a performance metric for NO_x and PM emissions is transformed into a quadratic cost function in α_{50} and α_{ID}. The second part of the chapter presents a more systematic approach to finding a reduced-dimension set of variables from the cylinder pressure trace that can be used to predict emissions, published in [Henningsson et al., 2012a; Henningsson et al., 2012b].

5.1 A Heuristic Approach

For low-load low-temperature diesel combustion, the main actuator variables are injection timing u_{SOI}, and EBP valve position u_{EBP}. The VGT should be kept fully open since there is enough air available without boosting, and extra boosting will reduce the efficiency and increase NO_x emissions. The target operating points are determined by an acceptable trade-off between emissions, efficiency, and audible noise. Control of emissions becomes more important at these low loads because the exhaust temperatures may be too low for the after-treatment systems to operate efficiently.

This type of combustion was studied in the D12 engine. Figure 5.2 shows steady-state NO_x, opacity, brake efficiency, and maximum pressure derivative d_p at a grid of operating points defined by start of injection u_{SOI} and χ_{EGR}, the ratio of CO_2 concentration in the intake to the CO_2 concentration in the exhausts. It can be concluded from these maps that the four variables are sensitive to both u_{SOI} and χ_{EGR}, and that the different performance variables are conflicting.

We now wish to characterize the trade-off between different variables in Fig. 5.2 in terms of feedback variables computed from the cylinder pressure data. The feedback variables should be chosen such that there are robust and invertible transformations from emissions to feedback variables, and from feedback variables to actuator variables. This means that the feedback variables need to be fairly orthogonal as u_{SOI} and χ_{EGR} are varied.

By trial-and-error it was found that the combustion phasing α_{50} and the ignition delay α_{ID} fulfill this property. Figure 5.3 shows α_{50} and α_{ID} mapped according to u_{SOI} and χ_{EGR}.

Figure 5.4 illustrate how these variables may be used for feedback. The figure shows emissions of NO_x and PM mapped according to α_{50} and α_{ID}, and a weighted sum of the emissions that could be used as a cost function for emission control. Note that the cost is heavily skewed in terms of feedback variables; deviations in some directions have a much larger influence than others. The figure suggests that a quadratic cost function in α_{50} and α_{ID} with a non-diagonal quadratic term could provide a good performance metric for a controller aimed at managing the NO_x-PM trade-off. Level curves for such a cost function are shown in the figure, and control design based on this quadratic function will be presented in Chapter 7.
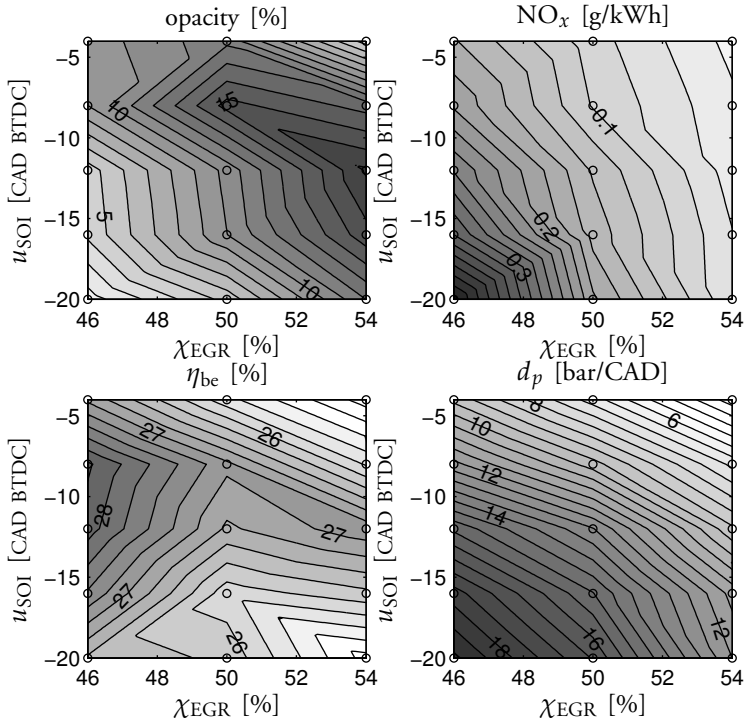
Figure 5.2 Emissions of NO_x and soot, brake efficiency η_{be}, and pressure derivatives d_p mapped according to u_{SOI} and χ_{EGR} in steady-state operation. Circles represent measurement points, intermediate values are obtained by linear interpolation. All data was collected at $IMEP_n$ = 4 bar and N_{engine} = 1200 rpm.

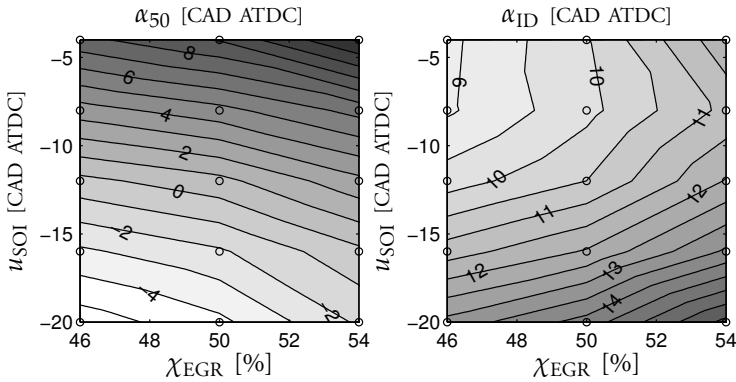**Figure 5.3** Feedback variables α_{50} and α_{ID} mapped according to u_{SOI} and χ_{EGR} for steady-state operation.
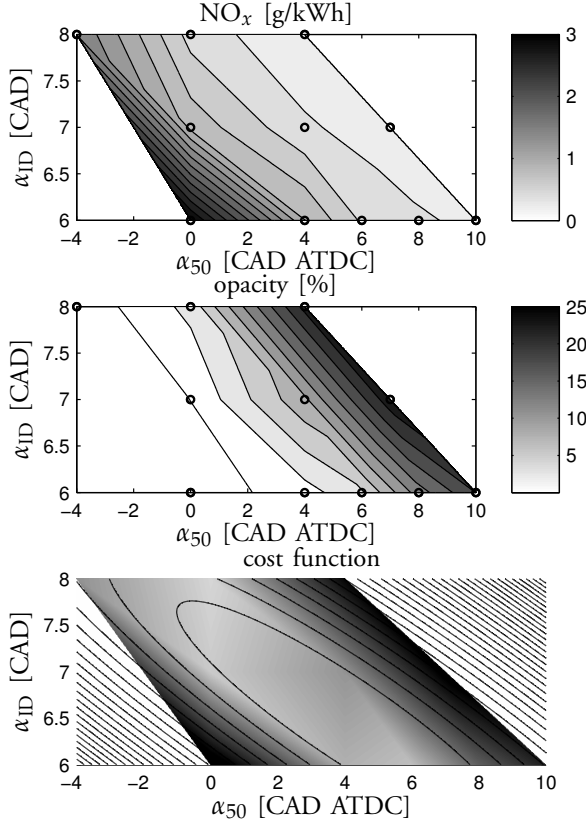
Figure 5.4   Upper two plots: Emissions of NO_x and soot mapped according to α_{50} and α_{ID} in steady-state operation. Circles represent measurement points, intermediate values are obtained by interpolation. Lower plot: Weighted sum of emissions and level contours of cost function to be minimized. Note that these data were collected at a different load than the data in Fig. 5.2. The levels of emissions are therefore different, but the NO_x-soot trade-off shows the same characteristics.

5.2   A Data-Mining Approach

In the previous section, α_{50} and α_{ID} were shown to provide good predictors of NO_x and PM at a fixed operating point. Much of the work on exploiting cylinder pressure information p_{cyl} for feedback or for prediction of target variables ζ take a similar approach, focusing on a few parameters q with physical interpretation that are related to the cylinder pressure p_{cyl} or the heat release rate dQ. This scheme is illustrated in Fig. 5.5. Such parameters include the combustion
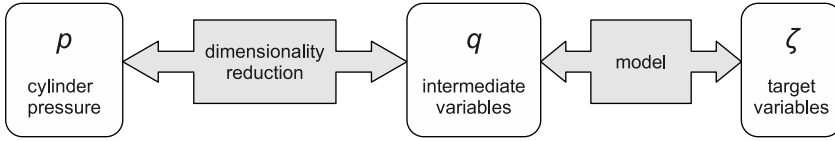
Figure 5.5   Illustration of common setup to predict target variables ζ such as emissions from cylinder pressure data. A common choice for intermediate variables q are physical quantities such as combustion phasing, ignition delay, or maximum pressure derivative.

phasing α_{50}, the indicated mean effective pressure IMEP, the crank angle degree of peak pressure α_{PP}, the maximum pressure derivative d_p, the ignition delay α_{ID}, etc.

However, such choice of feedback variables is somewhat heuristic since a large number of different quantities can be defined, many of which may be redundant. In the previous section, α_{50} and α_{ID} were chosen for q as they were shown to be 'fairly' orthogonal as the two actuator variables varied. Other choices of q could have been possible, such as α_{10} or α_{PP}. A trial-and-error process was needed to select an appropriate subset q of possible physical quantities.

In this section, an alternative approach is taken. Instead of physical insights, it focuses on the statistical properties of a set of experimental cylinder pressure observerations collected over a large operating range. The intermediate variables q are obtained by principal component analysis of the data set, which means that q captures the directions of the largest variability within the experimental training data.

We will distinguish between five different sets of variables:

- *Cylinder pressure p_{cyl}*: The measured pressure, high-dimensional data.

- *Reduced-dimension cylinder pressure representation w*: Reduced-dimension representation of p_{cyl}.

- *Input to nonlinear model q*: w combined with other measured engine variables v such as engine speed, injection timing, etc.

- *Target variables ζ*: The target variables for prediction, i.e., the cylinder-individual instantaneous cylinder-out emissions (not available for measurement).

- *Measured variables y*: The measured emissions used for inference of model parameters. These differ from ζ in that they are averaged over cylinders and corrupted by the dynamics in the exhaust manifold and the sensors.
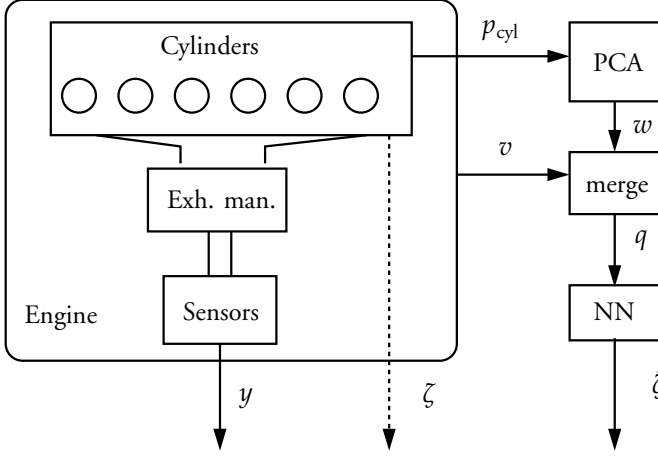
Figure 5.6   Overview of information flow: ζ are the true cylinder-out emissions (not measurable), y is the output from physical emissions sensors, and $\hat{\zeta}$ is the output of the cylinder-pressure based virtual sensor.

The relationship between the variables is illustrated in Fig. 5.6.

For the model step in Fig. 5.5, a neural network is introduced. The method will be evaluated for prediction of emissions,

$$\zeta = \begin{pmatrix} \lambda \\ \chi_{\text{NOx}} \\ X_{\text{op}} \end{pmatrix} \tag{5.3}$$

Dimensionality Reduction through PCA

Principal component analysis (PCA) is a method for dimensionality reduction of large data sets [Pearson, 1901; Hotelling, 1933; Bishop, 2006]. The key idea is to project the data observations on a subset that represents the maximal variability within the data set.

Method   Let $x \in \mathbb{R}^P$ be a high-dimensional, zero-mean stochastic variable. Let $\{x\}_{n=1}^N$ be a set of observations of x. We wish to approximate each x_n by a linear combination of a set of basis vectors, known as principal components,

$\{\phi\}_{l=1}^{L}$, where $L < P$,

$$x_n = \sum_{l=1}^{L} w_{ln}\phi_l + e_n = \Phi w_n + e_n \qquad (5.4)$$

such that the errors $\{e\}_{n=1}^{N}$ are minimized. The principal components algorithm finds an orthonormal matrix $\Phi \in \mathbb{R}^{P \times L}$ of basis vectors, and the weights w_n for each of the observations x_n by solving the optimization problem

$$\min_{\Phi, \{w_n\}} \sum_{n=1}^{N} ||x_n - \Phi w_n||^2 \qquad (5.5)$$

Now, let $x = p_{cyl} - \bar{p}_{cyl}$, where $\bar{p}_{cyl}$ is the average cylinder pressure over the entire set of observations. Only the crank angle range of the cylinder pressure that is of interest for combustion diagnosis needs to be included. Here, the range (-30,40) CAD after top dead center was chosen, which gives $P = 350$ with a sampling interval of 0.2 CAD.

We now assume that any cylinder pressure curve p_{cyl} can be well approximated by a weighted sum of the principal components, which means that the dimensionality of an observation is reduced from $x_n \in \mathbb{R}^P$ to $w_n \in \mathbb{R}^L$. The set of principal components $\{\phi_l\}$ are only computed once, off-line. To use the scheme for real-time dimensionality reduction, the weights w_n for each new observation x_n are obtained by a straight-forward matrix multiplication according to

$$w_n = \Phi^T x_n \qquad (5.6)$$

since, by construction, the columns of Φ are orthonormal vectors.

Results A random set of experimental cylinder pressure data, consisting of $N = 9,000$ observations was chosen. This set contained data from all six cylinders for experiments at different operating points in terms of load, speed, EGR rate, inlet pressure, and injection timings. Figure 5.7 shows the cylinder pressure from 50 random cycles to illustrate the variability within the data.

The cylinder pressure principal components were found using the Python package PCA Module [Risvik, 2008]. This software contains an implementation of the NIPALS algorithm [Geladi and Kowalski, 1986], which allows the principal components to be computed one at a time. Figure 5.8 shows the first 12 principal components $\{\phi_l\}_{l=1}^{12}$, normalized to have a square norm of one.

Figure 5.9 shows the measured cylinder pressure from one cycle along with the approximated cylinder pressure using a finite number l of principal components. The approximation is very good using only a few components, and the contribution from $l > 7$ is almost invisible.
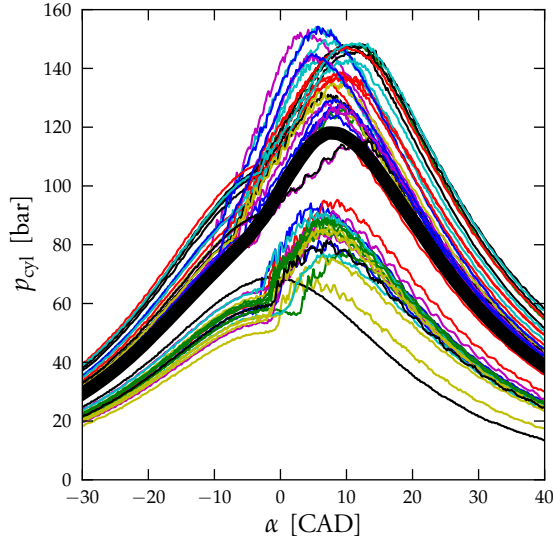
Figure 5.7   50 random observations of cylinder pressure taken from the experimental data set. The thick black line is the average of all observations in the data set.

L	0	1	2	3	4	5
error (%)	100.0	6.96	1.64	0.53	0.23	0.19

L	6	7	8	9	10
error (%)	0.15	0.13	0.11	0.10	0.10

Table 5.1   Norm of approximation error e as a function of the number of principal components L.

Table 5.1 shows the norm of the error e in (5.4) as a function of the number of components L. The first component explains 93% of the variance in the data set, the second component explains 5%, etc.

To conclude, the effect of different operating conditions on the cylinder pressure p_{cyl} can be compactly coded by the principal component coefficients w.
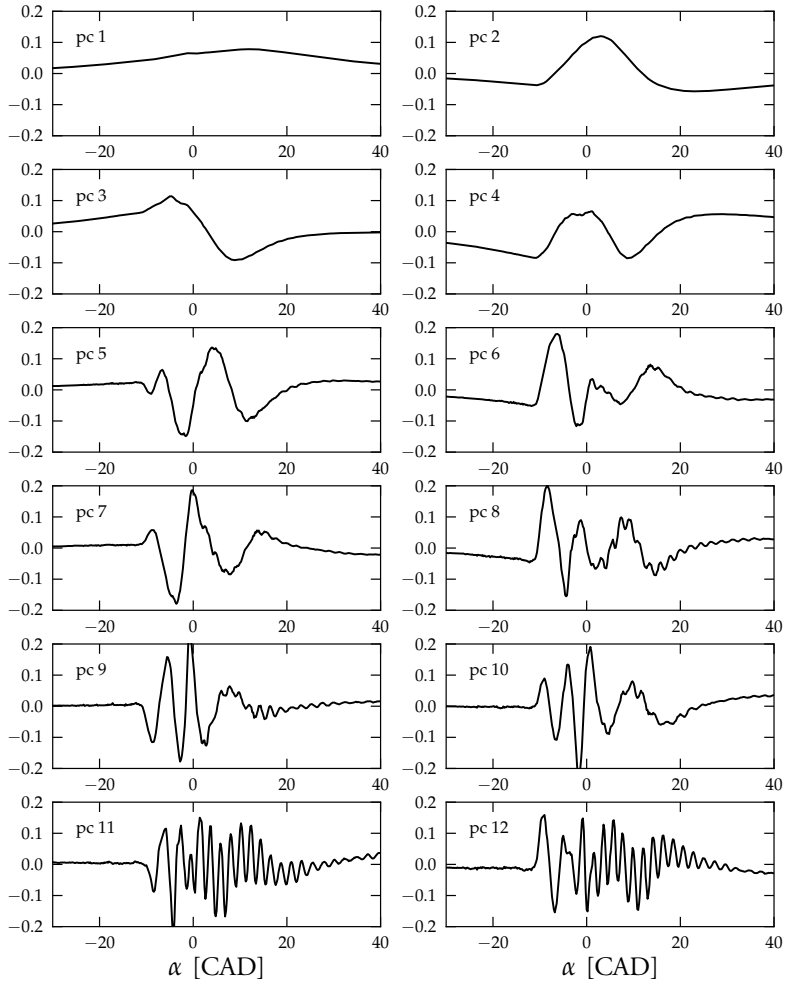
Figure 5.8 The first 12 principal components from the cylinder pressure data set.
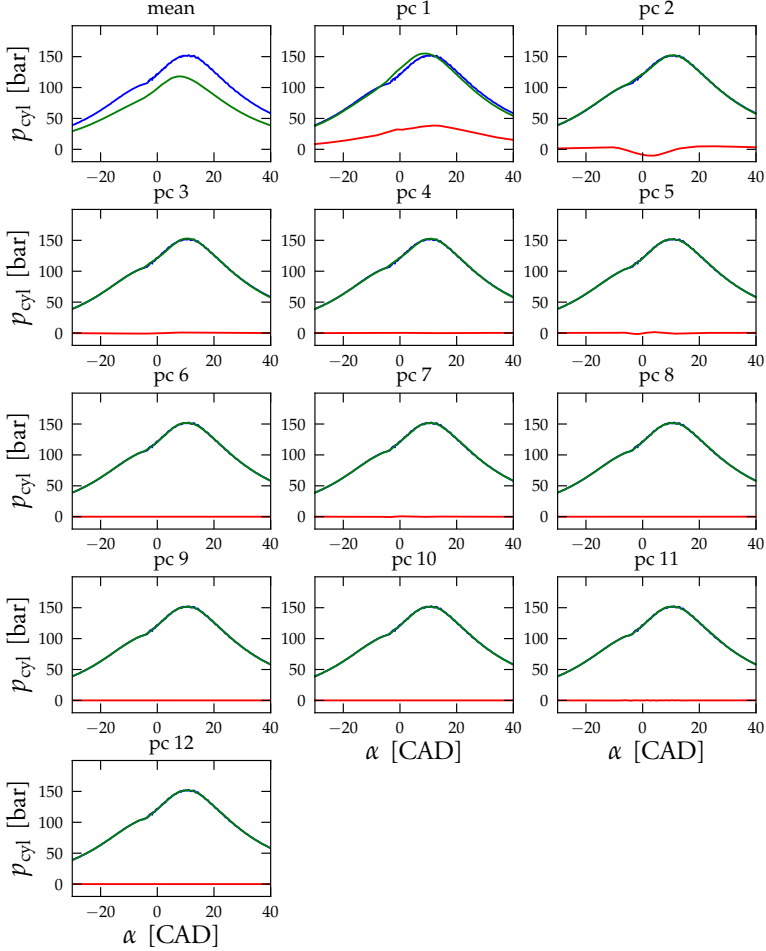
Figure 5.9 Measured pressure from one cycle (blue), approximation using l principal components (green), and the contribution from the lth principal component (red). The upper left plot shows the mean of all cylinder pressures in the PCA training data set.

Neural Network Emissions Model

We now address the second step in Fig. 5.5, predicting the target variable ζ from reduced set of variables q. We assume that q is available for each cylinder individually, but that the training data only provide the average ζ over the cylinders. We wish to train a neural network model $f_{\mathrm{NN}}(q_c, \theta)$ that predicts the the individual cylinder variables ζ_c by assuming that the network parameters θ are common to all cylinders,

$$\zeta = \frac{1}{C} \sum_{c=1}^{C} \zeta_c = \frac{1}{C} \sum_{c=1}^{C} f_{\mathrm{NN}}(q_c, \theta) \qquad (5.7)$$

The model is illustrated in Fig. 5.10.

Define:

- ζ_{nk}: output component k at time n, measured or estimated from sensor data

- $\hat{\zeta}_{nkc}$: predicted output component k at time n for cylinder c

- $\hat{\bar{\zeta}}_{nk}$: predicted output component k at time n, averaged over cylinders.

Network model   The neural network structure is built from the feedforward network with a single hidden layer and sigmoidal basis functions presented in Chapter 3, and the model for averaging over cylinders (5.7). The notation for indices used in this section is summarized in Table 5.2.
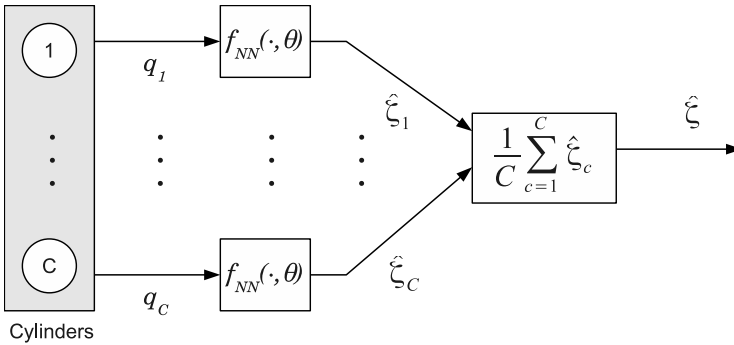

Figure 5.10   Structure of neural network for cylinder-individual prediction of emissions. Note that the structure of the functions $f_{\mathrm{NN}}(\cdot)$ and the parameters θ are the same for all cylinders.

N	number of data
K	dimension of ζ_n (number of network outputs)
L	dimension of q_n (number of network inputs)
M	dimension of z_n (number of hidden nodes)
C	number of cylinders

Table 5.2 Summary of notation for the neural network model.

The neural network model is given by

$$\hat{\zeta}_{nkc} = \beta_{k0} + \sum_{m=1}^{M} \beta_{km} z_{nmc} \tag{5.8}$$

$$\bar{\hat{\zeta}}_{nk} = \frac{1}{C} \sum_{c=1}^{C} \hat{\zeta}_{nkc} = \beta_{k0} + \sum_{m=1}^{M} \beta_{km} \bar{z}_{nm} \tag{5.9}$$

$$\bar{z}_{nm} = \frac{1}{C} \sum_{c=1}^{C} z_{nmc} \tag{5.10}$$

$$z_{nmc} = \sigma(\xi_{nmc}) \tag{5.11}$$

$$\xi_{nmc} = \alpha_{m0} + \sum_{l=1}^{L} \alpha_{ml} x_{nlc} \tag{5.12}$$

Cost function For training of the network, a cost function J built from a prediction error term J_{pe} and a regularization term J_{reg} is defined

$$J = J_{\text{pe}} + \gamma J_{\text{reg}} \tag{5.13}$$

where γ is constant weight. The prediction error cost is given by

$$J_{\text{pe}} = \frac{1}{2} \sum_{n=1}^{N} \sum_{k=1}^{K} (\zeta_{nk} - \bar{\hat{\zeta}}_{nk})^2 \tag{5.14}$$

and the regularization cost by

$$J_{\text{reg}} = \frac{1}{2C} \sum_{n=1}^{N} \sum_{k=1}^{K} \sum_{c=1}^{C} (\hat{\zeta}_{nkc} - \bar{\hat{\zeta}}_{nk})^2 \tag{5.15}$$

The regularization term is included to avoid overfitting by penalizing the difference between the predicted output of the individual cylinders $\hat{\zeta}_{nkc}$ and the predicted average $\bar{\hat{\zeta}}_{nk}$.

Network training Optimization of J with respect to $\theta = \{\beta_0, \beta, \alpha_0, \alpha\}$ is performed through a gradient descent method

$$\theta^{(\tau+1)} = \theta^{(\tau)} - \eta^{(\tau)} \frac{dJ}{d\theta}(\theta^{(\tau)}) \qquad (5.16)$$

Algebraic expressions for the derivative of J with respect to θ are found in Appendix B.1. The step size $\eta^{(\tau)}$ is chosen iteratively such that J is decreased in each iteration τ. The training scheme is summarized in Algorithm 1.

Algorithm 1 Scheme for training neural network from measured variables q to target variables ζ.

1: Rescale each input q_k to zero mean and unit sample variance.
2: Draw 20 initial estimates $\theta_{1:20}^{(0)} \in \mathcal{N}(0,1)$.
3: Compute $J(\theta)$ for each $\theta^{(0)}$ and select the one that gives the smallest cost.
4: Let $\eta^{(0)} = 1$.
5: **for** $\tau = 0$ to $\tau_{\max}$ **do**
6:   Compute the gradient of J with respect to θ for $\theta = \theta^{(\tau)}$,

$$\nabla J^{(\tau)} = \frac{dJ}{d\theta}(\theta^{(\tau)})$$

   according to Appendix B.1.
7:   Compute $\theta^* = \theta^{(\tau)} - \eta^{(\tau)} \nabla J^{(\tau)}$
8:   **while** $J(\theta^*) > J(\theta^\tau)$ **do**
9:     $\eta^{(\tau)} := \eta^{(\tau)}/2$
10:     $\theta^* = \theta^{(\tau)} - \eta^{(\tau)} \nabla J^{(\tau)}$
11:   **end while**
12:   $\theta^{(\tau+1)} = \theta^*$
13:   $\eta^{(\tau+1)} = 2\eta^{(\tau)}$
14: **end for**

Results

The method was applied to predict λ, NO_x, and opacity from cylinder pressure data,

$$\zeta = \begin{pmatrix} \lambda \\ \chi_{NOx} \\ X_{op} \end{pmatrix} \qquad (5.17)$$

Experimental data on cylinder pressure p_{cyl} and the target variables ζ were collected on the Volvo D13 engine. Eight nominal operating points for load

and speed were chosen. At each operating point, data was recorded in transient operation as fuel injection duration, start of injection, the EBP and EGR valve positions, and the VGT actuator position were varied. Around 30,000 cycles were recorded and included in the experimental data set.

Pre-processing the cylinder pressure data   The cylinder pressure sensor offset was estimated for each pressure trace individually by simultaneously finding the polytropic exponent and pressure offset before and after combustion, and interpolating the two values in between [Tunestål, 2009]. The offsets were then subtracted from the cylinder pressure data.

Pre-processing the target data   For model training and validation, λ and NO_x were measured using the Siemens VDO/NGK NOx sensor, and PM was measured using the opacimeter. The specified response times were 750 ms for NO_x and 550 ms for λ [Siemens VDO, 2005].

The sensors were modeled as

$$y = H(z)\zeta + e \tag{5.18}$$

where $H(z)$ is the linear transfer function from the true target variables ζ to the sensor output y. The sensor dynamics were modeled as a first-order low-pass filter with a time delay of d samples and unit stationary gain,

$$H(z) = \frac{(1-a)z^{-1}}{1-az^{-1}}z^{-d} \tag{5.19}$$

The parameter a governs the time constant of the low-pass filter.

The optimal estimate of ζ from y is obtained using a non-causal Wiener deconvolution [Hayes, 1996]. Modeling both ζ and e as white noise processes, the optimal filter is given as

$$\hat{\zeta}_{\text{wiener}} = G(z)y \tag{5.20}$$

where

$$G(z) = \frac{1}{H(z)}\frac{H(z)H(z^{-1})}{H(z)H(z^{-1}) + \frac{1}{\beta}} \tag{5.21}$$

and β is the signal-to-noise ratio between ζ and e.

The optimal filter is composed of two parts: the inverse of the dynamics $1/H(z)$, and a non-causal symmetric smoothing filter. The non-causal part can be implemented using spectral factorization of the transfer function and a forward-backward pass through the data. Note that the filter cannot be used for
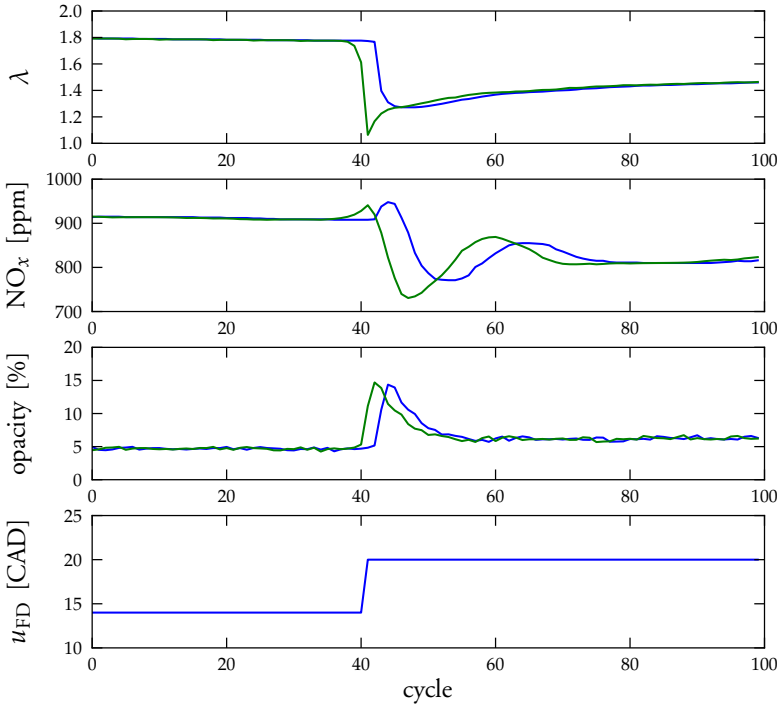
Figure 5.11 Measurements y of NO_x, λ, and opacity (blue) when load is increased, and Wiener filter output $\hat{\zeta}_{\text{wiener}}$ (green). Note that the time delay of the measurements has been removed without increasing the visual noise levels.

on-line estimation since it is non-causal. For off-line estimation of ζ from batch data, causality is however not required.

The filter parameters a, d, and β were determined for each output by considering the sensor response times and the noise characteristics of each signal. The effect of the filter is illustrated in Fig. 5.11. The figure shows y as well as the output of the Wiener filter $\hat{\zeta}$ (green) when fuel injection duration was increased by one third (blue).

Network training data   The full data set of 30,000 engine cycles was considered for training and evaluating the model for emissions prediction. Principal

	A	B
actuated variable	u_{EBP}	u_{FD}
average $IMEP_n$ (bar)	6.8	14.2
N_{engine} (rpm)	1700	1450
u_{SOI} (CAD ATDC)	-7	-7
nbr of cycles	1000	1000

Table 5.3 Operating conditions for data sets A and B, used for illustration of results.

component weights were computed for each cylinder pressure observation.

The input to the neural network q included the first eight principal component weights $w_{1:8}$, engine speed N_{engine}, start of injection u_{SOI}, and injection duration u_{FD},

$$q_c = (\begin{array}{cccc} w_{1:8} & N_{engine} & u_{SOI} & u_{FD} \end{array}) \tag{5.22}$$

The separation of the data into training and validation data was made considering the distribution of the target variables ζ. The desired size N_{train} of the training data was determined. For each of the outputs ζ_i, a subset $\mathcal{Z}_i$ of size $2N_{train}$ was selected such that the estimated probability distribution $p(\zeta_i)$ would be approximately uniform in $\mathcal{Z}_i$. The training subset $\mathcal{D}$ was finally selected as N_{train} random samples over the union of $\mathcal{Z}_i$ over the outputs. The purpose of of this approach was to include more samples from transients with large peaks in emissions.

To illustrate the neural network results, two different subsets of the data will be used, data set A and B. In data set A (low-load, high-speed), the fuel injection duration u_{FD} was varied, and in data set B (medium-load, medium-speed), the EBP valve position u_{EBP} was varied. The experimental conditions of these two operating conditions are given in Table 5.3.

Figure 5.12 shows the actuated variables for the two data sets, and their effect on the cylinder pressure from Cylinder 2. Figure 5.13 shows the first eight principal components for the two data sets.
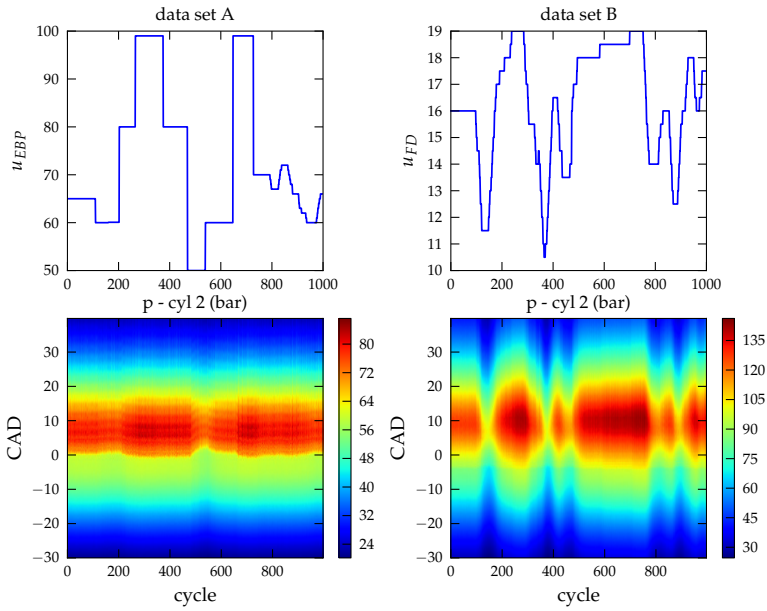
Figure 5.12   Illustration of actuated variable and cylinder pressure data for the two data sets in Table 5.3.
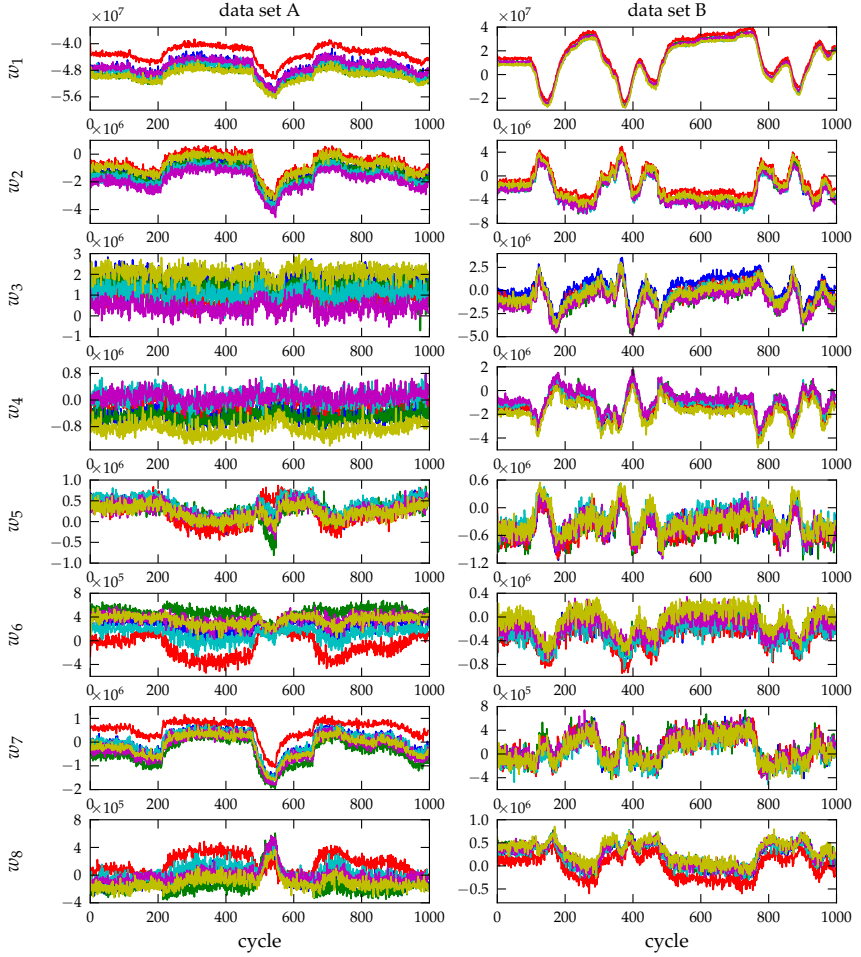
Figure 5.13   Principal component weights w for first eight components of data sets A and B.

Validation of neural network   The method was tested for prediction of λ, NO_x, and opacity. Results will here be presented for a network with $M = 10$ hidden nodes and regularization weight $\gamma = 0.5$, after 5,000 iterations of the gradient descent optimization algorithm. The computational effort corresponded to approximately 5 min on a standard PC for the implementation in Python. The implementation used three-dimensional arrays to represent the data and tensor operations for the computations to avoid looping over the indices. The choice of M was based on observation of prediction performance on validation data; however, no systematic analysis of optimal number of hidden nodes was performed. The choice of γ will be discussed below.

The results here thus aim to show what can be achieved by the method, but it is not claimed that the choice of parameters is optimal. By tuning the parameters and optimization algorithm, both predictive performance of the model and computational time could likely be improved.

Figure 5.14 shows neural network prediction $\hat{\zeta}_{NN}$ vs. the target variables ζ_{wiener} over the entire data set. Note that the targets ζ_{wiener} were obtained through the non-causal Wiener filter from the measured variables y, and should therefore not be interpreted as the 'truth'. They are merely the best estimates that can be obtained through the physical emissions sensors.

The R^2 and RMSE statistics for predition over the entire data set were

$$
\begin{aligned}
R_\lambda^2 &= 0.92 & \text{RMSE}_\lambda &= 0.079 \\
R_{NOx}^2 &= 0.90 & \text{RMSE}_{NOx} &= 77 \text{ ppm} \\
R_{op}^2 &= 0.71 & \text{RMSE}_{op} &= 1.9\%
\end{aligned}
\tag{5.23}
$$

Figure 5.15 shows cylinder-individual predictions of the outputs for the two data sets A and B.
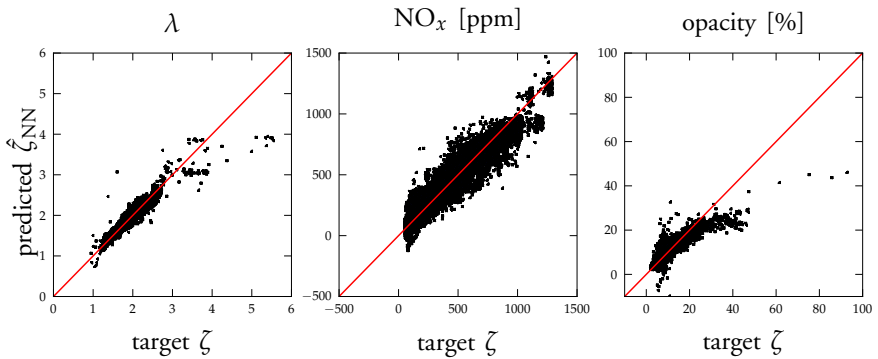

Figure 5.14   Predicted outputs from neural network vs. target outputs obtained from applying the non-causal Wiener filter to measurements.
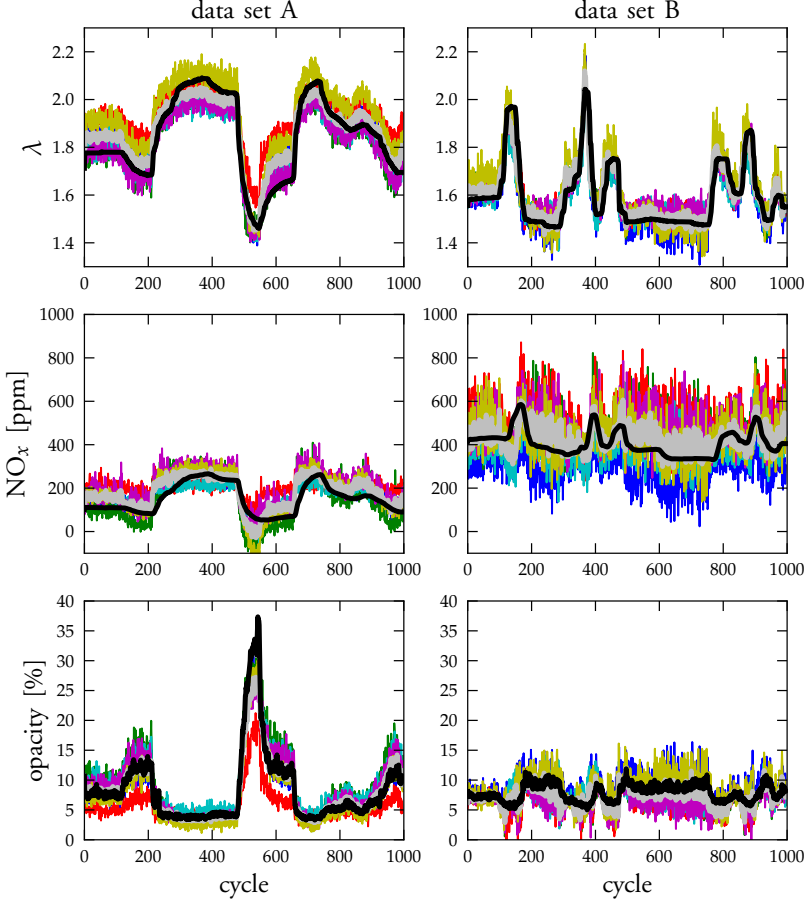
Figure 5.15 Target outputs ζ (black), predicted output averaged over cylinders $\bar{\bar{\zeta}}$ (grey), and cylinder-individual predicted outputs (colors), for the data sets A and B.

The neural-network predictions are fairly good; notably the trends are captured rather well. Cylinder-to-cylinder variations are significant. However, these variations are systematic; as an example we can see in data set B that Cylinder 1 (blue) appears to have slightly lower λ compared to the other cylinders and at the same time lower NO_x and higher opacity. This is in line with what would be expected from physical insight.

In some of the signals, e.g., NO_x for data set B, the cycle-to-cycle noise is

significant. There are a number of possible explanations for this,

- The number of nodes in the neural network was too small to provide good models at all operating points.

- The gradient descent algorithm converged to a local minimum.

- The training data did not provide sufficient information to train a successful model.

- The inputs to the neural network do not provide enough information to predict NO_x, regardless of model.

- The true cycle-to-cycle variations in NO_x are large.

Influence of the regularization term   The regularization term was included in the cost function to avoid overfitting. In practice, combustion will differ between the cylinders, and one of the key advantages of the proposed method is the ability to detect these differences. However, with a limited set of training data, the network may converge to solutions where the predicted output from the individual cylinders differ in manners that are not physically plausible, for example giving negative emissions concentrations. To avoid such overfitting, the regularization term is included.

To illustrate the effect of varying the weight γ for the regularization term, a neural network was trained to predict NO_x concentration. Only 0.5% of the data was used for network training, which implied that the predictive performance on the entire data set was intentionally made rather poor.

The neural network training algorithm is not deterministic. It finds a random starting point, and there is no guarantee that it will converge to a global optimum. To evaluate the effect of different γ, it is therefore not sufficient to train networks for a sweep of γ values. A Monte-Carlo approach was pursued instead, where neural networks were trained for a random set of γ, and their predictions were evaluated.

A sample $\{\gamma_1, \cdots, \gamma_D\}$ of size $D = 1{,}000$ was drawn from the exponential probability distribution

$$p_\gamma(\gamma) = b\exp(-b\gamma) \tag{5.24}$$

with $b = 0.5$. Neural networks were trained for each of γ_i using 8,000 iterations of the gradient descent algorithm, and evaluated on the validation data. The R^2-value for validation data was computed both for the cylinder-averaged predicted NO_x, and the cylinder-individual predictions. The result is illustrated in Figs. 5.16 and 5.17.

Figure 5.16 shows the R^2-values for the cylinder-averaged prediction compared to the target for the validation data (black dots). The probability density
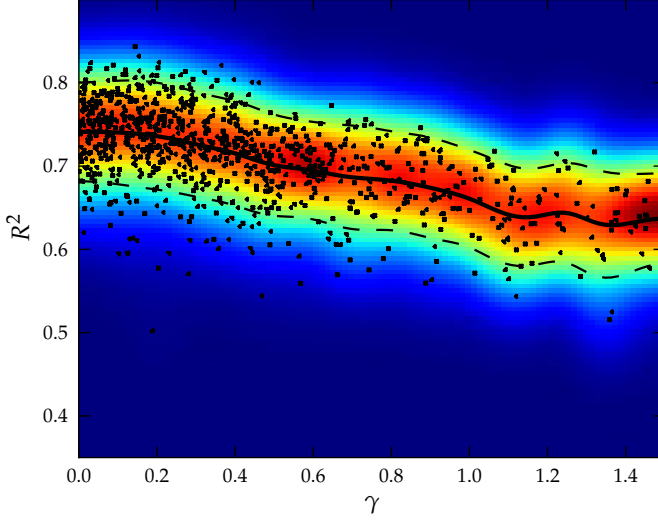
Figure 5.16   Monte-Carlo simulation where neural networks were trained for 1,000 random values of γ. R^2 denotes how well the cylinder-averaged predicted output match the cylinder-averaged target output in the validation data. The graph shows $p(R^2|\gamma)$, the estimated probability density of validation metric R^2 as a function of γ. The solid line is the estimated expected value $E(R^2|\gamma)$, and the dashed lines correspond to $\pm$ 1 standard deviation.

$p(R^2|\gamma)$ was estimated from this data using a kernel method with a Gaussian kernel [Hastie et al., 2009], and is visualized by the color scheme. Also shown in the plot is the expected value $E(R^2|\gamma)$ and the confidence bounds of $\pm$ 1 standard deviations. We can see that, on average, the fit between the cylinder-averaged predicted NO_x and the target decreases with increasing γ, as would be expected from the structure of the cost function.

Figure 5.17 shows the R^2-values for cylinder-individual predictions compared to the target for the validation data, and the expected value $E(R_c^2|\gamma)$. For $\gamma = 0$ (no regularization), there is a large spread in terms of how well the cylinder-individual predictions match the target. As γ increases, this spread decreases when the regularization term forces the predictions to be homogenized over the cylinders.

From these results, it can be concluded that the regularization term helps to obtain a closer match between the cylinder-individual and cylinder-averaged predictions. For the example studied here, the performance on the cylinder-averaged prediction does not increase significantly for small values of γ, while
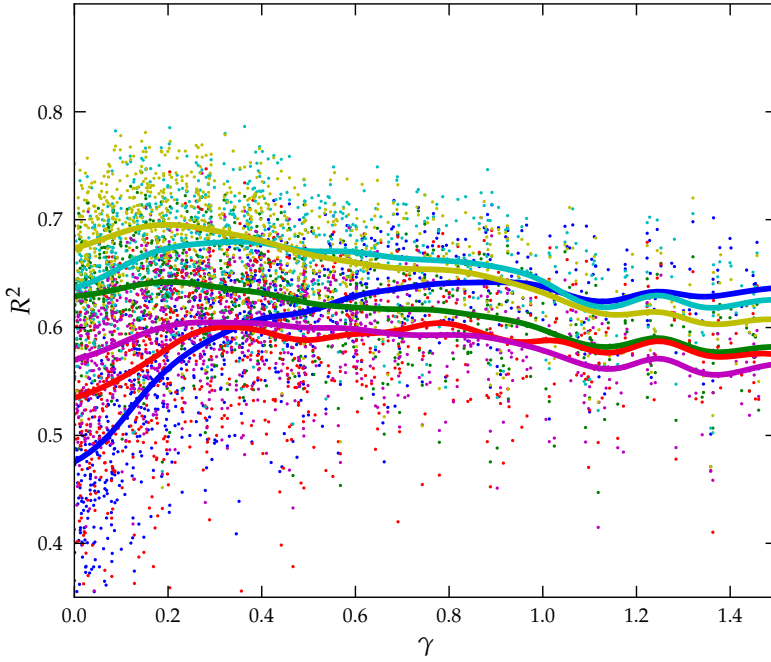
Figure 5.17   Monte-Carlo simulation where neural networks were trained for 1,000 random values of γ. R^2 denotes how well the cylinder-individual predicted outputs match the cylinder-averaged target output. The lines correspond to $\mathrm{E}(R_c^2|\gamma)$ for Cylinder c. Compared to Fig. 5.16, it can be seen that the optimal match between cylinder-individual inputs and cylinder-averaged target in this case occur for $\gamma > 0$. Blue = Cyl. 1, Green = Cyl. 2, Red = Cyl. 3, Cyan = Cyl. 4, Magenta = Cyl 5, Yellow = Cyl. 6.

the match for the cylinder-individual predictions improve substantially. The choice of γ is a trade-off between penalizing over-fitting and allowing the true cylinder-to-cylinder imbalances to be captured by the model.

Comments and Conclusions

In contrast to previously published work on predicting emissions from cylinder pressure data, the method presented here has been validated on a cycle-to-cycle cylinder-individual basis during transient operation for prediction of both λ, NO_x, and PM. None of the references mentioned in the beginning of the chapter [Traver et al., 1999; Seykens et al., 2009; Wilhelmsson et al., 2009; Çebi et al., 2011] present cycle-to-cycle transient predictions. In [Wilhelmsson et al.,

2009], a very small validation data set of 150 cycles collected at steady-state in a single-cylinder engine was used. Cycle-to-cycle variations in NO prediction were shown to be considerable. In [Traver et al., 1999], only two out of eight cylinders were equipped with pressure sensors and no results on cylinder-to-cylinder differences were shown. The cycle-to-cycle data were low-pass filtered using a five-point moving-average filter. The model was trained at steady-state but still proved to give qualitatively good predictions of NO_x, HC, and CO_2 emissions during an FTP transient. In [Seykens et al., 2009], only steady-state data were used. Cylinder-to-cylinder variations were shown to be fairly large, but it is not clear from the paper how large the cycle-to-cycle differences were or how the data was averaged. In [Çebi et al., 2011], an empirical model for PM calibrated at steady-state proved to give very good transient performance. However, it is unclear how many actuators that were manipulated independently in the training and validation data, i.e., which variables that were varied in open loop for excitation as opposed to being determined from other variable through the standard ECU calibration. It is therefore difficult to estimate how well the model would perform in general.

A key point of using cylinder-pressure based estimates of emissions is to obtain cycle-to-cycle cylinder-individual estimates that could be used for feedback control, for example tuning the start of injection to the optimal NO_x-PM trade-off for each cylinder individually. It is then essential that the emissions estimates are sufficiently accurate for each individual cycle and cylinder, so that no extensive low-pass filtering that decreases the bandwidth of the sensor is required for reasonable estimates. The method presented here has been shown to be promising in that respect. For future work, the performance of the virtual sensor should be evaluated on closed-loop cylinder-individual control of emissions.

6

Dynamic Engine Modeling

In this chapter, a method to find control-oriented cycle-to-cycle dynamic models from control variables u to target variables ζ is presented. The work was originally published in [Karlsson et al., 2010a]. The target application for the models is the model-based control design approach that will be presented in Chapter 7, where high-level engine specifications are transformed into a cost function to be optimized on-line through model predictive control. For this control design, on-line measurements of NO_x, opacity, combustion phasing, maximum pressure derivative, and $IMEP_n$ are exploited, to allow for explicit on-line management of the trade-off between different high-level objectives.

A key point of this work is that feedback control will be based on measured emissions. In this respect, the approach differs from almost all published work on engine control presented in Section 2.4. With feedback based on measured emissions, the requirements on the engine model shift from static to dynamic performance. The aim of this chapter is to find low-complexity models that capture the main dynamics of the engine, including emissions formation. The steady-state properties of the models are less important than the transient dynamics in this context, since a feedback controller can compensate for steady-state errors through integral action when the target variables are measured on-line.

Several papers have been published on control-oriented models of diesel engine emissions. However, most of them are based on approaches similar to what was presented in Chapter 5, where static models of emissions from other engine variables such as engine speed, inlet manifold pressure, fuel injection parameters, air mass flow, estimated EGR rate, etc., are derived, either from first principles or from empirical data. Examples of such models are given in [Hirsch et al., 2008; Westlund and Ångström, 2009; Mrosek et al., 2010; Tschanz et al., 2010; Sequenz and Isermann, 2011]. These models are intended to be used in combination with separate empirical or physical models that describe the engine dynamics.

A few publications introduce explicit dynamic models for emissions, e.g.

[Hafner et al., 2000; Ouladsine et al., 2004; Maaß et al., 2009] who all use various forms of neural networks such as nonlinear ARX-models for the emissions dynamics. Hafner et al. [2009] modeled emissions and fuel consumption, and used the model to optimize a weighted sum of emissions over injection timing. Ouladsine et al. [2004] had a more limited scope; a neural network model was developed to predict engine speed, inlet manifold pressure and opacity. Simulation results were shown for optimizing a cost function for tracking engine speed while minimizing opacity. Maaß et al. [2009] used a neural network to predict a set of emission concentrations from a set of 12 engine parameters such as torque, engine speed, and fuel injection parameters.

Instead of neural network models, the modeling approach in this chapter starts by identifying linear state-space models at a grid of operating points. The identification procedure is divided into two parts. First, linear models are identified separately for each operating point. Then, the number of models is reduced by introducing Wiener models and applying a clustering algorithm.

Problem Formulation

The combined influence of four main diesel engine actuator variables is considered: injection duration u_{FD}, injection timing u_{SOI}, EBP valve position u_{EBP}, and VGT actuator position u_{VGT}

$$u = \begin{pmatrix} u_{SOI} & u_{FD} & u_{EBP} & u_{VGT} \end{pmatrix}^T \tag{6.1}$$

The chosen output variables of the model,

$$y = \begin{pmatrix} y_{IMEP} & \alpha_{50} & d_p & \chi_{NOx} & X_{op} \end{pmatrix}^T \tag{6.2}$$

reflect high-level specifications for the engine controller. To manage emissions, NO_x concentration and opacity are included. For torque tracking, y_{IMEP} is included. To limit audible noise and ensure safe engine operation, maximum pressure derivative d_p is included. Fuel consumption would have been desired as an output, but since it is difficult to measure on a cycle-to-cycle basis, combustion phasing α_{50} was included instead. Defining a setpoint for combustion phasing in order to optimize fuel consumption is a widely adopted strategy. The setpoint could also be optimized on-line by an extremum-seeking controller if on-line estimation of fuel consumption is available [Larsson and Andersson, 2008; Killingsworth et al., 2009; Lewander et al., 2012].

The model setup is summarized in Fig. 6.1.

Experiment Design

Experimental data were collected on the D12 engine. The study was limited to low- and medium-load operating points where the interactions between gas-
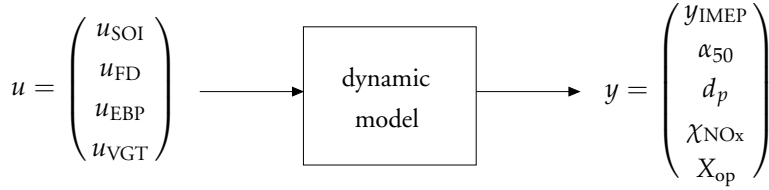
$$u = \begin{pmatrix} u_{\mathrm{SOI}} \\ u_{\mathrm{FD}} \\ u_{\mathrm{EBP}} \\ u_{\mathrm{VGT}} \end{pmatrix} \longrightarrow \boxed{\begin{array}{c} \text{dynamic} \\ \text{model} \end{array}} \longrightarrow y = \begin{pmatrix} y_{\mathrm{IMEP}} \\ \alpha_{50} \\ d_p \\ \chi_{\mathrm{NOx}} \\ X_{\mathrm{op}} \end{pmatrix}$$

Figure 6.1   Model inputs and outputs.

flow dynamics and in-cylinder combustion dynamics are most dominant and therefore interesting to model in the same framework.

A set of operating points spanned by the four model inputs were defined. A fixed engine speed of $N_{\mathrm{engine}} = 1200$ rpm was chosen, the study could be expanded to multiple engine speeds using the same methodology. Three different load operating points were chosen, corresponding to $y_{\mathrm{IMEP}} = \{4, 7, 10\}$ bar. At each load, three different values of injection timing u_{SOI} were chosen, and at each such value four points in the $u_{\mathrm{EBP}} - u_{\mathrm{VGT}}$ plane were decided. A few initial steady-state maps were used to define suitable operating points in terms of emissions and brake efficiency. In total, 30 operating points were defined: 6 at load $y_{\mathrm{IMEP}} = 4$ bar, 12 at load $y_{\mathrm{IMEP}} = 7$ bar, and 12 at $y_{\mathrm{IMEP}} = 10$ bar. For $y_{\mathrm{IMEP}} = 4$ bar, the VGT actuator was kept fully open as the flow over the compressor was sufficiently large without additional turbocharging. An overview of the operating points is given in Table 6.1.

Combustion phasing α_{50}, IMEP_n, and pressure derivative d_p were computed from the cylinder pressure data. The Siemens VDO / NGK NOx sensor was used to measure NO_x emissions, and the opacimeter for measuring PM emissions. Sensor dynamics compensation was not applied to the data. The models therefore represent the dynamic response of the system from actuator command to sensor reading.

At each operating point, suitable amplitudes for pseudo-random binary sequence (PRBS) excitation signals were determined. These were applied to the engine, and data of length 2800 engine cycles were collected at each operating point, corresponding to 280 s. Constant offsets were removed and subsets of the data were selected for identification and validation, each of length 1300 cycles. It was concluded that offsets differed between the cylinders whereas the dynamics were similar. Models were therefore only identified for Cylinder 5 which was determined to be representative of all six cylinders. The outputs were scaled to obtain the same order of magnitude.

Table 6.1 Operating points.

Op. point	IMEP$_n$ [bar]	u_{SOI} [CAD ATDC]	u_{FD} [CAD]	u_{EBP} [%]	u_{VGT} [%]
1	4	-5	5.8	10	100
2	4	-12	5.8	10	100
3	4	-20	5.8	10	100
4	4	-5	5.8	13	100
5	4	-12	5.8	13	100
6	4	-20	5.8	13	100
7	7	-5	7.1	53	33.5
8	7	-10	7.1	53	33.5
9	7	-15	7.5	53	33.5
10	7	-5	7.1	56	40
11	7	-10	7.3	56	40
12	7	-15	7.5	56	40
13	7	-5	7.2	50	23
14	7	-10	7.4	50	23
15	7	-15	7.6	50	23
16	7	-5	7.3	56	28
17	7	-10	7.4	56	28
18	7	-15	7.5	56	28
19	10	-9	10.4	76	29
20	10	-13	10.8	76	29
21	10	-17	10.7	76	29
22	10	-5	10.5	82	29
23	10	-10	10.6	82	29
24	10	-15	10.8	82	29
25	10	-5	10.6	82	40
26	10	-10	10.6	82	40
27	10	-15	10.8	82	40
28	10	-5	10.5	90	40
29	10	-10	10.6	90	40
30	10	-15	10.9	90	40

Identification of Local Linear Models

Linear state space models of the form

$$
\begin{aligned}
x_{k+1} &= Ax_k + Bu_k + Kw_k \\
y_k &= Cx_k + Du_k + w_k
\end{aligned}
\tag{6.3}
$$

where $x_k \in \mathbb{R}^n$, $u_k \in \mathbb{R}^m$, and $y_k \in \mathbb{R}^p$ were identified at each operating point using the `n4sid` algorithm from the System Identification Toolbox in Matlab [Mathworks, 2009]. Variance accounted for (VAF) was used as validation criterion, and a prediction horizon of 20 engine cycles was selected to evaluate the models. Since the target use of the models is closed-loop control, the choice of prediction horizon should reflect the desired closed-loop bandwidth. At the applied engine speed, a prediction horizon of 20 engine cycles corresponds to 2 s which is the same order of magnitude as the time constant of transient load tracking.

Models of orders $n = 2$ to $n = 12$ were identified at each operating point. The mean VAF over the five outputs for each of the operating points is shown in Fig. 6.2 as a function of model order.

Low model orders, $n < 5$, lead to poor prediction. At some operating points, low-order models even lead to negative VAF (not included in Fig. 6.2 for the sake of clarity) corresponding to a higher variance in the prediction error than in the measured outputs. Increasing the model order beyond $n = 7$ can give a small improvement in VAF, but not sufficient to motivate the greater
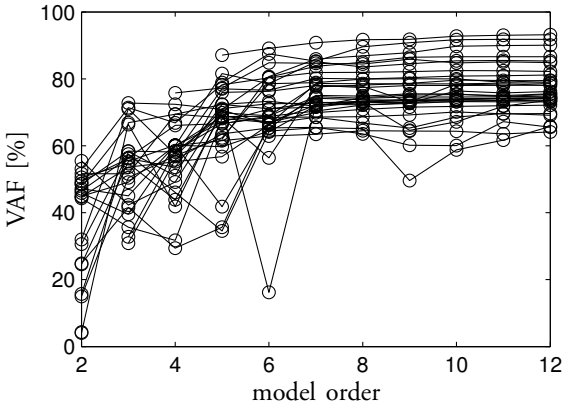

Figure 6.2 Variance accounted for (VAF) as a function of model order for the 30 operating points.

computational burden for control design. From Fig. 6.2, it was concluded that model order $n = 7$ was suitable to describe the data. There is a large spread in VAF between the operating points for a fixed model order. This spread is largely caused by different excitation of the outputs compared to the noise level at different operating points.

Reducing the Number of Models

We now wish to investigate the similarity between models at different operating points to see how the engine dynamics vary between operating points, and to investigate if a more compact engine model can be obtained be selecting a subset of the linear models to be used over a larger operating range. Because the system is known to be highly nonlinear, the linear systems identified at different operating points are expected to be differ by a degree that depends on the distance between the operating points.

Cross-validation was performed between all combinations of models and data from different operating points which results in a 30×30 cross-validation matrix. Figure 6.3 illustrates this matrix for 20-step predictions.

In general, it can be seen that the best model for data for a given operating point is the model identified at that same operating point, as would be expected. Some combinations of models and operating points give good predictions, others
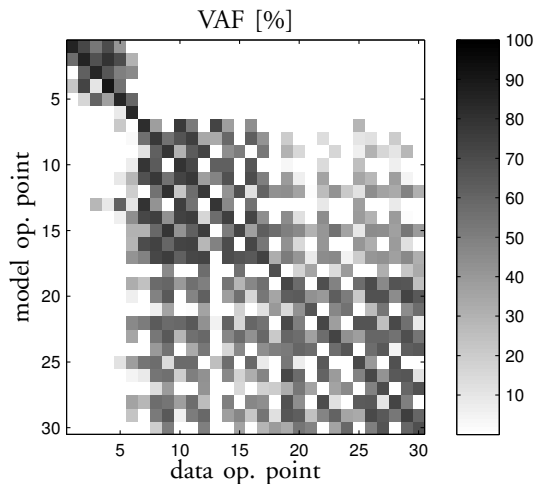

Figure 6.3 Mean VAF for cross-validation of the models identified at the 30 operating points with validation data at all operating points. Values on the diagonal are high, corresponding to a good fit between model and data at the same operating point.

do not. Note that models identified at low load (operating points 1 to 6) cannot be used at higher loads since the u_{VGT} signal was kept constant at these operating points.

Two steps are now proposed to find a limited number of dynamic models to model data at all operating points. First, Wiener models are introduced to compensate for different gains at different operating points. A clustering algorithm is then applied to group the operating points and find a suitable model for each group.

Wiener models   A Wiener model is a linear dynamic model with a static nonlinearity at the output, see Fig. 3.2. The static nonlinearity $f(\cdot)$ adds a large flexibility to the linear dynamic model at a moderate cost. If the nonlinearity can be inverted, control design can be based entirely on linear techniques.

Previously, models of the form

$$
\begin{aligned}
x_{k+1} &= A^i x_k + B^i u_k + K^i w_k \\
y_k &= C^i x_k + D^i u_k + w_k
\end{aligned}
\tag{6.4}
$$

where $x_k \in \mathbb{R}^n$, $u_k \in \mathbb{R}^m$, $y_k \in \mathbb{R}^p$, were identified for operating points $i = 1, \cdots, 30$. A Wiener model extends this representation to

$$
\begin{aligned}
x_{k+1} &= A^i x_k + B^i u_k + K^i w_k \\
\bar{y}_k &= C^i x_k + D^i u_k + w_k \\
y_k &= f^i(\bar{y}_k)
\end{aligned}
\tag{6.5}
$$

Consider the dynamic model $\mathcal{M}_i(A^i, B^i, C^i, D^i, K^i)$ at operating point i to be given from the previous identification procedure. We now wish to find a representation of the nonlinearities $f^i(\cdot)$ to let model i better fit data at another operating point j. This can be done through a local linearization of $f^i(\cdot)$ at operating point j,

$$
M^{ij} = \left. \frac{\partial f^i}{\partial \bar{y}} \right|_{\text{op point}=j}
\tag{6.6}
$$

From the set of local linearizations M^{ij} and the offsets removed at each operating point, approximations of the nonlinearities $f^i(\cdot)$ can be reconstructed, see Appendix B.2.

We now wish to find the matrices M^{ij} to optimize the fit between model i and identification data j. To make the representation simpler, the matrices M^{ij} are constrained to be diagonal,

$$
M^{ij} = \mathrm{diag}(m_1^{ij}, \cdots m_p^{ij})
\tag{6.7}
$$

such that the nonlinearity $f^i(\cdot)$ is decoupled into p scalar nonlinearities, one for each output.

Denote by $\hat{\mathcal{Y}}_{ij} \in \mathbb{R}^{N \times p}$ the data series of predicted outputs at operating point j using model i with the nominal gain matrix $M^{ij} = I$. It then holds for the output data series of Wiener model $\hat{\mathcal{Y}}_{ij}$

$$\hat{\mathcal{Y}}_{ij} = \hat{\mathcal{Y}}_{ij} M^{ij^T} \tag{6.8}$$

The optimal gains m_k^{ij}, $k = 1, \cdots, p$, can now be found by solving the convex optimization problems

$$\min_{M^{ij} \text{ diagonal}} ||\mathcal{Y}_j - \hat{\mathcal{Y}}_{ij} M^{ij^T}||_F^2 \tag{6.9}$$

where $\mathcal{Y}_j$ is the measured output data series at operating point j.

The cross-validation was performed again with an optimized scaling matrix M^{ij} for each pair of model and data operating points i and j. The resulting VAF can be seen in Fig. 6.4. Note the large improvement in VAF when matching models and data from different operating points, compared to Fig. 6.3.
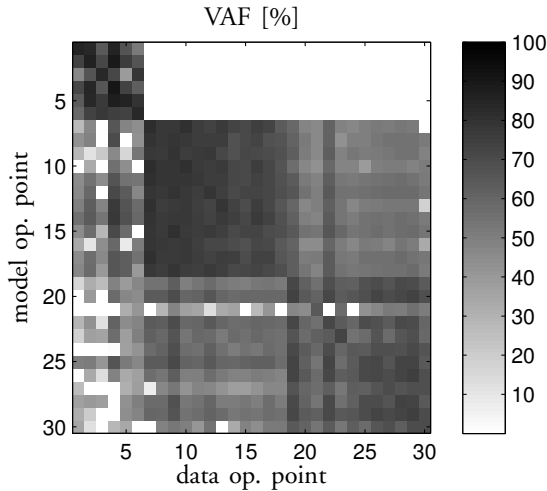

Figure 6.4 Mean VAF for cross validation of the models identified at the 30 operating points with validation data at all operating points with gains adapted to form Wiener models. Note the large improvement compared to Fig. 6.3.

Model clustering   From Fig. 6.4, we can see that data at many operating points can be described almost as well by dynamic models identified at other operating points with adapted Wiener gains, as by the model identifed at the same operating point. We will now present a clustering algorithm to select a subset of the linear dynamic models that can accurately describe the data together with the Wiener gain matrices.

Define by V the VAF matrix illustrated in Fig. 6.4, where element v_{ij} corresponds to the mean VAF over the five outputs when using Wiener model i for a 20-step prediction of validation data at operating point j. The matrix V can be used to group operating points to a limited number of models. A hierarchical agglomerative clustering algorithm is used to that respect [Manning et al., 2008].

The algorithm is based on the relative VAF loss matrix ΔV, where the elements are given by

$$\Delta v_{ij} = v_{jj} - v_{ij} \tag{6.10}$$

and a clustering matrix C initialized as

$$C = \Delta V \tag{6.11}$$

The element Δv_{ij} is a measure of how much VAF that is lost by removing model j and using model i instead for that operating point. The hierarchical clustering algorithm successively merges two of the existing clusters at each step until only one cluster remains. At each step, the algorithm first finds the minimum element of C, corresponding to the smallest VAF loss, and merges models in cluster j into the cluster for model i. A new column is added to C representing the new cluster. The distance to other models for the newly formed cluster is defined as the worst-case distance over the operating points assigned to the cluster model. The details of the algorithm are described in Algorithm 2.

Results

The result of the clustering procedure is illustrated in a dendrogram in Fig. 6.5. The dendrogram shows the merges of operating points into clusters as a tree structure, starting at the bottom where every operating point is in its own cluster. On the y-axis, the loss of VAF is shown for each merge. It can be seen that a few models may be removed at no loss at all, which means that a model identified at a different operating point proved to be marginally better than the corresponding model in some cases. This result is likely due to the choice of prediction horizon in the computation of VAF. A large number of models may be removed at a moderate cost; if a loss of 5% is accepted, only six clusters remain, if 10% can be accepted only four clusters are needed.

Algorithm 2 Clustering algorithm based on the relative VAF loss matrix ΔV and the clustering matrix C.

1: Let $K =$ number of operating points.
2: Initialize $C = \Delta V$.
3: Set $\mathrm{diag}(C) = \infty$ to reflect the fact that a cluster cannot merge with itself.
4: **for** $k = K + 1$ to $2K - 1$ **do**
5:     Find indices i, j of minimum element of C. By assigning operating point j to the model of cluster i, the smallest loss of VAF will occur.
6:     Merge cluster i and j into new cluster k, assign cluster i model to cluster k.
7:     Add a column to matrix C corresponding to cluster k, let $c_{\star k} = \max(\Delta v_{\star s_1}, \cdots, \Delta v_{\star s_L})$, where s_1 to s_L are the operating points previously assigned to clusters i and j, now to cluster k.
8:     Set $c_{\star k}$ to ∞ for models that have previously been removed.
9:     Remove clusters i and j by letting $c_{\star i} = \infty$, $c_{\star j} = \infty$.
10:    Remove the previous model for operating point j model by letting $c_{\mathrm{model}(j)\star} = \infty$.
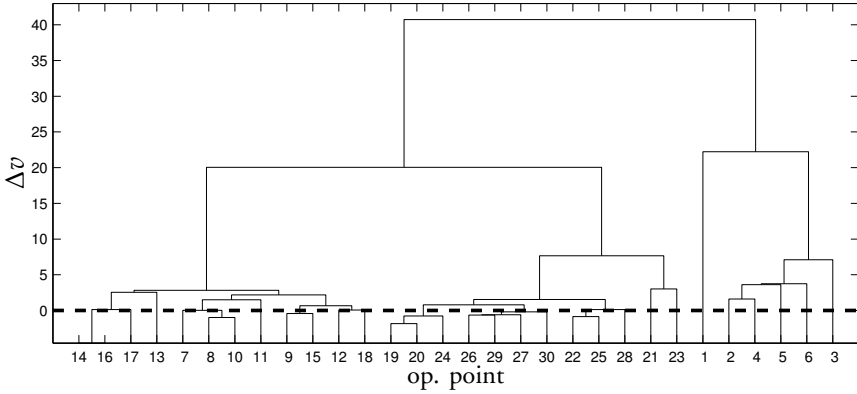11: **end for**

Figure 6.5 Dendrogram of operating point clustering. The vertical axis denotes the loss incurred for each merge of the clusters. The dashed line represents $\Delta v = 0$, the merges below this line do not decrease predictive performance of the model.

It can be noted that the clusters are not randomly assembled. With only two clusters remaining, one consists of the low-load operating points 1 to 6, and the other of the medium- and high-load operating points 7 to 30. The medium-to-high load cluster is further divided at a lower level into one cluster for medium-load operating points 7 to 18 and one for high-load operating points 19 to 30.

If we settle for five clusters, corresponding to a VAF loss of 7.5%, the worst-

case fit between model and operating point will occur for operating point 3 which has been assigned to model 5. Figure 6.6 shows the measured output validation data at operating point 3, the 20 step prediction using the original model 3, and the 20 step prediction using the assigned model 5 with the adapted Wiener gain for operating point 3. It can be concluded that prediction of all outputs is very good using model 3, and only slightly worse using the adapted model 5.

Conclusions and Comments

A novel approach to finding dynamic emissions models was presented. The system considered is complex; it has four inputs and five outputs, it is highly nonlinear, and it involves a number of complex physical processes that are hard to model from first principles. Standard system identification algorithms were used to fit dynamic black-box models of moderate model order to four-input-five-output data sets. Considering the complexity of the task, the results are surprisingly good. Furthermore, Wiener models combined with a clustering algorithm reduced the number of dynamic models needed significantly, while keeping the predictive ability of the remaining models high. The results are a promising start for model-based control design that uses direct emissions measurements.

Compared to the prior works in the field summarized in the beginning of the chapter, the presented method differs in at least one of the following respects:

- Experiment design for data collection.

- Model structure.

- Model evaluation criteria.

Some brief comments on the merits of the proposed method are given here.

Experiment design   Hirsch et al. [2008] makes an important remark regarding data collection for empirical emissions models. They notice that it is not uncommon in published work to use empirical data collected under closed-loop control of the standard ECU. This strongly reduces the dimension of the model space, and may greatly overestimate the quality of the models.

In this paper, all data were collected in open loop. By defining a grid of operating points, the region of validity of the model is explicitly known.

Model structure   The model structure with local linear state-space models was chosen because of their wide-spread use in model-based control-design algorithms. State-space models handle MIMO systems in a natural way both in terms of notation and computations. The subspace-based algorithms that were
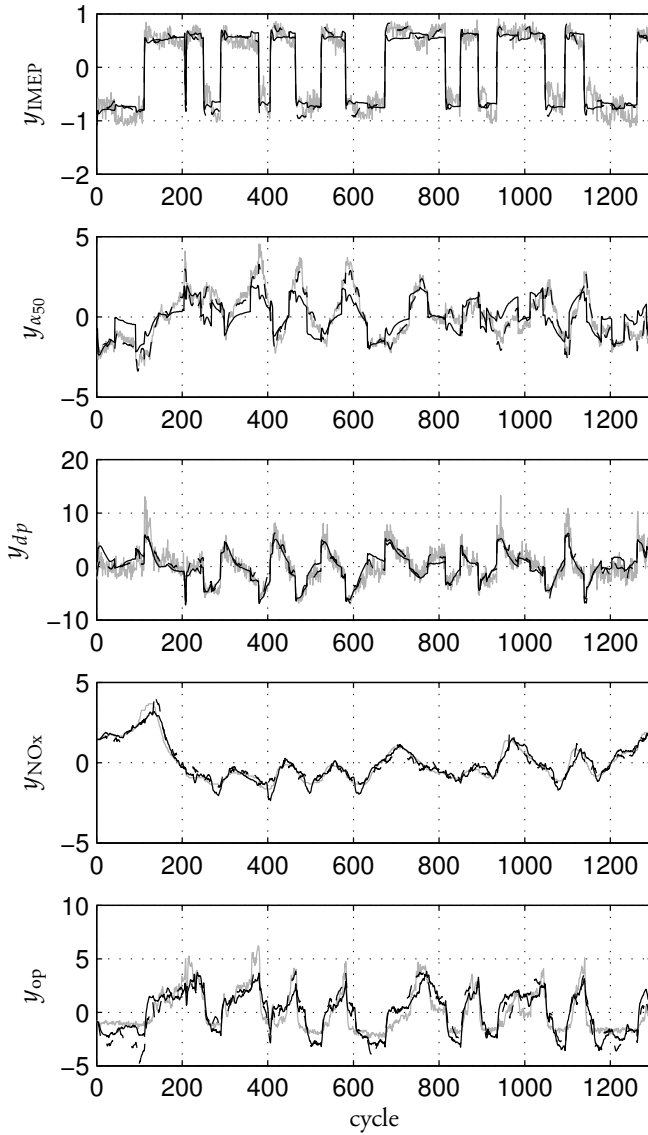
Figure 6.6 Measured output of validation data at operating point 3 (grey solid line), 20-step ahead predicted output of local linear model identified at operating point 3 (dashed line), 20-step ahead predicted output of operating 5 model with Wiener gain adapted to operating point 3 (black solid line). The Wiener model is the assigned model from the cluster algorithm at a level of accepted VAF loss of 7.5%, yielding 5 dynamic models for the 30 operating points. All data have been scaled and offsets have been removed.

used to identify the models also provide a noise model that may be used for Kalman filter design. Similar model structures with weighted local-linear or linear-parameter-varying models are used for engine control design in for example [Ortner and Re, 2007; García-Nieto et al., 2008; Alfieri et al., 2009; Wang et al., 2011], but for smaller sets of inputs and outputs.

An alternative approach to find local linear models is the LOLIMOT neural networks applied in for example [Hafner et al., 2000; Sequenz and Isermann, 2011]. The clustering method presented here starts with many local models and then merges them to find a reduced set of models. The LOLIMOT approach starts instead with a global model and successively adds models at operating points where the performance of the existing models is poor. The process of identifying locally valid dynamic engine models and merging them to a global model is also addressed in [Hametner and Nebel, 2012].

As mentioned in chapter's introduction, many publications present static models for emissions from measurements or estimates of other engine variables such as injection parameters, inlet manifold pressure, or EGR rate. For control design, these models need to be combined with separate models for the engine dynamics, e.g. mean-value models for the gas flow. An advantage of directly identifying dynamic models from control variables u to target variables ζ is that no assumptions need to be made regarding which dynamics that are important. At different operating points, different dynamics may be dominant. For example, in-cylinder effects such as cylinder-wall heating or properties of the residual gas are often not included in mean-value models, but may introduce significant dynamics for low-load, low-temperature dynamics. By directly modeling the influence of u to ζ, the dynamics that affect the high-level objectives at each operating point will automatically be included.

Evaluation criteria   Performance of the state-space models was defined in terms of 20-step prediction error, with prediction based on a Kalman filter obtained from the identified noise model. By selecting the prediction horizon, validation can be targeted to frequencies that are important for closed-loop control. If emissions are measured on-line, the steady-state properties of the models are less important since integral action can compensate for steady-state errors.

Future work   An interesting topic for future work could be to develop a systematic procedure for determining experimental operating points using design-of-experiments methods and concepts. Another direction is to apply alternative metrics in the clustering algorithm to determine the closeness of models, where closed-loop performance would be considered. Yet another area for future work is to use physical models for some phenomena such as gas exchange, and combine them with black-box models of the remaining processes such as emissions formation.

7

Optimal Control

This chapter presents work on optimal control of diesel engines, originally published in [Karlsson et al., 2008; Karlsson et al., 2010b]. As discussed in Chapters 1 and 2, there are several reasons optimal engine control is a difficult problem. One reason is that the problem is multivariable, another reason that the target variables for control are not generally measured on-line. Compared to the extensive body of previous research in the field, summarized in Chapter 2, the novelty of the work presented in this chapter lies in the combination of three features:

- Integrated fuel and gas flow control—fuel control variables (injection timing and injection duration), and gas flow control variables (EBP and VGT actuator positions) are incorporated on equal terms in the models and the controllers.

- Data-rich control—feedback from emissions sensors (for NO_x and opacity), and cylinder pressure sensors is exploited.

- The cost function for optimal control is directly related to high-level specifications, such as emissions.

The first part of the chapter is devoted to control of low-load low-temperature combustion (LTC). The control design is based on the heuristic virtual sensor for NO_x and opacity presented in Section 5.1, where a cost function for emissions is transformed into a cost function for combustion phasing and ignition delay. Low-temperature operation accentuates the need to consider interactions between fuel injection and airpath controllers ([Hillion et al., 2008; Alberer, 2009]). Joint control of start of injection and EGR to optimize emissions during transients is therefore studied.

When the work on low-load LTC was performed, the experimental platform was equipped with cylinder pressure sensors for fast feedback, but not with fast emissions sensors. Later, the Siemens Smart NOx sensor [Siemens VDO, 2005] was installed, which made it possible to measure both NO_x and opacity
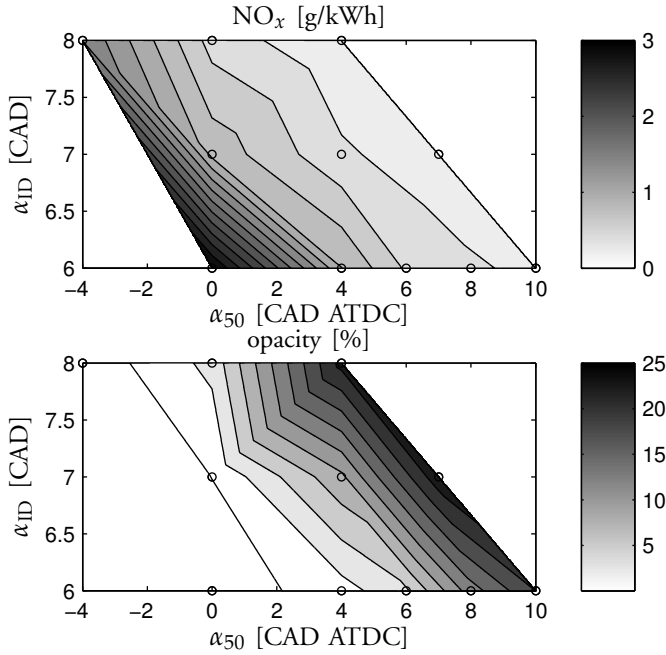
Figure 7.1 Emissions of NO_x and PM mapped according to α_{50} and α_{ID} for steady-state operation. Circles represent measurement points, intermediate values are obtained by linear interpolation.

on timescales appropriate for feedback control. The second part of this chapter presents work on model predictive control for MIMO optimization of the engine, where emissions measurements are used for feedback, and a multi-objective cost function is formulated.

7.1 LQG Control Based on Heuristic Virtual Emissions Sensor

In Chapter 5, it was shown how opacity and NO_x concentration can be related to combustion phasing and ignition delay for low-temperature diesel combustion. To recall, Fig. 7.1 shows the emissions mapped according to α_{50} and α_{ID} as the EGR rate and ignition timing were swept, and Fig. 7.2 shows a weighted sum of NO_x and opacity which defines a cost to be minimized. A quadratic function was fitted to this cost, with level curves also shown in Fig. 7.2.
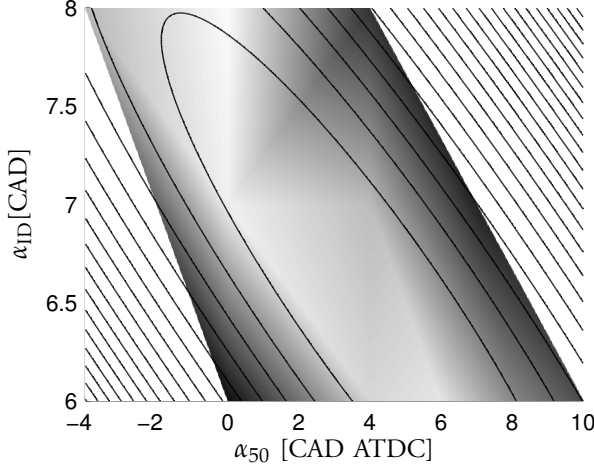
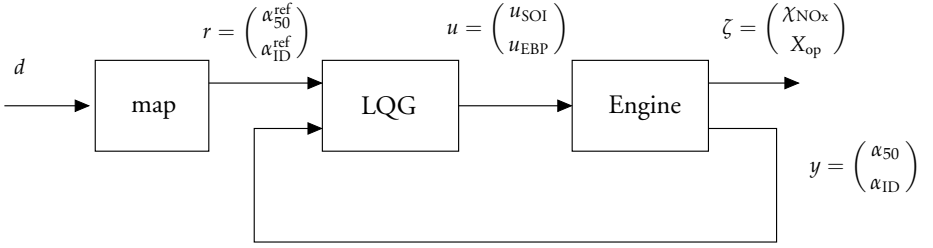**Figure 7.2** Weighted sum of emissions from Fig. 7.1 and level contours of quadratic approximation.

Figure 7.3 Control structure for optimal control of ζ based on feedback variables y. For a solution over the full operating range of the engine, a map would be needed for the setpoint r according to operating point d defined in terms of speed and load.

Control Design

The control structure is illustrated in Fig. 7.3. The control design aims to optimize ζ based on the approximated quadratic cost in Fig. 7.2. The feedback controller steer the measured variables y to a setpoint r. The unmeasured target variables ζ are indirectly controlled through an open-loop map that provides the setpoint r.

Problem Formulation Let the dynamics of cylinder i, $i \in \{1, \ldots 6\}$, from input u_{SOI}^i and u_{EBP} to output $y^i = (\alpha_{50}^i \quad \alpha_{\text{ID}}^i)^T$ be modeled by a linear

113

time-invariant discrete-time system

$$x^i_{k+1} = A^i x^i_k + (B^i_1 \quad B^i_2) \begin{pmatrix} u^i_{\text{SOI},k} \\ u_{\text{EBP},k} \end{pmatrix} + K^i w^i_k$$

$$y^i_k = C^i x^i_k + (D^i_1 \quad D^i_2) \begin{pmatrix} u^i_{\text{SOI},k} \\ u_{\text{EBP},k} \end{pmatrix} + w^i_k$$

(7.1)

where the input u_{SOI} can be set individually for each cylinder whereas u_{EBP} is a common control variable influencing all cylinders. Let n denote the system order, then $u^i_{\text{SOI}} \in \mathbb{R}$, $u_{\text{EBP}} \in \mathbb{R}$, $y^i \in \mathbb{R}^2$, $x^i \in \mathbb{R}^n$, and $w^i \in \mathbb{R}^2$. The sample time is one engine cycle. The noise w_k is zero-mean white Gaussian noise with

$$\text{E}(w^i_k w^{iT}_k) = P^i. \tag{7.2}$$

The objective of the controller is to minimize the quadratic cost function

$$J(u^i) = \lim_{k \to \infty} \text{E} \left(\sum_{i=1}^{6} (r^i_k - y^i_k)^T Q^i (r^i_k - y^i_k) + I^{iT}_k Q^i_I I^i_k + u^{iT}_k R^i u^i_k \right) \tag{7.3}$$

where I^i_k represents integrator states, the matrices Q^i define the level contours in Fig. 7.2, and the weight matrices Q^i_I and R^i represent cost on the integrator states and control variables. The setpoint r_k is assumed constant.

The dynamics of the full six-cylinder engine can now be written as

$$x_{k+1} = A x_k + B u_k + K w_k$$

$$y_k = C x_k + D u_k + w_k$$

(7.4)

where

$$A = \text{diag}\{A^1, \cdots, A^6\}$$

$$B = \begin{pmatrix} B^1_1 & 0 & \cdots & 0 & B^1_2 \\ 0 & B^2_1 & \cdots & 0 & B^2_2 \\ \vdots & \vdots & \ddots & \vdots & \vdots \\ 0 & \cdots & \cdots & B^6_1 & B^6_2 \end{pmatrix}$$

(7.5)

$$K = \text{diag}\{K^1, \cdots, K^6\}$$

$$C = \text{diag}\{C^1, \cdots, C^6\}$$

$$D = \begin{pmatrix} D_1^1 & 0 & \cdots & 0 & D_2^1 \\ 0 & D_1^2 & \cdots & 0 & D_2^2 \\ \vdots & \vdots & \ddots & \vdots & \vdots \\ 0 & \cdots & \cdots & D_1^6 & D_2^6 \end{pmatrix}$$

and

$$\begin{aligned} x &= (\, x_1^T \quad \cdots \quad x_6^T \,)^T, & x &\in \mathbb{R}^{6n} \\ u &= (\, u_{\text{SOI}}^1 \quad \cdots \quad u_{\text{SOI}}^6 \quad u_{\text{EBP}} \,)^T, & u &\in \mathbb{R}^7 \\ y &= (\, y_1^T \quad \cdots \quad y_6^T \,)^T, & y &\in \mathbb{R}^{12} \\ \text{E}(w_k w_k^T) &= P = \text{diag}\{P^1, \cdots, P^6\} \end{aligned} \tag{7.6}$$

The optimization problem (7.3) can now be reformulated as

$$J(\{u_k^*\}) = \min_{\{u_k\}} \lim_{k \to \infty} \text{E}\left((r_k - y_k)^T Q (r_k - y_k) + I_k^T Q_I I_k + u_k^T R u_k \right) \tag{7.7}$$

where $\{u_k\}$ is a causal function of $\{y_k\}$,

$$\begin{aligned} Q &= \text{diag}\{Q^1, \cdots, Q^6\} \\ Q_I &= \text{diag}\{Q_I^1, \cdots, Q_I^6\} \end{aligned} \tag{7.8}$$

and R represents the cost of the seven control variables.

Centralized LQG   A controller for the 7-input, 12-output system (7.4) that minimizes the cost (7.7) can be designed using standard LQG techniques [Åström and Wittenmark, 1997] by extending the state vector with the integrator states according to

$$z_k = \begin{pmatrix} x_k \\ I_k \end{pmatrix} \tag{7.9}$$

The standard integrator update equation is

$$I_{k+1} = I_k + r_k - y_k \tag{7.10}$$

but for the system (7.4) with $u_k \in \mathbb{R}^7$ and $y_k \in \mathbb{R}^{12}$, the extended system will not be stabilizable, and the optimization problem (7.7) will not be well posed because $\text{E}(I_k^T Q_I I_k)$ will not be finite for any control law $u_k = -L_C z_k$.

To find a modified integrator update equation, consider the extended system using the standard integrator update (7.9),

$$\begin{pmatrix} x_{k+1} \\ I_{k+1} \end{pmatrix} = \begin{pmatrix} A & 0 \\ -C & I \end{pmatrix} \begin{pmatrix} x_k \\ I_k \end{pmatrix} + \begin{pmatrix} B \\ -D \end{pmatrix} u_k + \begin{pmatrix} 0 \\ I \end{pmatrix} r_k + \begin{pmatrix} K \\ -I \end{pmatrix} w_k$$

$$(7.11)$$

Denote by W_c the controllability matrix for this system. The non-controllable part of I_k is given by

$$W_C^T \begin{pmatrix} x_k \\ I_k \end{pmatrix} = 0$$

$$(I \quad 0) \begin{pmatrix} x_k \\ I_k \end{pmatrix} = 0$$

$$(7.12)$$

which can be written as

$$\begin{pmatrix} W_C^T \\ (I \quad 0) \end{pmatrix} \begin{pmatrix} x_k \\ I_k \end{pmatrix} = (N_x \quad N_I) \begin{pmatrix} x_k \\ I_k \end{pmatrix} = 0 \tag{7.13}$$

where N_x and N_I are matrices of appropriate dimensions.

We wish to find a projection matrix M such that

$$\bar{I}_k = MI_k \tag{7.14}$$

where $\text{rank}(M) = \text{rank}(N_I)$, and $\bar{I}_k$ represents the controllable part of I_k.

The matrix M should then satisfy $N_I = N_I M$ and $\text{rank}(M) = \text{rank}(N_I) = 7$, since there are seven independent inputs to the system. From the singular value decomposition of N_I, we can choose M as an orthogonal projection according to

$$N_I = U\Sigma V^T = U\Sigma \begin{pmatrix} I_{7\times7} & 0 \\ 0 & 0_{5\times5} \end{pmatrix} V^T$$

$$= \underbrace{U\Sigma V^T}_{N_I} \underbrace{V \begin{pmatrix} I_{7\times7} & 0 \\ 0 & 0_{5\times5} \end{pmatrix} V^T}_{M} = N_I M$$

$$(7.15)$$

Now define the integrator update equation as

$$I_{k+1} = M(I_k + r_k - y_k) \tag{7.16}$$

which will only update I_k along its controllable modes, in practice yielding seven independent integrators for the seven-input system (7.4).

LQG controllers can now be designed for the extended system

$$z_{k+1} = \begin{pmatrix} A & 0 \\ -MC & M \end{pmatrix} z_k + \begin{pmatrix} B \\ -MD \end{pmatrix} u_k + \begin{pmatrix} 0 \\ M \end{pmatrix} r_k + \begin{pmatrix} K \\ -M \end{pmatrix} w_k$$

$$y_k = \begin{pmatrix} C & 0 \end{pmatrix} z_k + Du_k + w_k$$

(7.17)

The Kalman filter for state observation [Kalman, 1960] is given by

$$\hat{x}_{k+1} = A\hat{x}_k + L_F(y_k - C\hat{x}_k - Du_k) \tag{7.18}$$

and the optimal control law by $u_k = -L_C \left(\hat{x}_k^T \quad I_k^T \right)^T + L_R r_k$. The gains L_F and L_C are found by solving the corresponding Riccati equations, as described in [Åström and Wittenmark, 1997]. The optimal reference value weight matrix L_R is computed using the procedure in [Haddad and Moser, 1994].

Decentralized LQG   A disadvantage with the controller presented in the previous section is that measurements from all cylinders must be available to compute any single control variable. The resulting controller is designed for a seven-input, twelve-output system and with an n-state model for each cylinder, the extended system (7.17) will be of order $n_e = 6n + 12$.

We will now investigate an alternative approach where the control laws for u_{SOI}^i are based on local measurements of y^i only. The approach is a heuristic reformulation of the centralized optimal control problem, and relies on the following assumptions

1. all cylinders have identical dynamics

2. the controller for u_{EBP} should be slower than for u_{SOI}.

The decentralized approach relies on designing the controllers for u_{SOI} and u_{EBP} separately. First, u_{EBP} is considered as a constant, measurable disturbance, and an LQG controller for u_{SOI} is designed for the single cylinder system (7.1)

extended with integrator states

$$
\begin{pmatrix} x^i_{k+1} \\ I^i_{\mathrm{SOI},k+1} \end{pmatrix} = \begin{pmatrix} A^i & 0 \\ -M^i_{\mathrm{SOI}}C^i & M^i_{\mathrm{SOI}} \end{pmatrix} \begin{pmatrix} x^i_k \\ I^i_{\mathrm{SOI},k} \end{pmatrix}
$$

$$
+ \begin{pmatrix} B^i_1 \\ -M^i_{\mathrm{SOI}}D^i_1 \end{pmatrix} u^i_{\mathrm{SOI},k} + \begin{pmatrix} B^i_2 \\ -M^i_{\mathrm{SOI}}D^i_2 \end{pmatrix} u_{\mathrm{EBP},k}
$$

$$
+ \begin{pmatrix} 0 \\ M^i_{\mathrm{SOI}} \end{pmatrix} r_k + \begin{pmatrix} K^i \\ -M_{\mathrm{SOI}} \end{pmatrix} w_k
$$

$$
y_k = \begin{pmatrix} C^i & 0 \end{pmatrix} \begin{pmatrix} x^i_k \\ I^i_{\mathrm{SOI},k} \end{pmatrix} + D^i_1 u^i_{\mathrm{SOI},k} + D^i_2 u_{\mathrm{EBP},k} + w_k
$$

(7.19)

The integrator update projection matrices M^i_{SOI} are chosen such that the integrator states are only updated in directions controllable by u^i_{SOI}, analogous to the procedure described in the previous section.

Standard Kalman filters are used to estimate $\hat{x}^i$, and cylinder-individual controllers for u_{SOI}

$$
u^i_{\mathrm{SOI},k} = -L^i_{C,\mathrm{SOI}} \begin{pmatrix} \hat{x}^i_k \\ I^i_{\mathrm{SOI},k} \end{pmatrix} + L^i_V u_{\mathrm{EBP},k} + L^i_{R,\mathrm{SOI}} r_k
$$

(7.20)

are designed to minimize each cylinder's term in the cost function (7.3), where $\{u^i_{\mathrm{SOI}}\}$ are causal functions of $\{y^i\}$, r, and u_{EBP}. The control law for u^i_{SOI} depends on measurements y^i only, and the system dynamics (7.19) is of order $n_{ecyl} = n + 2$, six times less than in (7.17).

To design a controller for u_{EBP}, consider the closed-loop system obtained by inserting the control law (7.20) into the dynamics (7.19). Design an LQG controller that minimizes the cylinder cost function

$$
J(u_{\mathrm{EBP}}) = \lim_{k \to \infty} \mathrm{E}((r^i_k - y^i_k)^T Q^i (r^i_k - y^i_k) + I^{iT}_{\mathrm{SOI},k} Q_I I_{\mathrm{SOI},k}
$$

$$
+ I^{iT}_{\mathrm{EBP},k} Q_{I2} I^i_{\mathrm{EBP},k} + R_{\mathrm{EBP}} u^2_{\mathrm{EBP},k})
$$

(7.21)

subject to the dynamics given by (7.19) and (7.20) extended by integrator states I_{EBP} that are updated along directions controllable by u_{EBP}.

For cylinder i, the resulting optimal control law will then take the form

$$u_{\text{EBP},k}^i = -L_{\text{C,EBP}}^i \begin{pmatrix} \hat{x}_k^i \\ I_{\text{SOI},k}^i \\ I_{\text{EBP},k}^i \end{pmatrix} + L_{\text{R,EBP}}^i r_k \qquad (7.22)$$

where the optimal $u_{\text{EBP},k}^i$ will vary between the cylinders. With identical dynamics for all cylinders, $L_{\text{C,EBP}}^i = L_{\text{C,EBP}}$ and $L_{\text{R,EBP}}^i = L_{\text{R,EBP}}$ are the same for all cylinders. Choose u_{EBP} as the average optimal u_{EBP}^i given the u_{SOI} controller

$$u_{\text{EBP},k} = -L_{\text{C,EBP}} \begin{pmatrix} \frac{1}{6}\sum_{i=1}^6 \hat{x}_k^i \\ \frac{1}{6}\sum_{i=1}^6 I_{\text{SOI},k}^i \\ I_{\text{EBP},k} \end{pmatrix} + L_{\text{R,EBP}} r_k \qquad (7.23)$$

and update I_{EBP} according to

$$I_{\text{EBP},k+1} = M_{\text{EBP}} \left(I_{\text{EBP},k} + r_k - \frac{1}{6}\sum_{i=1}^6 y_k^i \right) \qquad (7.24)$$

Experimental Conditions

Experiments for modeling and evaluation of control designs were performed on the D12 engine. All engine actuator variables except for u_{SOI} and u_{EBP} were kept constant. The experiments were performed at a constant fuel injection duration of $u_{\text{FD}} = 7$ CAD, corresponding to $\text{IMEP}_n = 5.8$ bar, and at engine speed $N_{\text{engine}} = 1200$ rpm. Inlet valve closing was kept constant at $u_{\text{IVC}} = 560$ CAD ATDC. The VGT actuator was also fixed, giving an absolute inlet pressure of $p_{\text{in}} = 1.12$ bar.

Modeling

Dynamic models for the system were found using system identification. Data were collected in open loop when the system was excited with PRBS (pseudo-random binary sequence) signals for the two inputs. Data sets of length 900 engine cycles were used for identification and validation respectively. Identification of state-space models was performed using the Matlab System Identification Toolbox method `pem`, which uses a combination of subspace identification and numerical optimization of prediction error.

Figure 7.4 shows variance accounted for (VAF), for models of order $n = 1$ to $n = 5$ for one cylinder. Prediction of α_{50} is as good with a first-order model as
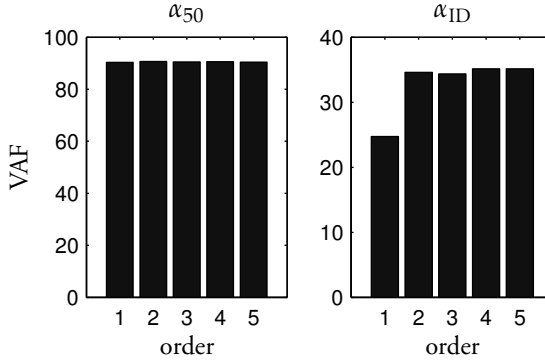
Figure 7.4 Variance accounted for (VAF) for models of different orders for one of the cylinders.

higher orders, but prediction of α_{ID} improves significantly using a second-order model. Second-order models were therefore used for control design.

It can be seen that the model captures a larger portion of the variance in α_{50} compared to α_{ID}. This effect is caused by larger excitation from u_{SOI} and u_{EBP} to α_{50}.

Models estimated from identification data from the six cylinders were simulated against validation data from all cylinders, and VAF for all combinations are shown in Fig. 7.5. There is no clear trend that models from the same cylinder better predict data than models estimated from different cylinders, which would have been indicated by higher VAF values on the diagonals in the figure. A model from one cylinder was selected and applied for all cylinders.

Figure 7.6 shows validation data and predicted output for one cylinder with a second-order model. Validation was performed on data with the same input amplitudes and parameters for generation of the PRBS sequence.

Results

The controllers were tested in both simulation and experiment. All model parameters, including noise characteristics, were taken from the identified model. The costs for the output errors, $Q^i = Q^0$, were defined by the level contours demonstrated in Fig. 7.2 with identical costs for all cylinders, and the integrator costs were chosen as $Q_I^i = \gamma Q^0$, $Q_{I2}^i = \gamma_2 Q^0$. The control variable cost R was adjusted to keep the cycle-to-cycle changes in the control variables within realistic bounds. The setpoint for y_k, i.e., the center point in Fig. 7.2, is shifted in the results presented because the optimal point varies somewhat with operating conditions such as speed and fuel injection pressure.
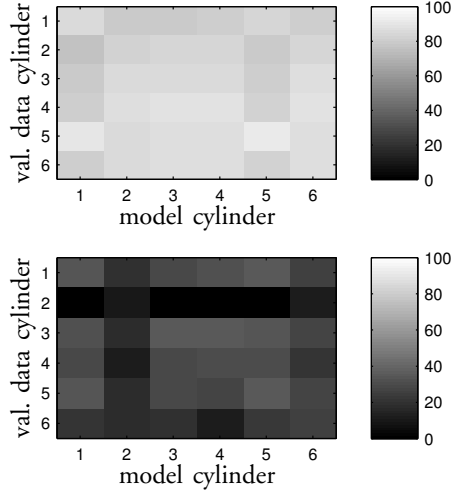
Figure 7.5 Variance accounted for (VAF) for α_{50} (top), and α_{ID} (bottom), for validation data for the six cylinders matched to models estimated from identification data for the six cylinders.
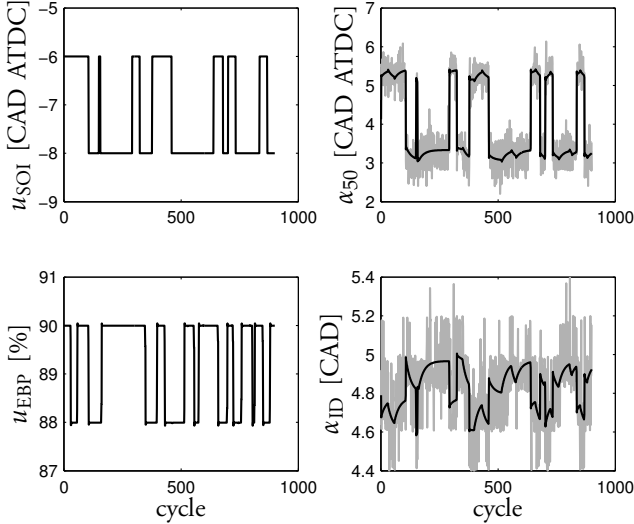

Figure 7.6 Cross-validation of identified model for one cylinder with validation data. The plots to the right show measured outputs (gray), and predicted outputs (black). The small overshoot in the u_{EBP} signal are caused by the internal position controller of the valve servo.

121

In all presented results, the setpoint was first set different from the cost function optimum, and then shifted to the optimum after a few cycles. This way, we can observe the transient performance of the closed-loop system after a disturbance has shifted the system from its setpoint.

Simulations   Results from a Simulink simulation of the engine with the centralized LQG controller are shown in Fig. 7.7. In this figure, a large overshoot in α_{50} can be seen when the setpoint is changed. In Fig. 7.8, the process output y_k is shown in relation to the cost function level contours. Here, it can be seen that the overshoot in α_{50} occurs in a direction of decreasing cost, and that the cost demonstrates a monotonic convergence to its stationary value. The reason why this convergence does not happen in the shortest geometrical path from the initial to the final setpoint is the combined effect of the skewed cost function level contours, the cost on the control signals, and the system dynamics, i.e., because of the slow changes of u_{EBP} and the slower effect on α_{ID} compared to α_{50}.

Simulation results using the decentralized controller are shown in Figs. 7.9 and 7.10. Performance is similar to the centralized controller, and the differences are primarily caused by different weighting matrices in the cost function.

Experiments   Experimental results using the centralized controller are shown in Figs. 7.11 and 7.12. Though there are large overshoots in the step response transients in Fig. 7.11, it can be seen in Fig. 7.12 that the transient takes place in a direction associated with low cost, as defined by the NO_x-PM trade-off. The control variable u_{EBP} saturated at its upper value when the setpoint was changed. An anti-windup feature would be desirable but was not implemented here, nevertheless the control variable gets out of saturation rapidly and the effect of the saturation on control performance appears to be limited.

Experimental results using the decentralized controller are shown in Figs. 7.13 and 7.14. It is less clear that the cost function is minimized subject to the control variable cost in this case, and the decentralized controller was more difficult to tune compared to the centralized controller. The reason is thought to be the two-stage design method, where the effect of changing one of the weighting matrices is less transparent than for the one-stage design method used for the centralized controller.

In the experimental results, it can be seen that the cylinder-to-cylinder differences are quite small, so that performance is not in practice limited by the configuration with more outputs $y \in \mathbb{R}^{12}$ than inputs $u \in \mathbb{R}^{7}$.
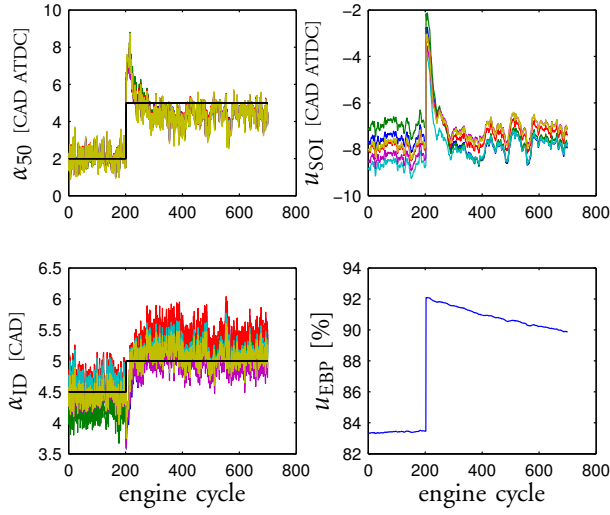
Figure 7.7   Simulation results using the centralized controller. At engine cycle 200, the setpoint is changed to the cost function optimum.
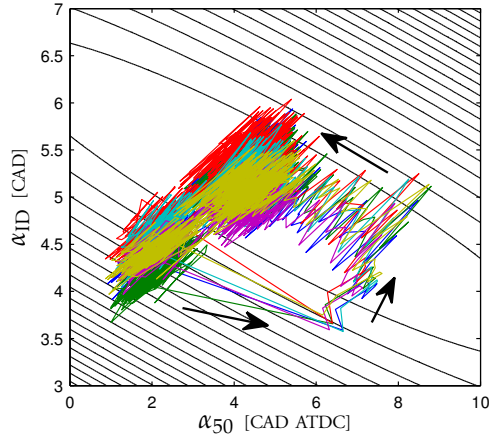

Figure 7.8   Simulation data from Fig. 7.7 illustrated in relation to cost function level curves. The setpoint is first $\left(\alpha_{50}^{\text{ref}}, \alpha_{\text{ID}}^{\text{ref}}\right) = (2,4.5)$, and at engine cycle 200 changed to the cost function optimum at $\left(\alpha_{50}^{\text{ref}}, \alpha_{\text{ID}}^{\text{ref}}\right) = (5,5)$. The arrows indicate the direction of the trajectories.
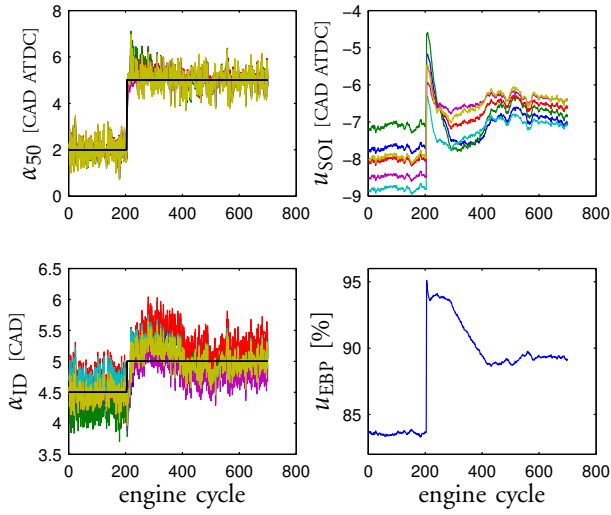
Figure 7.9 Simulation results using the decentralized controller. At engine cycle 200, the setpoint is changed to the cost function optimum.
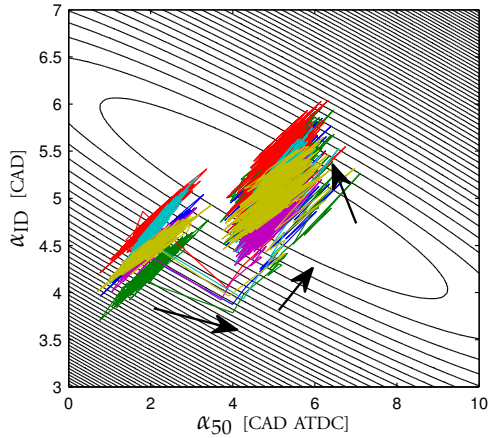

Figure 7.10 Simulation data from Fig. 7.9 illustrated in relation to cost function level curves. The setpoint is changed from $\left(\alpha_{50}^{\text{ref}}, \alpha_{\text{ID}}^{\text{ref}}\right) = (2,4.5)$ to $\left(\alpha_{50}^{\text{ref}}, \alpha_{\text{ID}}^{\text{ref}}\right) = (5,5)$ at engine cycle 200. The arrows indicate the direction of the trajectories.
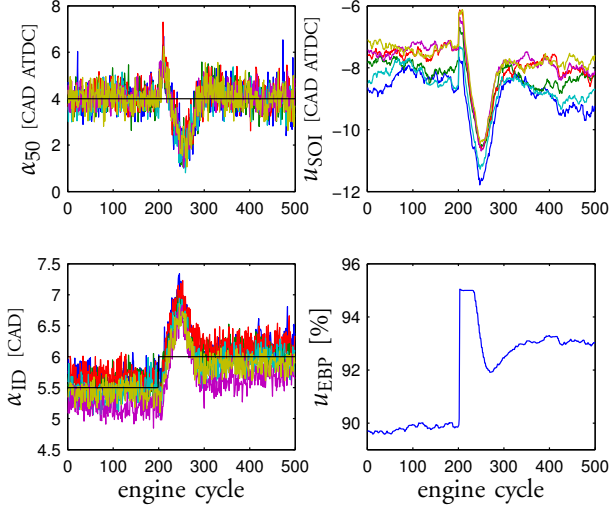
Figure 7.11 Experimental results using the centralized controller. At engine cycle 200, the setpoint was changed to the cost function optimum.
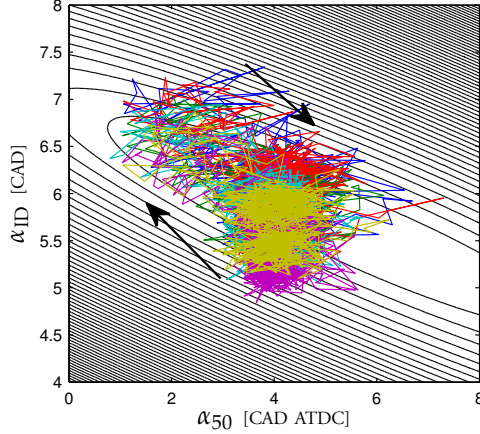

Figure 7.12 Experimental data from Fig. 7.9 illustrated in relation to cost function level curves. At engine cycle 200, the setpoint was changed from $(\alpha_{50}^{\text{ref}}, \alpha_{\text{ID}}^{\text{ref}}) = (4, 5.5)$ to $(\alpha_{50}^{\text{ref}}, \alpha_{\text{ID}}^{\text{ref}}) = (4, 6)$. The arrows indicate the direction of the trajectories.
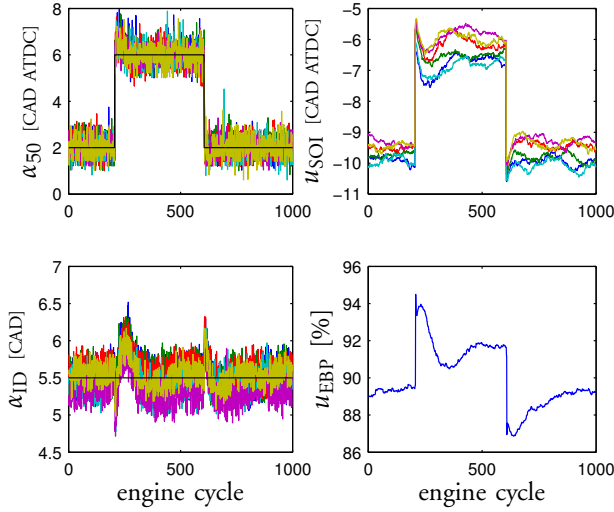
Figure 7.13 Experimental results using the decentralized controller. At engine cycle 200, the setpoint was changed to the cost function optimum. At engine cycle 600, the setpoint was changed back to the original value. From the different responses on the positive and negative setpoint step, it can be concluded that the process is nonlinear even for these small changes in operating conditions.

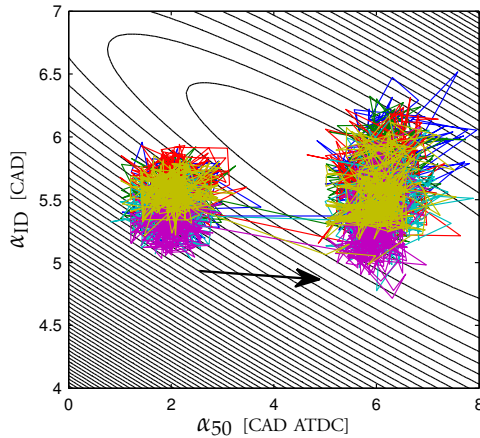**Figure 7.14** Experimental data from engine cycle 1 to 500 in Fig. 7.9 illustrated in relation to cost function level curves. At engine cycle 200, the setpoint was changed from $(\alpha_{50}^{\text{ref}}, \alpha_{\text{ID}}^{\text{ref}}) = (2,5.5)$ to the cost function optimum at $(\alpha_{50}^{\text{ref}}, \alpha_{\text{ID}}^{\text{ref}}) = (6,5.5)$. The arrow indicates the direction of the trajectory.

7.2 Direct Optimal Engine Control Using MPC

The previous section described indirect control of NO_x and PM emissions, by using feedback from parameters computed from cylinder pressure data. In this section, we will assume that NO_x and PM emissions are measured on-line, and use them for direct feedback control. The previous section was limited to control of the NO_x-soot trade-off around a fixed operating point in load and speed. This section extends the scope to multiple high-level engine control objectives:

- Tracking the desired torque trajectory.

- Keeping fuel-optimal combustion phasing (often known as MBT timing).

- Managing the NO_x-soot trade-off.

- Limiting audible noise.

The task of optimizing a trade-off between several objectives subject to a large number of constraints fits nicely into the model predictive control formulation. In this work, the main control variables for gas exchange and fuel injection were considered simultaneously

$$u = \begin{pmatrix} u_{\text{SOI}} & u_{\text{FD}} & u_{\text{EBP}} & u_{\text{VGT}} \end{pmatrix}^T \tag{7.25}$$

As far as possible, measurements directly related to high-level objectives were used for feedback, i.e., direct measurement of NO_x, opacity measurement for soot, and measurements from cylinder pressure sensors of indicated mean effective pressure (IMEP_n) for torque tracking, combusion phasing α_{50} for keeping MBT timing, and peak pressure derivative d_p to limit audible noise.

NO_x concentration χ_{NOx} was measured using the Siemens Smart NOx sensor. The opacimeter was used to measure soot, X_{op}. Formation of soot is highly nonlinear, with gain from actuator variables to measured opacity being much higher at high soot levels compared to lower levels. In order to make the process more linear to facilitate closed-loop control, opacity was rescaled based on an inverted empirical map when used for system identification and feedback to the controller.

Five measured variables were thus used in the control design,

$$y = \begin{pmatrix} y_{\text{IMEP}} & \alpha_{50} & d_p & \chi_{\text{NOx}} & X_{\text{op}} \end{pmatrix}^T \tag{7.26}$$

Control Design

Dynamic model   The controller was based on one of the dynamic models from Chapter 6. The scope of this work was control around a fixed operating point;
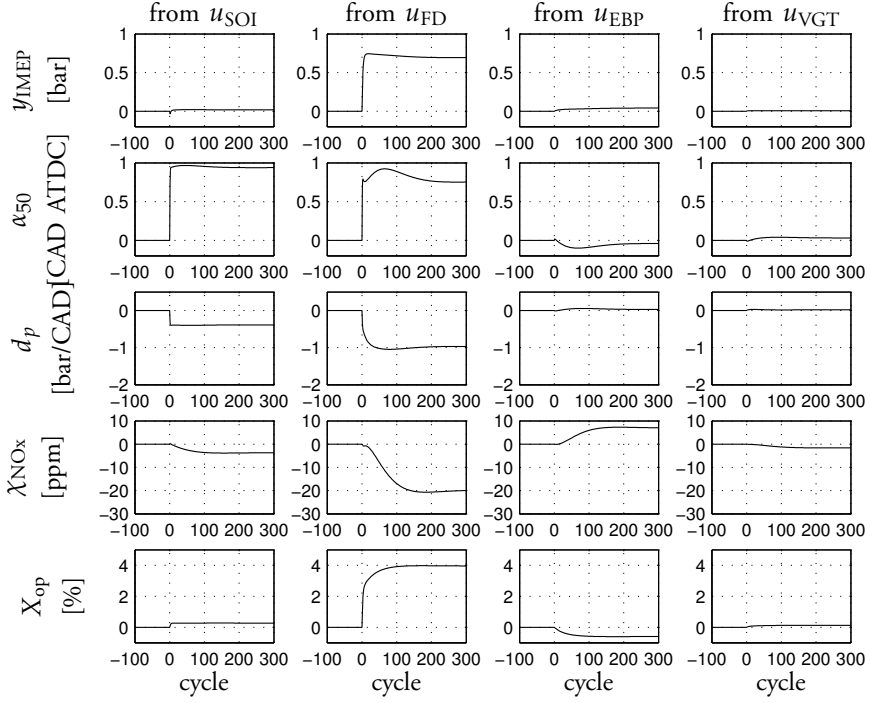
Figure 7.15 Step response of dynamic model used for model predictive control.

a controller over a large operating range that exploits the full nonlinear model found in Chapter 6 is left for future work. A fixed sixth-order linear model was used for control design, of the form

$$
\begin{aligned}
x_{k+1} &= Ax_k + Bu_k + Kw_k \\
y_k &= Cx_k + Du_k + w_k
\end{aligned}
\tag{7.27}
$$

where $u_k \in \mathbb{R}^4$, and $y_k \in \mathbb{R}^5$. In Chapter 6, models of order seven were investigated. To reduce the computational effort, a lower order was chosen for this work.

Step responses for the model are shown in Fig. 7.15. The model incorporates both fast dynamics, as in e.g. the step response from u_{SOI} to α_{50} which is almost instantaneous, and slow dynamics as, e.g., the step response from u_{EBP} to χ_{NOx} which takes more than 100 cycles to settle.

Design choices for the model predictive controller   A general overview of linear MPC was presented in Chapter 3. A number of measures were taken to transform

the high-level control objectives into this MPC framework. The following design choices were made in the setup of the model predictive controller:

- A high weight was put on reference tracking of y_{IMEP} to obtain a fast torque response.

- A reference value was set for α_{50} to achieve combustion phasing close to maximum brake torque timing. Prior information is needed to determine the correct reference value.

- A reference value of 0 was specified for χ_{NOx}.

- A load-dependent reference value was set for X_{op}. The reference value was set low enough to avoid excessive soot formation. It would be preferred to have an asymmetric cost function for X_{op} that penalized opacity above the reference, but not under. As this was not possible in the MPC implementation, a load-dependent reference was used.

- A maximum limit was set on X_{op} to avoid very large peaks in soot emissions during transient operation, where reference tracking of y_{IMEP} would otherwise take precedence over keeping the reference value for X_{op}. Such high values of soot emissions may exceed the capacity of the aftertreatment system for soot, and may also clog engine pipes.

- A maximum limit was set on d_p to avoid excessive audible noise.

- A target value was set for u_{VGT}. Without such a target, maximum allowed turbocharging would be applied in stationarity in order to obtain the best possible NO_x-soot trade-off. In such case, u_{VGT} would loose control authority through saturation during transients, and fuel consumption might also suffer.

- A slack variable was used for constraint softening.

- Constraints were specified for minimum and maximum values and rates of all control variables in order to take into account physical constraints on the actuators and include some safety margins.

- A prediction horizon of 100 engine cycles was used.

- The set of control action samples was chosen as $\mathcal{T}_u = \{0, 2, 4\}$, which was deemed to give an acceptable trade-off between performance and computational complexity.

All six cylinders of the engine were operated, but for simplicity, the controller was based on feedback from Cylinder 5 only for the cylinder-individual measured variables y_{IMEP}, α_{50}, and d_p. Also, the same values were used for all cylinders for the cylinder-individual actuator variables u_{SOI} and u_{FD}.

Experimental Results

The experiments were performed on the D13 engine. The Model Predictive Control Toolbox of Matlab R2008b was used to implement the controllers [Mathworks, 2008].

Change in reference load   Experimental results for changes in reference value for y_{IMEP} around the chosen operating point are shown in Fig. 7.16. It can be seen that reference tracking of y_{IMEP} was fast and accurate. A change in load from $y_{IMEP} = 6$ bar to $y_{IMEP} = 8$ bar was achieved in 7 engine cycles, corresponding to 0.7 s at an engine speed of $_{engine} = 1200$ rpm. The variance in y_{IMEP} was substantially larger at load $y_{IMEP} = 6$ bar, indicating that the model is less accurate at this operating point.

When load was increased at engine cycle 250, opacity increased and momentarily exceeded the limit. The controller took several actions to bring down opacity. When the load reference value was increased, the EBP valve was adjusted to reduce the amount of recycled exhaust gases, and thus reducing soot formation. Injection timing was also advanced in order to get earlier combustion and less soot formation. Airpath and fuel-path actuators were thus automatically coordinated to satisfy the control objectives.

Also, the controller successfully combined feedforward and feedback functionality. When load was increased, the model predicted that opacity would come to exceed the limit, and immediately adjusted u_{EBP} and u_{SOI}—corresponding to feedforward control. When the measured opacity exceeded the limit a few cycles after the change in reference load, all variables were further adjusted to quickly bring opacity below the limit—corresponding to feedback control.

Combustion phasing α_{50} was maintained close to its reference value throughout the experiment. Peak pressure derivative d_p did not approach its limit of $d_p = 20$ bar/CAD during the experiment. Emissions of NO_x were minimized subject to constraints and reference values of all other variables throughout the experiment. Compared to other variables, χ_{NOx} varied slowly throughout the experiment. This was due to the fact that NO_x formation is influenced by many slow processes such as EGR flow and heating and cooling of cylinder walls (see Fig. 7.15), as well as response time in the NO_x sensor (0.75 s for 33% to 66% rise). The influence of the VGT was negligible at the investigated operating point, and it was kept close to its setpoint.

Change in load and speed around the operating point   Figure 7.17 shows experimental results for changes of both load and speed around the reference point. Tracking of y_{IMEP} was accurate throughout the experiment, tracking of α_{50} was successful except for the cases where load was increased and the opacity limit was exceeded. Emissions of NO_x were as low as possible given the
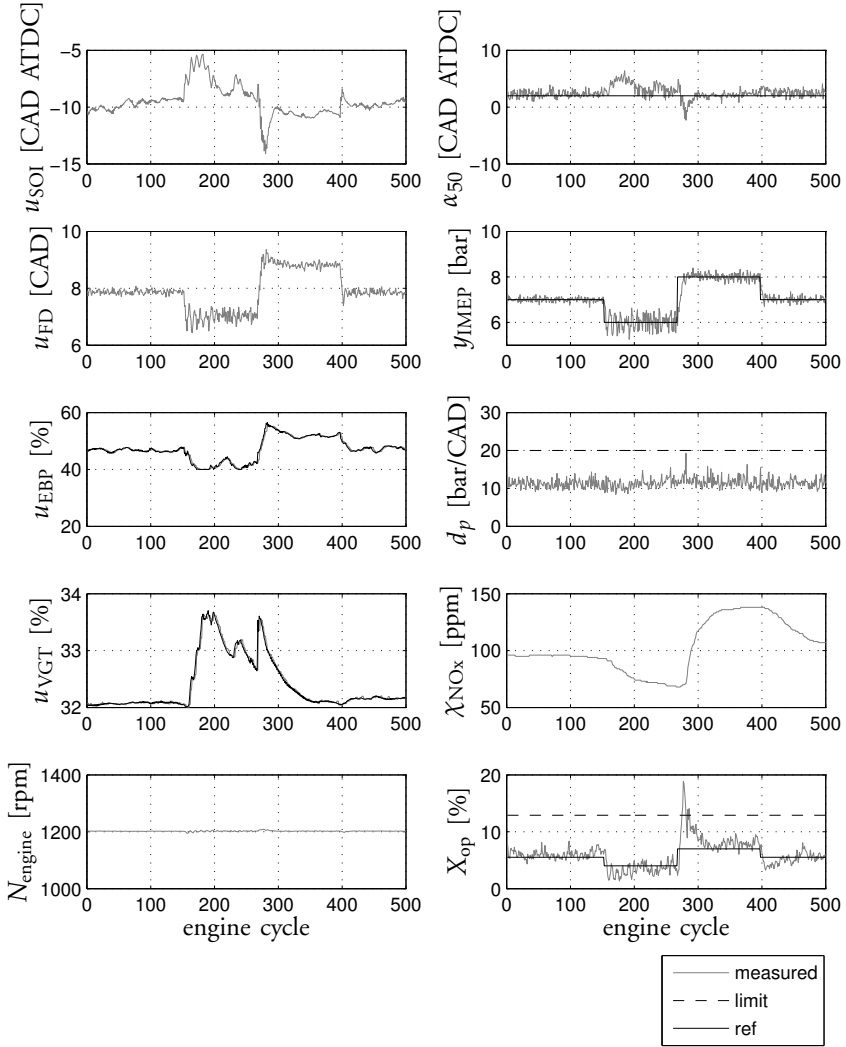
Figure 7.16   Experimental results using the MPC controller for changing the load around the investigated operating point.

specifications on opacity. The controller appears to be fairly robust to changes in load and speed in the investigated operating range.

Influence of opacity constraint   Figure 7.18 shows a change in load from $y_{IMEP} = 6$ bar to $y_{IMEP} = 8$ bar for two different experiments. The first, labeled

131

'original' is the same as shown in Fig. 7.16. In the second experiment, the same controller was used, except that the constraint on opacity was removed. As can be seen, the peak in opacity after the change in reference load was larger for the second case. The largest difference between the two controllers can be seen in u_{SOI} and α_{50}. With the opacity constraint present, the controller advances combustion phasing compared to the setpoint, in order to reduce opacity.

Comments and Conclusions

Model predictive control was used for engine control with the aim of simultaneously controlling load, combustion phasing, and emissions in an optimal manner, with correct trade-offs both in steady-state and during transients. The controller used direct measurements of emissions which facilitates relating high-level specifications directly to control design. Experimental results demonstrated the potential of the controller to use the available degrees of freedom from the actuators to achieve several objectives simultaneously.

There are many directions to extend the work. One direction is to further reduce the number of maps that require experimental calibration. The following a priori information is used for the controller:

- A load-varying setpoint for opacity. It would be desirable to replace this with an asymmetrical cost function, and a fixed setpoint based on what the after-treatment system can handle.

- A setpoint for α_{50} that is determined to be optimal in terms of fuel consumption. It would be better to directly measure fuel consumption and use that for feedback control. However, significant effort is required to integrate fuel consumption optimization into the MPC formulation. Fuel consumption cannot be modeled as the output of a linear(-ized) model of type (7.27) because it is not a monotonically increasing/decreasing function of the control variables. Some kind of extremum-seeking feature must be included into the controller to minimize fuel consumption on-line.

- A setpoint for u_{VGT}, also obtained from experience on optimal settings for fuel consumption. This setpoint should be removed and instead handled through on-line optimization of fuel consumption.

- Experimental data is required for identification of a dynamic model. It would be desirable to replace it by a (semi-)physical model, possibly with physical models for lower-level control loops combined with a higher-level model obtained through system identification.

There is also a great potential in designing the optimization criteria, setpoints, and constraints considering the capability of the after-treatment system.
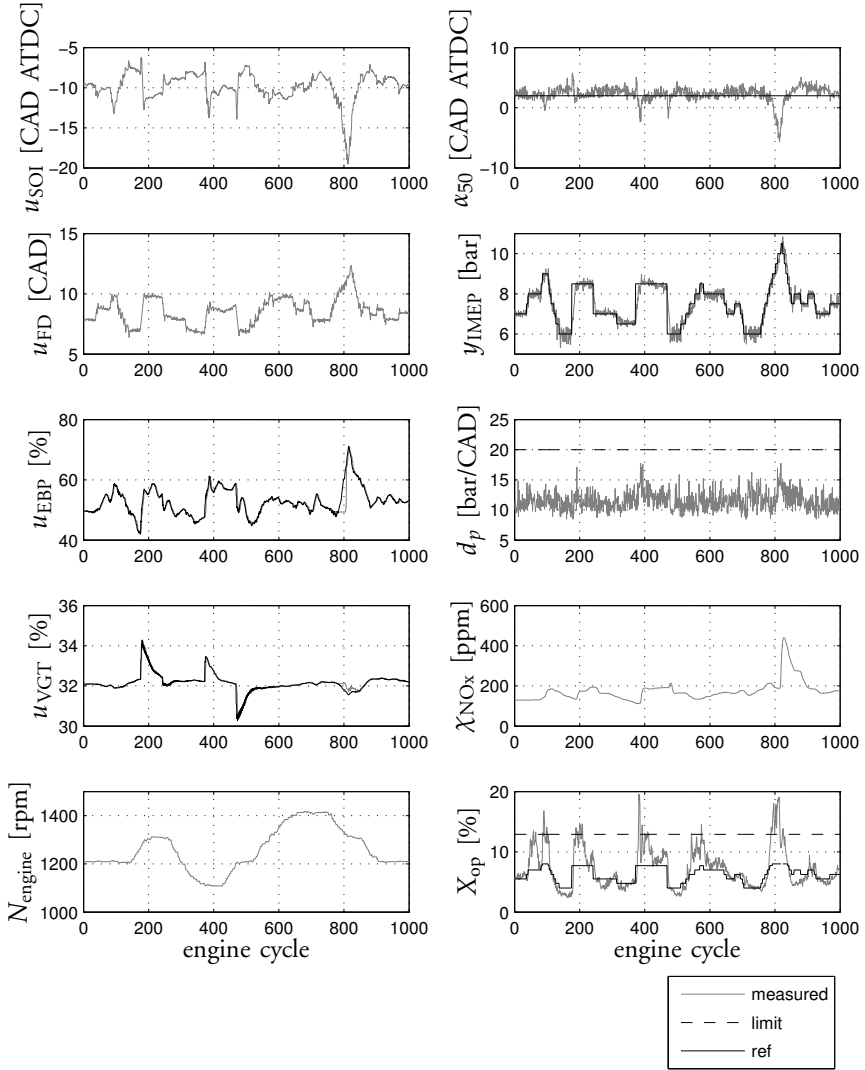
Figure 7.17 Experimental results using the MPC controller for changes of load and speed around the investigated operating point.
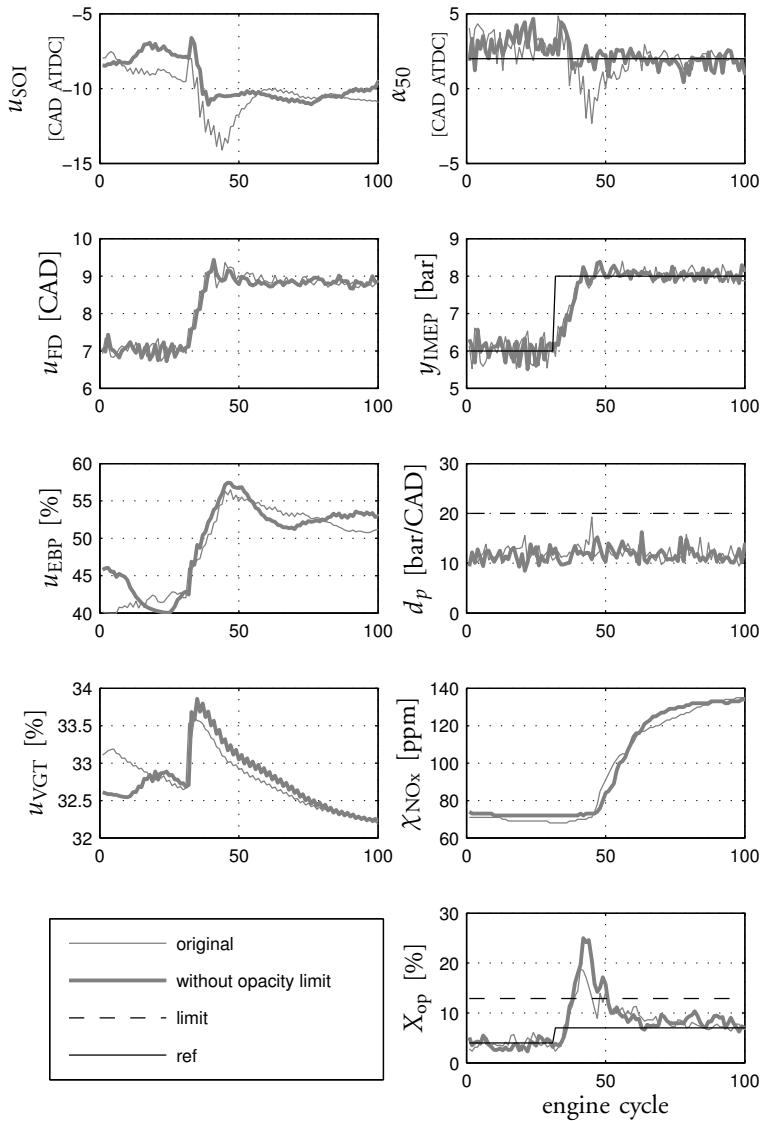
Figure 7.18 Experimental results for a load increase. The original controller had a constraint on X_{op} which it fulfills by advancing combustion phasing. The controller without opacity constraint kept the setpoint for α_{50} at the expense of a larger peak in X_{op} during the transient. The engine speed was fixed at $N_{engine} = 1200$ rpm.

8

Control of Sensitive Combustion Modes

Low-emission combustion modes such as HCCI, PPC, and LTC are inherently more difficult to control than conventional diesel combustion, since they are more sensitive to operating conditions. Also, these engine concepts push operation closer to physical limits such as the knocking limit or misfiring limit.

In the previous chapter, feedback control aimed to optimize the combustion process and manage the trade-offs in terms of high-level specifications. For highly sensitive combustion concepts, feedback control is not only a means to optimize the combustion process, but also a necessity as it is not possible to achieve reliable operation without feedback. In this chapter, control as an enabling technology is studied in two different contexts. The first is fully premixed HCCI combustion, where a control structure is presented for extending the operating range of combustion phasing control. The second is a form of dual-fuel operation, where feedback control of the fuel injection gives an automatic calibration of cylinder-to-cylinder variations.

8.1 Stabilization of Combustion Phasing in an HCCI Engine

The HCCI engine does not have an actuator that directly controls ignition, such as the spark in SI engines or the fuel injector in diesel engines. This makes combustion phasing very sensitive to operating conditions such as speed, load, and inlet temperature. Cylinder wall temperature also influences the combustion, introducing cycle-to-cycle couplings that make the combustion phasing process a dynamic system. At high loads, the combustion phasing dynamics have been shown to be unstable; early combustion leads to high cylinder wall temperatures which advances combustion even further in the subsequent cycle [Olsson et al., 2002].

The cycle-to-cycle and cylinder-to-cylinder variations in combustion phasing should be kept small in order to ensure reliable operation of the engine. To maximize efficiency, the combustion should occur shortly after the top dead center, but it may have to be retarded to avoid damaging the engine. If combustion occurs too early, there will be large in-cylinder pressures that may harm the engine. If combustion phasing is too late, combustion may be incomplete and result in high HC and CO emissions, as well as reduced efficiency [Olsson et al., 2002]. Closed-loop control of the combustion phasing enables reliable operation over the operating range of the engine [Zhao and Asmus, 2003].

Various actuator options have been suggested for control of combustion phasing in HCCI engines. With *dual-fuel actuation*, the ratio of two fuels with different auto-ignition properties is varied [Olsson et al., 2001; Strandh et al., 2004]. With *variable valve actuation* (VVA), the crank angle degrees of inlet and exhaust valve openings and closings are varied. Different setups are possible where some valve timings are fixed and others are varied, e.g., variable inlet valve closing (IVC) [Agrell et al., 2003; Strandh et al., 2005]. Variable valve actuation can influence the combustion process in more than one way; inlet valve closing can be used to alter the effective compression ratio, and exhaust valve timings can be used to manipulate the amount of residual gases in the cylinder from one cycle to next [Shaver et al., 2006]. Other actuator options for combustion phasing control are variable compression ratio (VCR) [Haraldsson et al., 2002], or fast thermal management [Martinez-Frias et al., 2000].

In multi-cylinder engines, cylinder-individual actuation is required since thermodynamic conditions may vary greatly between cylinders. All the previously mentioned actuation options can be made cylinder-individual with appropriate instrumentation. Other means of influencing combustion phasing may have to be common to all cylinders. Such actuation options include variable EGR or variable inlet temperature if a common heater is to be used for the inlet air to all cylinders.

Independent of the choice of actuator, saturation will limit the operating range in HCCI mode by not providing enough energy to the fuel-air mixture for auto-ignition at low loads, and not being able to limit the heat release sufficiently at high loads. It is therefore of interest to study combinations of actuators to increase capacity to adapt to operating conditions thus extending the HCCI operating range.

This chapter is based on [Karlsson et al., 2007] and presents a method of combining IVC and EGR valve actuation to control combustion phasing over a larger operating range than is possible using IVC actuation alone. The idea of a controller that combines these two control variables was first suggested as a topic of future work in [Agrell et al., 2003], and elaborated upon in [Agrell and Linderyd, 2005]. In that work, no specific control structure or control

design approach was suggested, and multi-cylinder engine issues were not treated explicitly. The publication [Karlsson et al., 2007] presented the first experimental verification of successfully combined IVC and external EGR actuation.

Effect of EGR and IVC on Combustion Phasing

The relationship between inlet valve closing u_{IVC} and combustion phasing α_{50} in steady-state is shown in Fig. 8.1. It can be seen that the same α_{50} can be obtained by closing the inlet valve either during the expansion stroke before bottom dead center or during the compression stroke after bottom dead center. In this work, only valve closing after bottom dead center is applied.

A step response from u_{IVC} to α_{50} is shown in Fig. 8.2. It can be seen that the effect on α_{50} is almost immediate.

The position of the exhaust back pressure valve u_{EBP} was used as actuator to manipulate the EGR rate. In Fig. 8.3, the steady-state effect of the valve position u_{EBP} on α_{50} at engine speed $N_{engine} = 1000$ rpm and fuel energy $W_{in} = 1000$ J/cycle is shown. Valve positions should here be interpreted as percentage closed, where $u_{EBP} = 0$ corresponds to a fully open valve and $u_{EBP} = 100$ to a fully closed valve. The inlet manifold CO_2 concentration is also shown in the figure. In general, increasing u_{EBP} also increases the concentration of CO_2 in the intake. The relationship between u_{EBP} and CO_2 is nonlinear, whereas the relationship between intake CO_2 and α_{50} is fairly linear in the investigated interval.

A step response from u_{EBP} to α_{50} is shown in Fig. 8.4. Due to dynamics in the EGR gas path, the effect of u_{EBP} on α_{50} is slow, compared to the effect of u_{IVC}. The time constant of this step response will vary depending on engine load and speed.
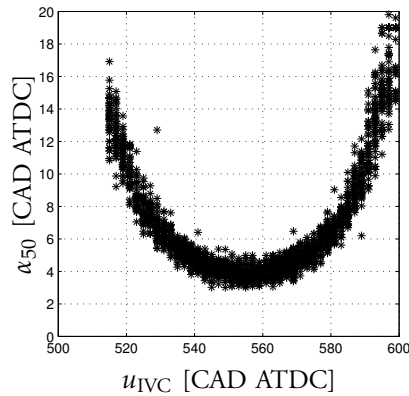

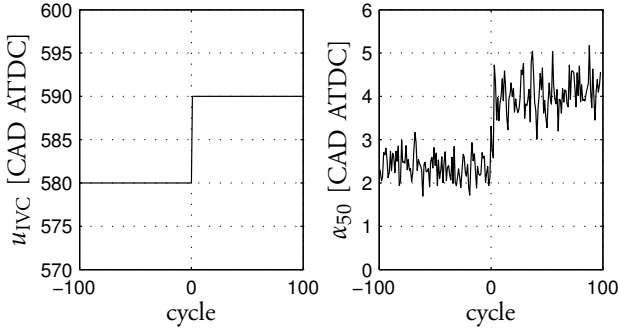**Figure 8.1** Nonlinear steady-state relation between u_{IVC} and α_{50}.

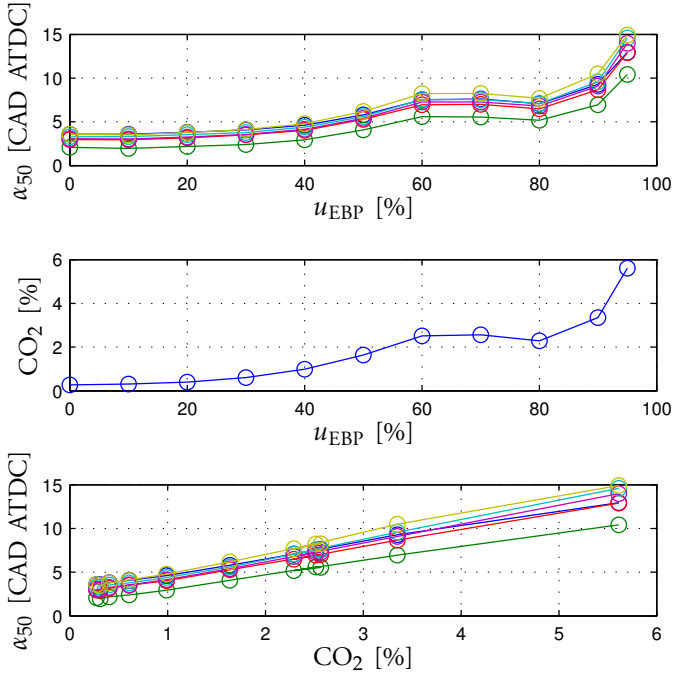**Figure 8.2** Step response from u_{IVC} to α_{50}.

Figure 8.3 Measured steady-state relations between the exhaust back pressure valve position u_{EBP}, the CO_2 concentration in the intake, and the resulting α_{50} for the six cylinders. It can be noted that the relationship between u_{EBP} and α_{50} is nonlinear, whereas the relationship between inlet manifold CO_2 and α_{50} is approximately linear for these data.
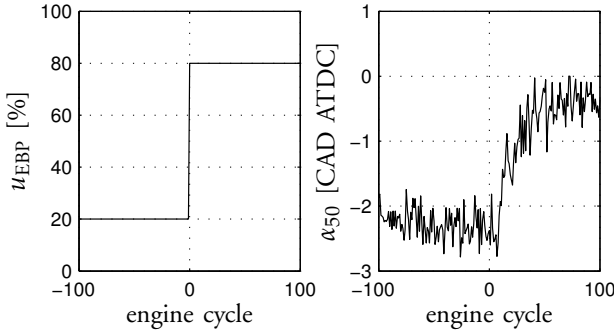
Figure 8.4   Step response from u_{EBP} to α_{50}.

Control Structure

While both u_{IVC} and u_{EBP} can be used to control the combustion phasing α_{50}, the effects of these control variables are not identical. The input u_{IVC} is cylinder-individual whereas u_{EBP} is a scalar control variable that will affect the combustion phasing of all cylinders. And while the effect of u_{IVC} on α_{50} is almost immediate, the time constant from u_{EBP} to α_{50} is in the order of 30 engine cycles. To find a suitable control structure, the different characteristics of the two control variables, u_{IVC} and u_{EBP}, must be taken into account.

As described in Chapter 3, mid-ranging is a control structure designed for processes with two control variables and only one process variable to control. Typically it is used to combine a fast accurate control variable with a small operating range with a slow, less accurate control variable to extend the operating range. Here it will be shown that the control structure is well suited for the combustion phasing control problem.

A control structure for $u_{\mathbf{IVC}}$ and $u_{\mathbf{EBP}}$ The structure of the basic mid-ranging controller is shown in Fig. 8.5.

The task of using u_{IVC} and u_{EBP} to control α_{50} fits nicely into this scheme, with $u_1 = u_{\mathrm{IVC}}$ and $u_2 = u_{\mathrm{EBP}}$. With one cylinder only, the structure in Fig. 8.5 could be immediately adopted. To handle a multi-cylinder engine with N_{cyl} cylinders, a modification is suggested where the inlet valve closing signals $u_{\mathrm{IVC},1} \ldots u_{\mathrm{IVC},N_{\mathrm{cyl}}}$ are mapped into a single input to C_2 according to Fig. 8.6.

The control structure leaves much freedom for design. The controllers C_1 and C_2, the setpoints u_r, and the map $f(\cdot)$ can be chosen to achieve the desirable speed and robustness of the system. The function $f(\cdot)$ should reflect
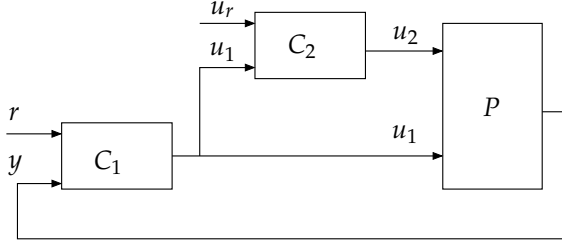
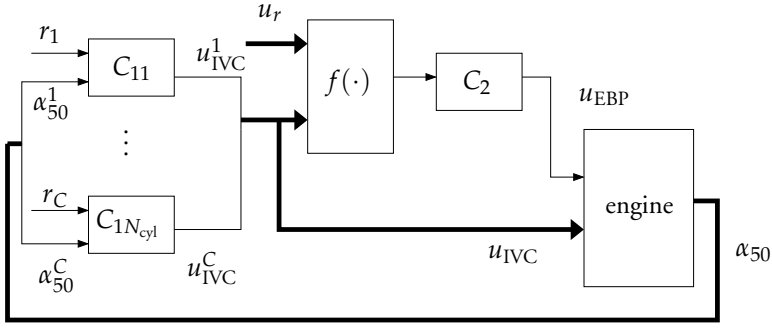**Figure 8.5**   The basic mid-ranging control structure.

Figure 8.6   Control scheme for control using u_{IVC} and u_{EBP} for C-cylinder engine. Thick arrows represent vector signals.

how far u_{IVC} is from saturation. One choice may be

$$f(u_{\text{IVC}}, u_r) = \frac{1}{N_{\text{cyl}}} \sum_{i=1}^{N_{\text{cyl}}} (u_r^i - u_{\text{IVC}}^i) \qquad (8.1)$$

where average deviation from the setpoints u_r^i is computed. The setpoints u_r^i should then lie in the middle of the operating range of u_{IVC}. Another option is to increase the weighting of a signal when it saturates, such as in the map

$$f(u_{\text{IVC}}, u_r) = \frac{1}{N_{\text{cyl}}} \sum_{i=1}^{N_{\text{cyl}}} (u_r^i - u_{\text{IVC}}^i) + \frac{K_s}{N_{\text{cyl}}} \sum_{i=1}^{N_{\text{cyl}}} (\text{sat}(u_{\text{IVC}}^i) - u_{\text{IVC}}^i) \qquad (8.2)$$

where K_s is some positive constant, or to only consider the maximum and

minimum u_{IVC}^i, as in

$$f(u_{\text{IVC}}, u_r) = u_{r0} - \frac{\max(u_{\text{IVC}}) + \min(u_{\text{IVC}})}{2} \tag{8.3}$$

Process nonlinearities   The effect of u_{IVC} on α_{50} is nonlinear, as seen in steady-state in Fig. 8.1. Tuning a linear controller with satisfactory performance in a large operating range may therefore be difficult. Assuming that the nonlinear process can be modeled by a Hammerstein system, a compensation for the nonlinearity can be included in the controllers $C_{11}, \ldots, C_{1N_{\text{cyl}}}$, as suggested in [Strandh et al., 2005]. The output of the controller is transformed using the inverse of the estimated nonlinearity such that the system from the output of the linear controller to the process output α_{50} is approximately linear, see Fig. 8.7.

A similar compensation for the nonlinearity from u_{EBP} to α_{50} would be appropriate, but was not included in the experimental work presented here.
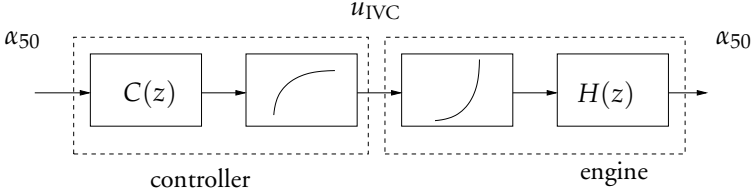

Figure 8.7   The structure of the controllers C_{1i} where a linear controller $C_{\text{nom}}(z)$ is combined with the inverse of the process nonlinearity to achieve an approximately linear closed-loop system.

Experimental Setup

The Volvo D12 engine was operated in pure HCCI mode with port fuel injection only. The two injectors at the inlet of each cylinder were supplying ethanol and n-heptane, respectively. The fuel energy ratio was fixed at 75% ethanol and 25% n-heptane. Inlet air temperature was controlled by the electrical heater, and was kept constant by a feedback controller.

Experimental Results

The mid-ranging control structure was implemented in the engine control system. PID controllers were used for $C_{11}, \ldots, C_{1N_{\text{cyl}}}$ and a PI controller was used for C_2. The implementation structure of the discrete-time controllers was taken from [Åström and Wittenmark, 1997], and included anti-windup and a filter on the derivative term. The controllers were implemented with a sampling time

of one engine cycle. The tuning was performed manually, and robustness was prioritized over closed-loop bandwidth.

The mapping $f(\cdot)$ from the vector u_{IVC} to the input to C_2 was chosen as

$$f(u_{\mathrm{IVC}}, u_r) = u_{r0} - \frac{1}{6}\sum_{i=1}^{6} u_{\mathrm{IVC}}^{i} \tag{8.4}$$

which proved to work well in practice.

The inputs u_{IVC}^{i} were constrained to the range $u_{\mathrm{IVC}}^{i} \in [568,607]$ CAD where the nonlinearity in Fig. 8.1 could be inverted in a robust way and the cycle-to-cycle variations were kept at an acceptable level. The setpoint for u_{IVC} was chosen as $u_r = 587$ CAD.

Step responses at constant speed   In Fig. 8.8 the results of an experiment where the EBP valve was fixed at $u_{\mathrm{EBP}} = 45$ is shown. The engine speed was $N_{\mathrm{engine}} = 1000$ rpm and the total fuel energy $W_{\mathrm{in}} = 1200$ J/cycle. It can be seen that there is a large difference among the cylinders when it comes to the u_{IVC} required to hold a constant α_{50}. These imbalances could arise from different thermodynamic conditions; the cylinders located furthest from the heater will have a cooler mixture entering the cylinder and therefore a later combustion phasing for the same u_{IVC}. The temperature of the cooling water will also affect the combustion phasing. In the figure, we can see that taking this span into account, there is a very narrow operating range for u_{IVC}. At the lower α_{50} setpoint, u_{IVC} saturates at its lower limit for one cylinder, and when the setpoint is retarded by only 3 crank angle degrees, u_{IVC} saturates at its upper limit for other cylinders.

Results from an experiment using the mid-ranging control structure are shown in Fig. 8.9. The same values for speed, total fuel energy and fuel ratio as in Fig. 8.8 were used. We can now see the benefits of adjusting the EGR rate. When the setpoint for α_{50} was increased, u_{IVC} also increased and approached its upper limit. The second controller then reacted by increasing u_{EBP} which means that a lower u_{IVC} was required to keep the setpoint for α_{50}, and u_{IVC} was eventually reset to the middle of the operating range.

Speed transients   To test the performance of the control system during transients, experiments were performed with fuel energy $W_{\mathrm{in}} = 1200$ J/cycle and engine speed varying from $N_{\mathrm{engine}} = 1000$ rpm to $N_{\mathrm{engine}} = 1400$ rpm.

In Fig. 8.10, results are shown for the speed transient with constant u_{EBP}. It can be seen that u_{IVC} rapidly saturates at its lower value as the engine speed increases, and the setpoint for combustion phasing cannot be held. At $N_{\mathrm{engine}} = 1000$ rpm, u_{IVC} saturates at its upper limit for some cylinders. It can
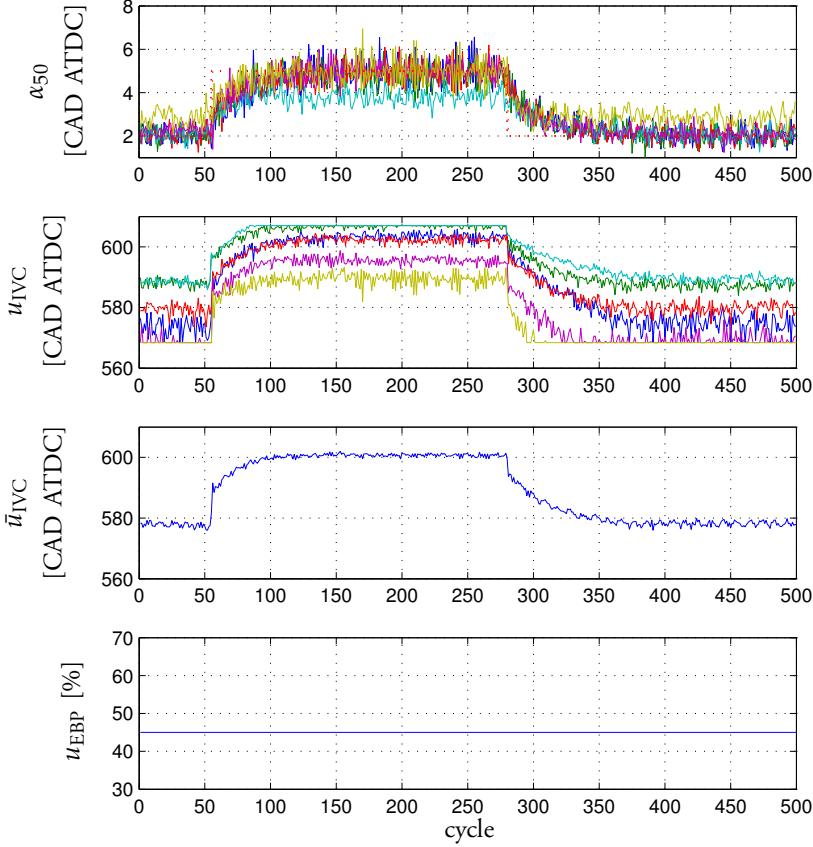
Figure 8.8 Step response experiment with constant u_{EBP}. In the upper two plots, α_{50} and u_{IVC} are shown for all six cylinders. The third plot shows the average u_{IVC}. Saturation occurs for some cylinders both for the low and high combustion phasing setpoint.

be concluded that the control variable u_{IVC} cannot keep a constant combustion phasing, even over this modest variation in speed.

In Fig. 8.11, results from a corresponding experiment with the mid-ranging control structure are shown. The combustion phasing α_{50} is kept at its setpoint throughout the experiment. The second control variable u_{EBP} adjusts so that u_{IVC} will remain within its operating range for all cylinders, allowing for rapid cycle-to-cycle adjustments.

The effect of the nonlinearity from u_{EBP} to α_{50} shown in Fig. 8.3 can
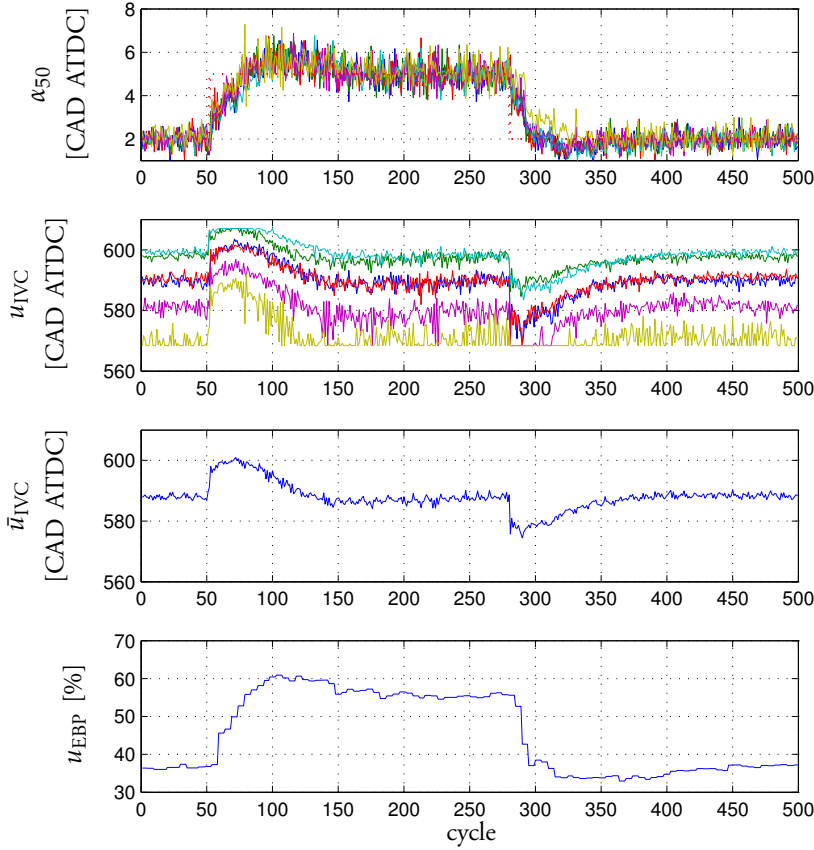
Figure 8.9   Step response experiment with the mid-ranging control structure. By adjusting the slow actuator u_{EBP}, the controller prevents permanent saturation of the fast actuator variable u_{IVC}, compare Fig. 8.8.

be seen towards the end of this experiment. Here, u_{EBP} passes through the range $[60, 80]$ where the effect on α_{50} is small. Therefore, there is a delay in the reset of u_{IVC} which causes a small control error in α_{50} at engine cycles around 950. The error is eventually reset, but a compensation for the nonlinearity could improve performance.

The control system was also tested with variations in injected fuel energy with similar results.
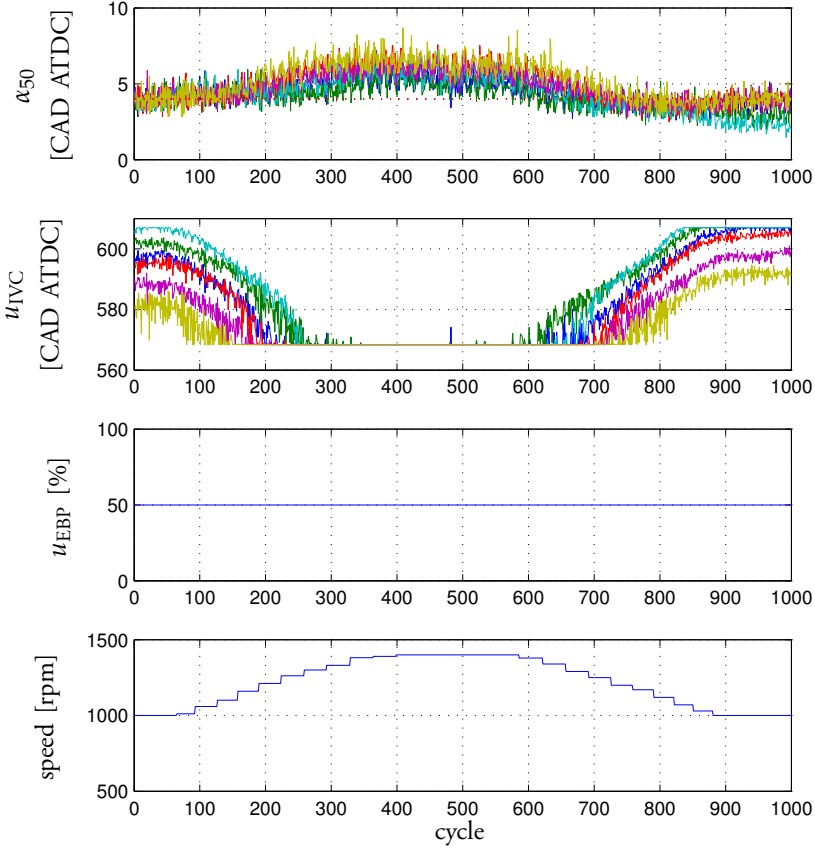
Figure 8.10   Speed transient with constant u_{EBP}. Even for this modest variation in speed, the actuator variables u_{IVC} hit both their upper and lower saturation limits. The setpoint $\alpha_{50}^{ref} = 4$ CAD ATDC cannot be maintained due to actuator saturation.

Conclusions on HCCI Combustion Control

The experimental results verified that the problem with a limited operating range of u_{IVC} for control of α_{50} can be successfully remedied by automatically adjusting the EGR rate, and the mid-ranging control structure was shown to be well suited for the combustion phasing control problem. The control structure is intuitive and simple to implement. Since it changes u_{EBP} continuously to reset u_{IVC} to its setpoint, it does not require extensive calibration of engine maps and could also be considered for other actuator combinations, e.g., valve timings and
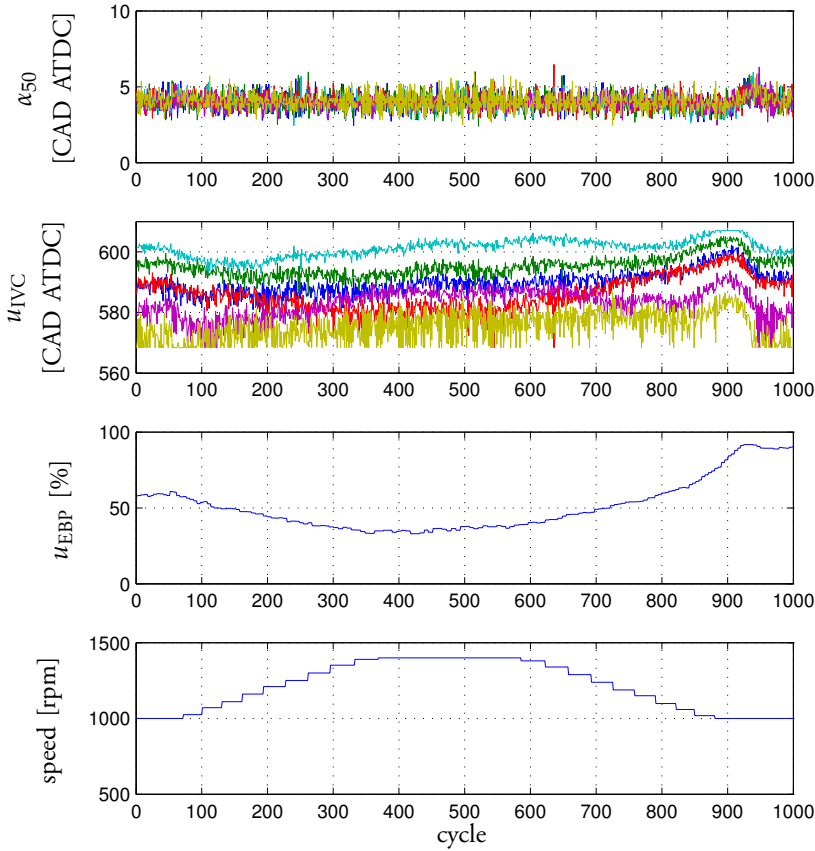
Figure 8.11   Speed transient with mid-ranging controller. Compared to Fig. 8.10, the mid-ranging controller prevents saturation and maintains combustion phasing at α_{50}^{ref} for almost the entire transient by adjusting u_{EBP}.

intake air heating.

A few shortcomings in the performed experiments can be mentioned. In Figs. 8.9 and 8.11, it can be seen that setpoint tracking was rather slow. The controllers were tuned conservatively. Feasible controller gains were limited by the slow dynamics of the u_{EBP} signal and by the process noise. It is likely that faster convergence to the setpoint could be achieved using more carefully tuned controllers. Alternatively, an MPC controller with a cost function designed to produce the mid-ranging effect could considered. The EGR rate has other

effects on the engine besides combustion phasing. When u_{EBP} is fixed by the α_{50} control structure, the possibility to manipulate u_{EBP} to optimize efficiency and emissions is reduced.

8.2 Control of Dual-Fuel Combustion

Fumigation is a form of dual-injection engine operation where part of the fuel is injected into the intake port and premixed with the intake air, and part of the fuel is injected directly into the cylinder. The premixed and direct-injected fuels may be of the same kind, or fuels with different properties may be used to achieve the desired combustion process. The two fuel injection systems provide a large flexibility in influencing the combustion, which implies that different combustion modes could be used in different parts of the operating range of the engine. There is thus a potential to combine the best features of port-fuel injection and direct injection to achieve low-emission combustion over a large operating range.

Various motivations to study fumigation have been presented in the literature. With low levels of premixed fuel, operation is close to that of a diesel engine. In this case, the premixed fuel can reduce the ignition delay and pressure oscillations, ensuring a smoother operation at high loads [Zaidi et al., 1998], similar to a pilot injection. With diesel used for both the premixed and direct injected fuel, fumigation is a way of avoiding the knock problem associated with diesel HCCI with port fuel injection [Odaka et al., 1999; Canova et al., 2007]. With high levels of premixed high-octane number fuel, engine operation is close to that of a spark ignition engine with the direct injected fuel replacing the spark [Kim et al., 2004; Alger et al., 2005]. With biogas as the premixed fuel and biodiesel as the direct injected fuel, this method has been presented as an engine concept for alternative fuel operation [Volvo Group, 2007].

Another term for fumigation is RCCI (reactivity-controlled compression ignition), introduced by researchers at the University of Wisconsin in a series of publications [Kokjohn et al., 2009; Curran et al., 2010; Kokjohn et al., 2011; Splitter et al., 2011]. These publications have shown that the RCCI concept can provide high thermal efficiency with very low NO_x and PM emissions.

This section presents experimental work on fumigation originally published in [Ekholm et al., 2008]. In the study, ethanol was used as premixed fuel, and was then ignited by a small diesel injection into the cylinder. A major advantage compared to the work on pure port-fuel injection HCCI presented previously is that no preheating is required for the ethanol to auto-ignite. The diesel fuel injection also provides additional degrees of freedom for controlling combustion.

The direct-injected fuel could be expected to introduce stratification during

the combustion process. A major point of interest was therefore to study emissions and achievable operating range in this combustion mode. The aim was to obtain HCCI-like emissions over a large operating range.

Motivation for Closed-Loop Control

The fumigation setup used in this work has some similarities to dual-fuel HCCI operation. By increasing the ratio of fuel energy coming from diesel, combustion becomes faster. The fumigation setup also presents additional features and complications. With the direct-injection diesel system, it is possible to modify not only the amount of diesel injected but also injection timing. With early injection, operation is closer to HCCI because the diesel fuel has time to partially mix with the ethanol-air mixture before combustion.

The setup thus opens for the same difficulties in terms of controlling the combustion process as dual-fuel HCCI operation [Olsson et al., 2001]. A too high diesel ratio would cause early ignition and thus high peak pressures and high pressure derivatives, whereas a too low diesel ratio could result in incomplete combustion and high HC emissions.

To illustrate the challenge of fumigation operation, Fig. 8.12 shows in-cylinder pressure, cumulative heat released, and heat release rate for the six cylinders during one engine cycle. Nominal fuel injection parameters were the same for the six cylinders, i.e., the same signals were sent to the injector hardware. As can be seen, there is a large difference in the combustion process between the cylinders. It appears that for Cylinder 1, the initial heat released from combustion of the diesel fuel is not sufficient to ignite the ethanol. On the other hand, for Cylinder 6, heat release is very rapid, leading to high pressure derivatives.

There are many plausible causes for cylinder-to-cylinder differences in combustion, including:

- Fuel injectors do not inject equal amounts of fuel.

- Compression ratio differs between cylinders due to geometrical variations.

- Volumetric efficiency varies due to variations in inlet manifold fluid flow.

- Temperature varies in cylinder walls or intake air/EGR, which results in different thermodynamic conditions for auto-ignition.

Cylinder-to-cylinder variations have been reported as an issue also in a previous fumigation study [Alger et al., 2005], where EGR concentration variations were thought to be the main cause.

A major contributor to cylinder-to-cylinder variations in combustion in the current study was thought to be the diesel fuel injection system, where unit injectors designed for conventional diesel operation were used. These injectors
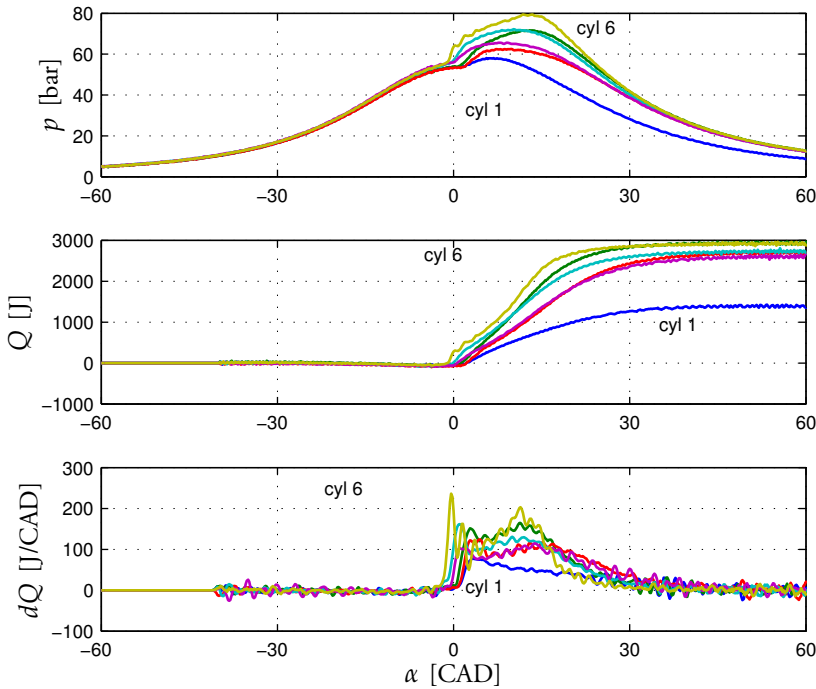
Figure 8.12   Pressure p, cumulative heat released Q, and filtered heat release rate dQ for the six cylinders during one cycle of steady-state dual-fuel operation with equal control variable commands for all cylinders. Note the large cylinder-to-cylinder variations. Combustion is incomplete in Cylinder 1, and heat release is too rapid in Cylinder 6.

are calibrated for substantially larger diesel flows, meaning that the accuracy may be poor for the small flows used here. That implies that even though the injection duration was nominally the same for all cylinders, the injected amount may vary by a large factor. For extended studies of this fumigation setup, the injection system should be adapted to lower diesel flows. Such measures would probably reduce the cylinder-to-cylinder variations seen in Fig. 8.12 substantially, but even so, there are other sources of cylinder-to-cylinder combustion variations that must be managed, as noted in [Alger et al., 2005].

The cylinder-to-cylinder variations severely limit the ability to perform the fumigation experiments as well as the validity of the results. Cylinder-averaged measurements of parameters of interest such as emissions and efficiency are of little interest when the combustion processes differ as much as in Fig. 8.12. Moreover, too high peak cylinder pressures or high pressure derivatives in one

cylinder would activate the safety mechanisms in the control system and shut down fuel injection. In short, in order to perform the experiments on fumigation, it is required to compensate for the variations.

Control Structure

To harmonize combustion between cylinders, a feedback controller was developed to manipulate the amounts of the two fuels. As feedback variables, the maximum pressure derivative d_p, and the net indicated mean effective pressure, $IMEP_n$, were used. It was observed that by balancing $IMEP_n$ and d_p between the cylinders, the heat release profiles were also harmonized.

Experimental testing showed that the maximum pressure derivative d_p was strongly correlated with the amount of diesel injected. Therefore, the duration of diesel injection u_{FD} was used to control the pressure derivative to a setpoint, and the amount of ethanol injected u_{PF} was used to control $IMEP_n$ to a setpoint. The effect of varying the amount of diesel could be studied by varying the maximum pressure derivative setpoint. PI controllers were used to control both d_p and $IMEP_n$. The control structure is shown in Fig. 8.13.

Controllers were designed ignoring the coupling between the two control variables, diesel and ethanol injection, and the two measured variables, d_p and $IMEP_n$. Such couplings do exist, e.g., with a larger amount of diesel injected, $IMEP_n$ will increase as the diesel fuel energy also contributes to the work output. To avoid exciting these cross-couplings, the controllers were tuned conservatively, which was satisfactory for the steady-state operation that was the target for this work. For transient operation, a MIMO control design that takes into account the cross-coupled dynamics of the process should be developed.
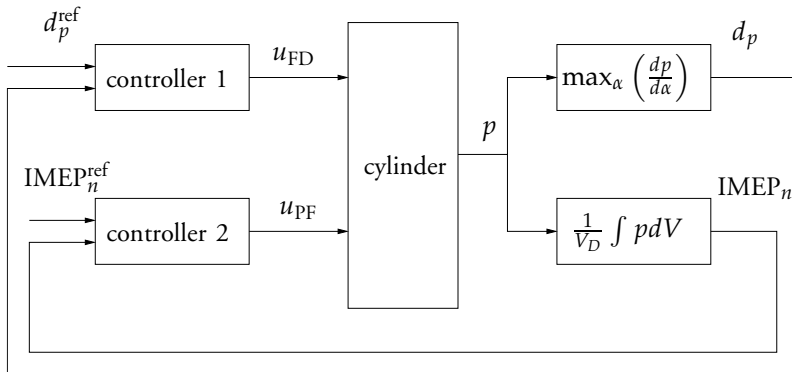

Figure 8.13 Control structure used for control of d_p and $IMEP_n$. The control variables are u_{FD} = injection duration for direct-injected fuel (diesel). u_{PF} = injection duration for port-injected fuel (ethanol).

Experimental Conditions

Experiments were performed on the D12 engine. Diesel was injected in the direct injection system, and ethanol in the port injection system. Inlet valve closing u_{IVC} was fixed at $u_{IVC} = 570$ CAD ATDC throughout these experiments. The engine speed was kept constant at $N_{engine} = 1450$ rpm. The EGR rate, the VGT actuator position, and the injection timing were adjusted manually according to operating point, as described below.

Closed-Loop versus Open-Loop Operation

Figure 8.14 shows the spread in the two measured variables d_p and $IMEP_n$ for 100 consecutive cycles with and without the controller activated. It can be seen that the cylinder-to-cylinder variations are significant in the latter case. Cylinders 1 and 6 with the lowest and highest $IMEP_n$, also demonstrate large cycle-to-cycle variations which are likely caused by incomplete combustion for Cylinder 1, and large sensitivity of d_p for high loads for Cylinder 6.

The controller successfully eliminates the systematic cylinder-to-cylinder variations, and also reduces the cycle-to-cycle variations by placing all cylinders in an operating range where the combustion process is more stable.

The control setup is thus very successful as a tool for automatic calibration in a laboratory setting. In practice, open-loop operation is preferred because it does not require sensors. An experiment was performed to see how well open-loop operation works once the diesel fuel injection system has been cal-
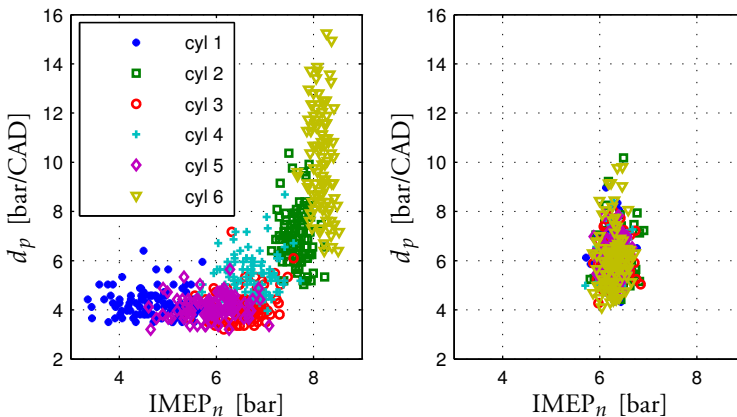

Figure 8.14   Maximum pressure derivative d_p and $IMEP_n$ for 100 consecutive cycles for the six cylinders, with all nominal conditions set equally (left), and with controller activated (right). Both cylinder-to-cylinder and cycle-to-cycle variations are reduced significantly by the controller.
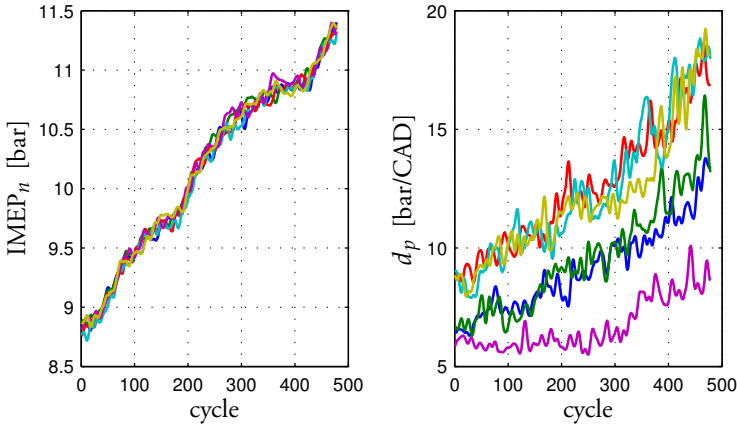
Figure 8.15 $IMEP_n$ and d_p during a load transient in open loop. Diesel injection settings were first calibrated individually for each cylinder in steady-state. These diesel injection settings were then fixed, and $IMEP_n$ was increased by increasing ethanol injection. We see that off-line cylinder-individual calibration of the injectors at one operating point does not extend well to other operating points. The data were low-pass filtered to make trends more clearly visible.

ibrated. The controller was activated to find diesel injection parameters that maintained $d_p = 7$ bar/CAD at $IMEP_n = 8.5$ bar. These diesel injection settings were then frozen and the ethanol injection duration was slowly increased to $IMEP_n = 11$ bar. Figure 8.15 shows the resulting d_p for the six cylinders.

Two conclusions can be drawn from Fig. 8.15. First, in order to keep d_p low, the amount of diesel must be carefully adjusted according to operating point. Second, settings for diesel injection duration that compensate for the cylinder-to-cylinder variations in the fuel injection system at one operating point are not immediately applicable at another operating point. Therefore, to enable operation in open loop, diesel parameters must be carefully mapped individually for each cylinder according to operating point. Open-loop operation is not impossible; there are very little dynamics from diesel injection duration to d_p, so there are no issues concerning instability necessitating closed-loop control. But to successfully operate the engine open-loop in a safe manner, careful calibration based on either extensive experimental testing or accurate models of the combustion process is required.

Heat Release Rate, Efficiency, and Emissions

Operation was tested with the controller active at 25%, 50%, and 100% of the maximum load specified for diesel operation of the engine, corresponding to BMEP = {4.6, 9.2, 18.4} bar.
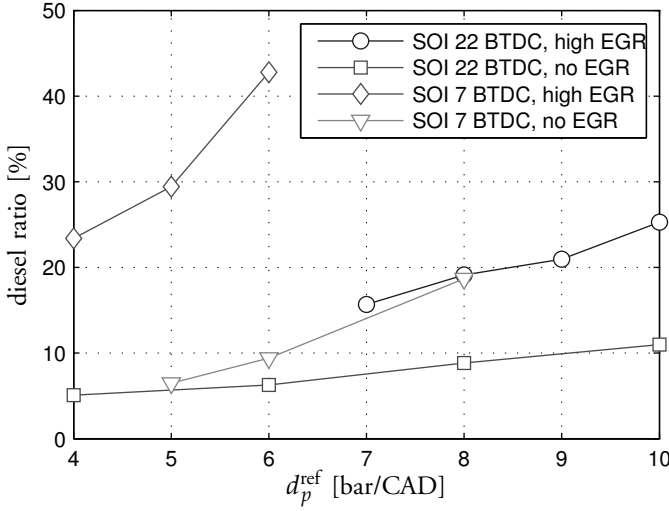
Figure 8.16 Ratio of diesel energy to total fuel energy required to keep a certain d_p for the four operation modes tested at BMEP = 4.6 bar. With pure diesel operation without EGR, average d_p was 5.4 bar/CAD.

Low load – BMEP = 4.6 bar   Four operation modes were tested:

1. Early fuel injection with high EGR rate,
   $u_{\mathrm{SOI}} = 22$ CAD BTDC, $\chi_{\mathrm{EGR}} = 50\%$.

2. Early fuel injection without EGR, $u_{\mathrm{SOI}} = 22$ CAD BTDC.

3. Late fuel injection with high EGR rate,
   $u_{\mathrm{SOI}} = 7$ CAD BTDC, $\chi_{\mathrm{EGR}} = 45\%$.

4. Late fuel injection without EGR, $u_{\mathrm{SOI}} = 7$ CAD BTDC.

For comparison purposes, the same operating point was also run with pure diesel operation without EGR.

For each of the operation modes, the ratio of fuel energy coming from diesel was varied by changing the setpoint for d_p. Figure 8.16 shows d_p setpoint versus diesel ratio for the four combustion modes. The range of d_p that was tested correspond to the range that was possible to obtain by modifying the diesel ratio without risk of misfire or too large cycle-to-cycle variations.

Heat release rates for the four combustion modes with different setpoints for d_p are shown in Fig. 8.17.
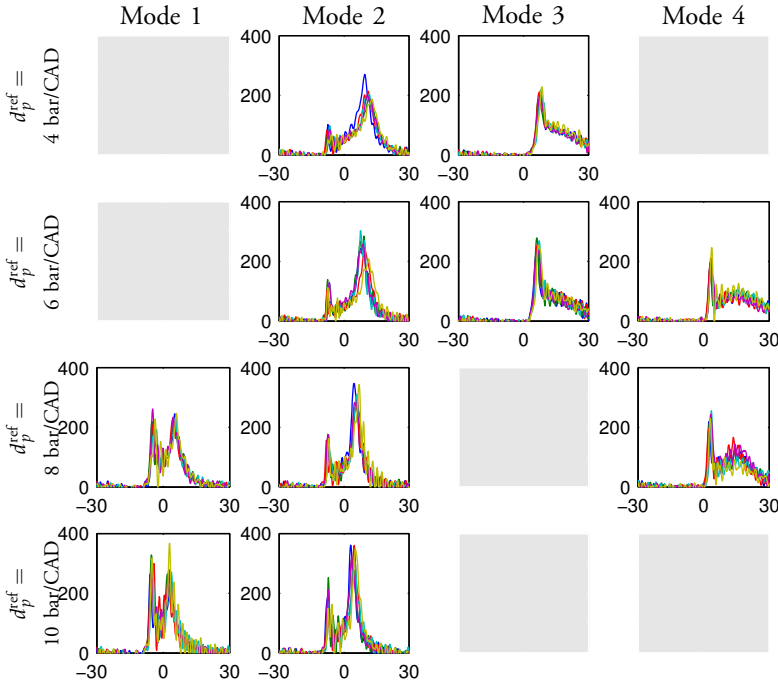
Figure 8.17   Experiments at BMEP = 4.6 bar. Heat release rates dQ [J/CAD] vs. α [CAD] for Mode 1–4 (left to right), for d_p^{ref} = 4, 6, 8, 10 bar/CAD (top to bottom).

A few things can be noted. First of all, cylinder-to-cylinder variations in heat release are small. This means that by harmonizing d_p and IMEP_n between the cylinders, the entire combustion process is harmonized. It can be concluded that d_p and IMEP_n are suitable feedback variables.

With early diesel injection, a two-stage combustion was obtained. The magnitude of the first heat release peak was strongly correlated to the amount of diesel injected, cf. Fig. 8.16. With a higher diesel ratio, the delay until the second heat release peak became shorter, and the heat release was faster. Without EGR, a smaller diesel ratio was required, and a larger part of the fuel burned in the second heat release peak.

With late diesel injection, there was a single peak in the heat release rate. Heat release started shortly after TDC, then there was a short period of high heat release rate followed by a slowly decaying combustion rate.

Brake efficiencies and emissions are shown in Fig. 8.18. HCCI-like levels of NO_x emissions were only obtained through late diesel injection and high EGR
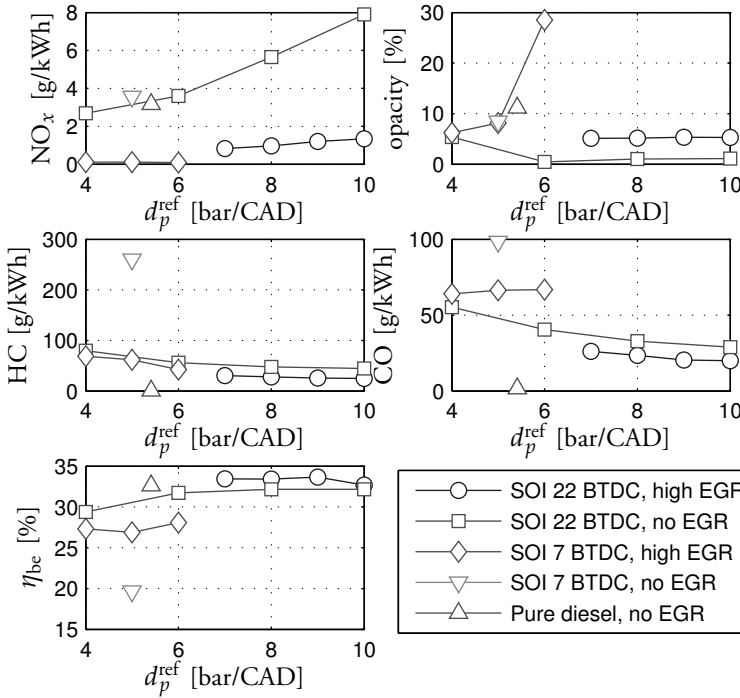
Figure 8.18 Emissions and brake efficiency for experiments at BMEP = 4.6 bar.

rate. In this combustion mode, CO emissions were very high and brake efficiency was low. The highest efficiency at this low-load operating point, $\eta_{be} = 33\%$ was obtained with early diesel injection and high EGR. In this combustion mode, soot was reduced compared to pure diesel operation, as was NO_x. However, NO_x emissions were still in the order of 1 g/kWh and the maximum pressure derivatives were increased compared to the case of pure diesel operation.

Medium load – BMEP = 9.2 bar Two operation modes were tested:

1. Early diesel injection, $u_{SOI} = 22$ CAD BTDC, $\chi_{EGR} = 45\%$.

2. Late diesel injection, $u_{SOI} = 10$ CAD BTDC, $\chi_{EGR} = 29\%$.

Operation without EGR was not possible due to risk of knock and too large cylinder-to-cylinder variations. Pure diesel operation was also tested for comparison purposes. Diesel ratio versus d_p is shown in Fig. 8.19. With early diesel
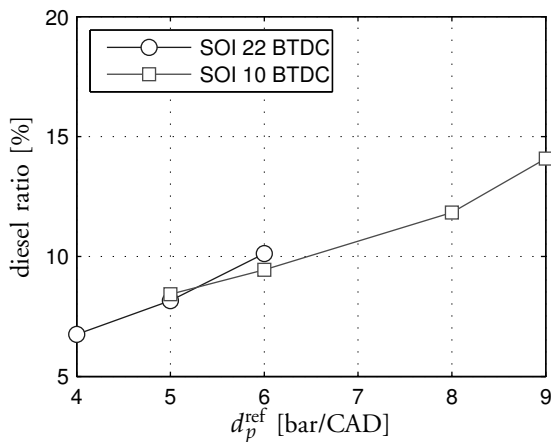
155

Figure 8.19 Diesel ratio required to keep a certain d_p for the two operation modes tested at BMEP = 9.2 bar. With pure diesel operation, average d_p was 4.0 bar/CAD.

injection, the engine could be operated at a diesel ratio of 7–12%, and with late diesel injection at a diesel ratio of 9–17%.

Heat release rates for the two modes for different d_p setpoints are shown in Fig. 8.20. With early diesel injection, there was a long ignition delay followed by a steadily increasing heat release rate. With late diesel injection, there was a two-stage combustion, with two peaks in the heat release.

Emissions and brake efficiencies are shown in Fig. 8.21. Examining the emissions data, operation in Mode 1, with early diesel injection, shows interesting characteristics. Compared to pure diesel operation, NO_x emissions were reduced from the order of 3 g/kWh to the range 0.08–0.11 g/kWh. We can conclude that in this operation mode we obtain HCCI-like NO_x emissions. As is commonly observed for low-temperature premixed combustion, HC and CO emissions were high, likely due to crevice effects and locally incomplete combustion.

High load – BMEP = 18.4 bar   Experiments were performed to find the high-load limit of fumigation operation. With closed-loop control, operation at BMEP = 18.4 bar was possible with start of diesel injection $u_{\mathrm{SOI}} = 9$ CAD BTDC. Data from this operating point are presented in Table 8.1. Pressure curves and heat release rates from one cycle are shown in Fig. 8.22.

Using the EGR system, the equivalent air fuel ratio λ was manually controlled to close to stoichiometric operation, which proved to give the most stable combustion at high load. Earlier diesel fuel injection did result in lower NO_x, in analogy with the medium-load results, but also unstable combustion. Calibration
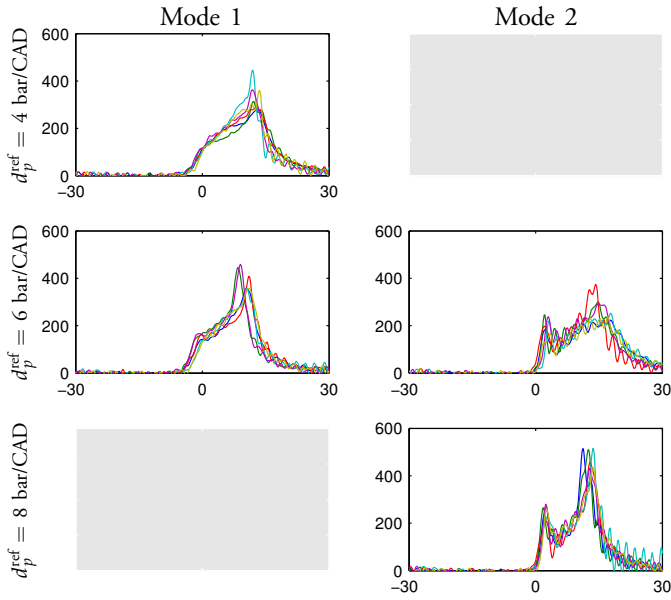
Figure 8.20   Experiments at BMEP = 9.2 bar. Heat release rates dQ [J/CAD] versus α [CAD] for Mode 1–2 (left to right), for d_p^{ref} = 4, 6, 8 bar/CAD (top to bottom).

Table 8.1   Data from high-load operation.

BMEP	18.4 bar
speed	1450 rpm
SOI	9 CAD BTDC
intake pressure	2.25 bar
d_p^{ref}	5.5 bar/CAD
diesel ratio	4.5%
brake efficiency	38.0%
NO_x	0.34 g/kWh
CO	33.7 g/kWh
HC	24.9 g/kWh
opacity	14%

157

Figure 8.21 Emissions and brake efficiencies for experiments at BMEP = 9.2 bar.

around the BMEP $=$ 18.4 bar test point showed reasons to expect that even higher loads could have been achieved, if the turbocharger had allowed higher boost. With higher inlet manifold pressures, a higher EGR rate could have been used which could possibly reduce NO_x emissions.

Pressure derivatives were modest, the setpoint for d_p was 5.5 bar/CAD. Figure 8.23 shows the distribution of d_p over 500 cycles. In 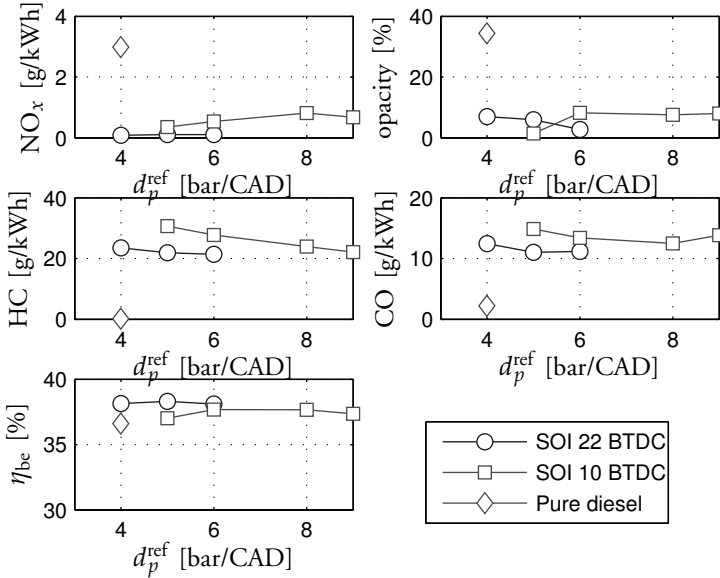most cycles, d_p is close to the setpoint. The frequency of cycles where d_p exceeded 15 bar/CAD was 0.53%. The distribution of d_p is highly non-Gaussian, it appears that an exponential distribution could model the data well. The non-Gaussian character of the process noise needs to be taken into account in the control design if a faster controller that can handle transients is to be developed.

Conclusions and Comments on Dual-Fuel Experiments

The experiments proved that dual-fuel fumigation can be a successful operating strategy for a multi-cylinder heavy-duty engine even for full load operation. The challenges for enabling the combustion concept was large cylinder-to-cylinder imbalances and the sensitivity of the combustion process to operating conditions.

A key feature for enabling the experiments was to introduce feedback control
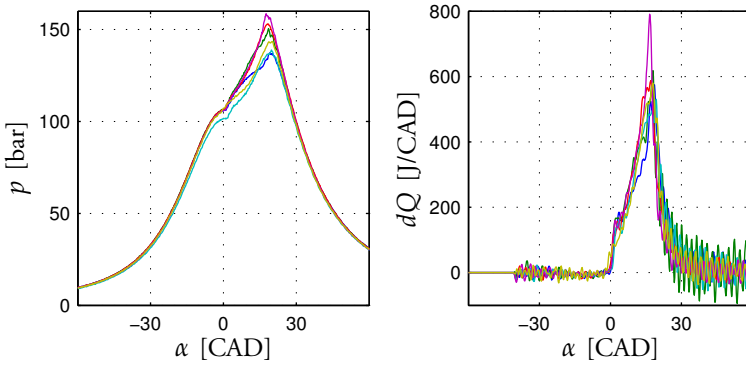
Figure 8.22 Cylinder pressure curves and heat release rates for operation at BMEP = 18.4 bar.
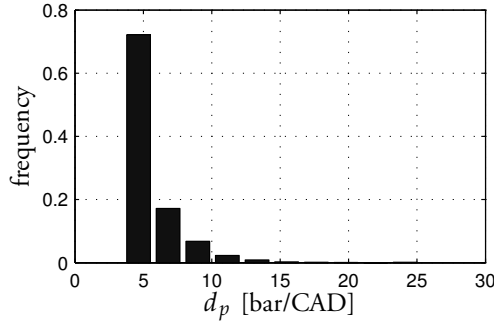
Figure 8.23 Distribution of d_p for operation at BMEP = 18.4 bar.

of peak pressure derivative d_p, to avoid misfiring or knocking combustion. Combustion proved to be very sensitive to diesel ratio; increasing the diesel fuel ratio by a few percent had a large impact on the combustion process. Feedback control could be expected to be necessary to avoid misfire and knock, analogous to SI engine operation.

The scope of the work was to show that operation in the entire load range was possible. For further studies, improvements may be pursued in terms of hardware, calibration, and control design. Hardware improvements would include injectors that are better adapted to low diesel flows to reduce cylinder-to-cylinder imbalances. The mechanical design of the piston bowl and crevices should be modified to minimize wall area for reducing HC and CO emissions. The turbocharger should be optimally matched to the engine. On the calibration side, a

full study of optimal injection timing, EGR rate, and λ is required, and could be expected to improve the results for emissions and fuel consumptions presented here. The RCCI publications from University of Wisconsin have to some extent pursued this direction. Their setup is slightly different from what was used here: gasoline instead of ethanol as the premixed fuel, earlier injection timing, lower compression ratio. With this setup, they have been able to combine high thermal efficiency with low NO_x and PM emissions. Other researchers have verified the results [Leermakers et al., 2011]. However, to the author's knowledge, no results have yet been published on RCCI full-load multi-cylinder operation. The results presented in this chapter indicate that feedback control may be the key to enable such operation, and that peak pressure derivative is a promising candidate feedback variable.

In terms of control design, the main focus in this work was to use the controller for automatic calibration in the laboratory setting. A simple ad-hoc structure of two slow PI controllers was therefore chosen. For transient operation, a more sophisticated model-based design would be needed. It would be interesting to further investigate different choices of sensors and feedback variables. With more precise diesel injectors, it could be possible to eliminate the in-cylinder pressure sensors, and let feedback be based on some other signal that could indicate when the combustion process is near the misfiring or knocking limit. The SI engine knock sensor could be one candidate.

9

Conclusions

The interplay between control and calibration is a key factor towards making combustion engines cleaner. Three current trends accentuate the need for increased focus on control and calibration:

- As more actuators are added to engines, calibration becomes a bottleneck in the development process because the time required for calibration increases exponentially in the number of free variables. One way to approach this challenge is to add more sensors to the engine and shift focus from empirical map-based open-loop calibration, to model-based closed-loop control. A fine grid of steady-state pre-calibrated maps could then be replaced by a coarse grid of dynamic models that would be used to fine-tune the calibration on-line.

- With low-temperature combustion, the process is more sensitive to conditions such as amount of residual gases in the cylinder or cylinder wall temperatures. Significant dynamics is then introduced for the in-cylinder combustion process. The traditional assumption that fuel path and gas path control can be separated because they operate on different time-scales may then not be valid.

- Tighter bounds on emissions enforced by legislation have already brought down steady-state emissions to such low levels that transient spikes now make up a significant part of the total drive-cycle emissions. To make further improvements, it is not sufficient to calibrate for steady-state operation only.

In this context, the contributions of the thesis may now be summarized

Sensing

Feedback control requires appropriate sensors. Most of the currently published literature on engine control are based on sensors that are available for production engines today, for example air mass flow and inlet manifold pressure. By contrast,

the work in the thesis was based on emissions sensor- and cylinder pressure sensor feedback.

Two different setups for moving feedback variables closer to high-level control objectives were presented, using virtual- or physical sensors. Chapter 5 described how cylinder pressure data can be used for a virtual emissions sensor. The advantage of cylinder pressure sensors is that they provide cylinder-individual data with high temporal resolution. The virtual sensor was tested on a large data set, and both cylinder-to-cylinder and cycle-to-cycle variability during transient operation were explicitly evaluated. This distinguishes the work from the referenced prior art, where variability of predictions was only analyzed in more limited contexts.

In Chapters 6 and 7, direct measurements of NO_x and opacity were used for engine modeling and feedback control. Physical emissions sensors may be more accurate and reliable than the virtual cylinder pressure-based sensors. However, emissions sensors are normally placed downstream of the turbine because of the lower pressure and temperature. Therefore, they only provide low-pass-filtered, cylinder-averaged information.

A natural direction for future work would be to integrate the virtual and physical sensors in a sensor-fusion framework to combine the best properties of both approaches.

Modeling

Chapter 6 presented a method to find dynamic MIMO models with the main engine actuator variables as inputs, and variables related to high-level engine specifications as outputs. The conclusion was that fairly simple, low-order models may be sufficient to capture the main engine dynamics. The method of identifying local linear state-space models, adapting the Wiener gains, and clustering the models according to similarity, is one approach to find a parametric low-order engine model. To the author's knowledge, this method has not previously been presented. Other approaches, e.g., based on dynamic neural networks, have been pursued in the literature. An advantage of the proposed method is that it yields models in a form suitable for many control design algorithms, including a noise model for prediction.

It is important to note that the choice of sensors determines the requirements on the engine model. Normally, steady-state performance is heavily emphasized in validation of emissions models in the literature. If emissions are measured online, steady-state predictions become less important than dynamic performance.

Control

Chapter 7 presented two approaches to address high-level engine specifications directly in closed-loop control. Compared to most previous work on diesel engine

control, fuel injection and gas exchange were considered in the same framework for both modeling and control. It was shown experimentally that a standard out-of-the-box implementation of MPC could be applied to successfully control the complex four-input-five-output system. The novelty in the work lies in the integration of rich feedback data, integration of fuel- and gas path control, and control design directly based on high-level objectives.

When using cylinder-pressure sensors for feedback, selection of feedback variables is non-trivial. Two ad-hoc setups were applied in the thesis. In Chapter 7, combustion phasing and ignition delay were proposed for indirectly controlling the NO_x-PM trade-off. In Chapter 8, $IMEP_n$ and maximum pressure derivative were used to harmonize dual-fuel combustion between cylinders. Further analysis of optimal feedback variables using statistical properties of the data, similar to the virtual sensor presented in Chapter 5, is an interesting topic for future work.

It would also be of interest to integrate the different ideas suggested in the thesis. A sensor-fusion approach to combine virtual- and physical emissions sensors has already been mentioned, and this scheme should be evaluated for feedback control. The MPC work was performed at a single operating point using a single linear model. Extending this to a nonlinear model like the one presented in Chapter 6 would be a next step. Also, the MPC work only used feedback from a single cylinder, and the extension to cylinder-individual fuel control is left for future work.

A constraint arising from using the Matlab MPC toolbox was the choice of cost function. The tuning variables in this implementation were the quadratic cost matrices, the constraints, and the constraint softening variables. When tuning the multivariable system, these degrees of freedom were perceived to be somewhat restrictive. When one of the outputs deviates significantly from its setpoint, the controller may put too much emphasis on this one variable compared to the others. By allowing a Huber-type cost function robustness may improve, while the optimization problem can still be formulated as a quadratic program.

Open Questions

Above, some directions for future work were presented that are mainly a matter of implementing ideas from the thesis in a more general context. Some more fundamental open research topics can also be mentioned:

- What can be gained by cylinder-individual emissions control? How much do emissions vary from cycle to cycle, and from cylinder to cylinder?

- How can data-mining techniques be exploited for optimal engine control? How much can performance improve by taking advantage of rich sensor data from the combustion process?

- What is an appropriate modeling framework for integrated control of various different engine subsystems, such as fuel injection, EGR, VGT, or variable valve timings?

- How should after-treatment systems be integrated into engine control design?

- How should the trade-off between different performance objectives such as NO_x, PM, and CO_2 emissions be formulated?

A

A Historical Perspective on Engine Control

John Cassidy, a pioneer of engine control at GM, here gives a historical perspective on the development of engine control in industry. Personal communication.

Observations on the Early Days of Automotive Engine Control

In September 1969, I joined the General Motors Research Lab. I was a cofounder of the GM computer-in-the car project. The objective was to make use of real time computing technology to control engine, drivetrain, and vehicle functions. Minicomputers were in use, e.g., DEC pdp8, solid-state integrated circuits were in production and the microprocessor would soon become available.

For over 50 years the primary control variables for spark ignition automotive engines were air-fuel ratio and spark advance. Initially manually set and later automatically using vacuum powered mechanical devices. Vehicle speed control was in use as early as 1910 and more widely available in the U.S. in the 1950's.

In 1967 California passed laws regulating automotive exhaust emissions and Federal U.S. laws were introduced in 1970. As the regulations tightened, tinkering with the conventional mechanical devices including carburetors became inadequate. In 1973 exhaust gas recirculation was introduced to reduce oxides of nitrogen and in 1975 the oxidizing catalytic converter went into ptoduction to further reduce carbon monoxide and unburned hydrocarbons.

Increasing the precision and complexity of mechanical controls was inadequate to meet the more stringent regulations. In 1978 Oldsmobile eliminated the mechanical distributor and introduced the MISAR system which electronically scheduled spark advance as a function of engine speed and manifold absolute pressure. This 3D map allowed more precise management of engine behavior over various operating conditions.

As exhaust emissions standards became even more stringent, open-loop methods proved inadequate. The standards required chemical oxidation and reduction. The so-called three-way catalyst was introduced and is still present today on all spark-ignited engines. Based on fundamental principles, simultaneous chemi-

cal reduction and oxidation is not possible. However averaged over time and a container volume, catalyst materials based on platinum and palladium were developed that allowed this to occur. This required that the air-fuel ratio be regulated to within a few tenths of stoichiometry. To put this in perspective a high-end carburetor of the 1970's would exhibit up to a transient of 10 ratios during a heavy acceleration event. Fortunately a sensor was developed that made closed loop control possible. Westinghouse was using zirconium oxide sensors to measure flue gas oxygen levels near stoichiometry. An engineer from Westinghouse went to work for Bosch in Germany where the approach was applied to the 3-way catalyst. I recall a meeting with Ed Cole, an engineer by background, who was then president of GM. A workable closed-loop system was possible using a fairly simple circuit based on an operation amplifier. Mr. Cole made the decision at that meeting that GM would take an advanced technical approach based on the newly emergent microprocessor technology. Others in the industry followed.

The early solutions reduced exhaust emissions at the expense of fuel economy. So additional applications were pursued to meet exhaust emission standards and improve fuel economy. For example idling in traffic is a significant waste of fuel. Lowering idle speed to the lowest possible value was accomplished with closed-loop control with vacuum and later stepper motor actuation of the throttle. Also accelerometers installed on the engine block allowed advancing the spark to improve fuel economy until engine knock was detected.

From the early days of automobiles to recent times, the architecture of controlling engine functions was flawed. The driver had unfettered control of the fastest variable in the system, namely the airflow into the intake manifold. The engine equipment then had to scramble to catch up to the air flow (fuel, mechanical devices and inertias). A more appropriate approach was to "drive by wire" The drivers foot is connected to the supervisory controller which then dynamically coordinates engine functions. This was demonstrated in a test cell in 1980. Lawyers at that time that it was too impractical an idea to be worthy of patenting. Today a number of production automobiles make use of the concept.

In the beginning the U.S. laws and major automotive companies doing business in the U.S. led progress. Smaller OEM companies bought technology and parts from the major OEM's and suppliers.

Control of diesel engines was slower to be introduced. Until recently passenger car diesels were not popular in the U.S. and the regulations were less stringent. Also, the problem is more difficult because of the physics and chemistry of diesels and less mature actuator and sensor technology.

John F. Cassidy

B

Technical Details

B.1 Gradients of Neural Network Cost Function

Algebraic expressions for the gradients of the two cost functions J_{pe} and J_{reg} used for neural network training in Section 5.2 are presented here. The input q is a three-dimensional tensor, with the dimensions representing sample index, input index, and cycle index, respectively.

The derivatives with respect to $\alpha_0 \in \mathbb{R}^M$, $\alpha \in \mathbb{R}^{M \times L}$, $\beta_0 \in \mathbb{R}^K$, $\beta \in \mathbb{R}^{K \times M}$ are derived element-wise to avoid introducing notation for tensor operations. Note that computations can be implemented efficiently using multi-dimensional arrays and tensor multiplication.

$$\frac{\partial J_{\text{pe}}}{\partial \alpha_{m0}} = -\frac{1}{C} \sum_{n=1}^{N} \sum_{k=1}^{K} \sum_{c=1}^{C} (\zeta_{nk} - \bar{\bar{\zeta}}_{nk}) \beta_{km} \sigma'(\xi_{nmc}) \tag{B.1}$$

$$\frac{\partial J_{\text{pe}}}{\partial \alpha_{ml}} = -\frac{1}{C} \sum_{n=1}^{N} \sum_{k=1}^{K} \sum_{c=1}^{C} (\zeta_{nk} - \bar{\bar{\zeta}}_{nk}) \beta_{km} \sigma'(\xi_{nmc}) q_{nlc} \tag{B.2}$$

$$\frac{\partial J_{\text{pe}}}{\partial \beta_{k0}} = -\sum_{n=1}^{N} (\zeta_{nk} - \bar{\bar{\zeta}}_{nk}) \tag{B.3}$$

$$\frac{\partial J_{\text{pe}}}{\partial \beta_{km}} = -\sum_{n=1}^{N} (\zeta_{nk} - \bar{\bar{\zeta}}_{nk}) \bar{z}_{nm} \tag{B.4}$$

$$\frac{\partial J_{\text{reg}}}{\partial \alpha_{m0}} = \frac{1}{C} \sum_{n=1}^{N} \sum_{k=1}^{K} \sum_{c=1}^{C} \hat{\zeta}_{nkc} \beta_{km} \left(\sigma'(\xi_{nmc}) - \frac{1}{C} \sum_{d=1}^{C} \sigma'(\xi_{nmc}) \right) \tag{B.5}$$

$$\frac{\partial J_{\text{reg}}}{\partial \alpha_{ml}} = \frac{1}{C} \sum_{n=1}^{N} \sum_{k=1}^{K} \sum_{c=1}^{C} \hat{\zeta}_{nkc} \beta_{km} \left(\sigma'(\xi_{nmc}) q_{nlc} - \frac{1}{C} \sum_{d=1}^{C} \sigma'(\xi_{nmd}) q_{nld} \right) \tag{B.6}$$

$$\frac{\partial J_{\text{reg}}}{\partial \beta_{k0}} = 0 \tag{B.7}$$

$$\frac{\partial J_{\text{reg}}}{\partial \beta_{km}} = \frac{1}{C} \sum_{n=1}^{N} \sum_{c=1}^{C} \hat{\zeta}_{nkc}(z_{nmc} - \bar{z}_{nm}) \tag{B.8}$$

B.2 Reconstruction of Wiener Nonlinearity Functions

We consider the problem of reconstructing the nonlinearity $f(\cdot)$ in the model (6.5) using the local linearizations M^{ij} and the offsets from model and data operating points. The function $f(\cdot)$ may be parameterized in different ways, here, polynomial approximations will be used.

Denote by i the operating point where the dynamic model was identified. With input offsets u^{0i} explicitly included, the Wiener model $\mathcal{M}_i$ is given by

$$\begin{aligned}
x_{k+1} &= A^i x_k + B^i(u_k - u^{0i}) + K^i w_k \\
\bar{y}_k &= C^i x_k + D^i(u_k - u^{0i}) + w_k \\
y_k &= f^i(\bar{y}_k)
\end{aligned} \tag{B.9}$$

Denote by $\mathcal{D}(i)$ the set of data operating points that were assigned to model $\mathcal{M}_i$ by the clustering algorithm.

We will assume that the offsets u^{0j} and y^{0j} for each operating point represent the steady-state relationship between u and y. As the nonlinearity $f(\cdot)$ is assumed to be diagonal, we can constrain the discussion to the single-output case.

We have two sources for information on the structure of $f(\cdot)$: the Wiener scaling matrices M^{ij} that are approximations of the derivative of $f(\cdot)$

$$M^{ij} = \left. \frac{\partial f^i}{\partial \bar{y}} \right|_{\text{op. pt. } j} \tag{B.10}$$

and the offsets u^{0j} and y^{0j} for $j \in \mathcal{D}(i)$ that represent the steady-state relation

$$\begin{aligned}
\bar{y}^{0j} &= G_i(0)(u^{0j} - u^{0i}) \\
y^{0j} &= f(\bar{y}^{0j})
\end{aligned} \tag{B.11}$$

where $G_i(0)$ is the steady-state gain of model $\mathcal{M}_i$

$$G_i(0) = C^i(I - A^i)^{-1}B_i + D_i \tag{B.12}$$

We now wish to approximate $f(\cdot)$ by a polynomial of order ν

$$\hat{f}(\bar{y}) = p(\bar{y}) = \sum_{l=0}^{\nu} a_l \bar{y}^l \tag{B.13}$$

This approximation could be based on the offsets, the Wiener scaling matrices, or both. To use the model for control design, input-output gain is more important than the steady-state map. Therefore, it is suggested that the approximation is based on the M^{ij}-data.

First, we find a polynomial $q(\bar{y})$ from $\bar{y}^{0j}$ to M^{ij} for the observations $j \in \mathcal{D}(i)$.

$$M^{ij} \approx q(\bar{y}) = \sum_{l=0}^{\nu-1} b_l (\bar{y}^{0j})^l \tag{B.14}$$

The polynomial $p(\bar{y})$ can then obtained by integration,

$$p(\bar{y}) = a_0 + \sum_{l=0}^{\nu-1} \frac{b_l}{l+1} \bar{y}^{l+1} \tag{B.15}$$

The constant term a_0 can be found by minimizing the least-squares error between y^{0j} and $p(\bar{y}^{0j})$.

The performance of the algorithm is illustrated in Fig. B.1 for finding the nonlinearity of the NO_x output y_{NO_x} from the data-set in Chapter 6. Here, all medium- and high-load operating points were assigned to a single cluster with the model from operating point 8. The input $\bar{y}$ to the nonlinearity $f(\cdot)$ was computed according to (B.11). In the figure, the circles show y_{NO_x} as a function of $\bar{y}_{NO_x}$ for all operating points in the cluster. The lines through the circles point in the direction of M^{ij}, the local linearization derivative. A third-order polynomial was fit to the data by first fitting M^{ij} to y^{0j} and then integrate to find $\hat{f}(\cdot)$, as described above.

We can see that the polynomial $p(\cdot)$ approximate the nonlinearity from $\bar{y}_{NO_x}$ to y_{NO_x} rather well. The modeling errors are likely due to the assumption that the nonlinearity is decoupled into a scalar nonlinearity for each output.
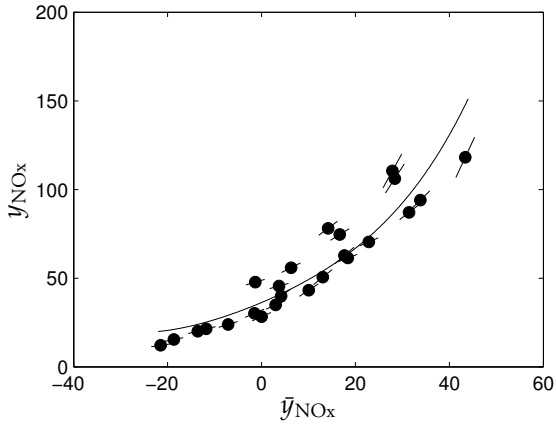
Figure B.1   Reconstruction of Wiener nonlinearity $f(\cdot)$ by a polynomial approximation $p(\cdot)$. A single dynamic model (from op. pt. 8) was used for all medium- and high-load operating points. y_{NOx} is the average NO_x (scaled) at each of the operating points, and $\bar{y}_{NOx}$ is the output of the dynamic linear system when feeding it with the mean input for the same operating point. The lines through the circles illustrate the direction of the local linearization.

References

Agrell, F., H. Ångström, B. Eriksson, J. Wikander, and J. Linderyd (2003): "Transient control of HCCI through combined intake and exhaust valve actuation." In SAE Technical Paper 2003-01-3172.

Agrell, F. and J. Linderyd (2005): "Swedish patent: SE525677 C, Arrangemang och förfarande för att styra en förbränningsmotor."

Akihama, K., Y. Takatori, K. Inagaki, S. Sasaki, and A. M. Dean (2001): "Mechanism of the smokeless rich diesel combustion by reducing temperature." In SAE Technical Paper 2001-01-0655.

Alberer, D. (2009): Fast Oxygen Based Transient Diesel Engine Control. PhD thesis, Institute for Design and Control of Mechatronical Systems, Johannes Kepler Universität, Linz, Austria.

Alfieri, E., A. Amstutz, and L. Guzzella (2009): "Gain-scheduled model-based feedback control of the air/fuel ratio in diesel engines." Control Engineering Practice, **17:12**, pp. 1417–1425. Special Section: The 2007 IFAC Symposium on Advances in Automotive Control.

Alger, T., S. Hanhe, C. E. Roberts, and T. W. Ryan (2005): "The heavy duty gasoline engine—a mutli-cylinder study of a high efficiency, low emission technology." In SAE Technical Paper 2005-01-1135.

Allison, B. and A. Isaksson (1998): "Design and performance of mid-ranging controllers." Journal of Process Control, **8(5,6)**, pp. 469–474.

Amstutz, A. and L. del Re (1995): "EGO sensor based robust output control of EGR in diesel engines." Control Systems Technology, IEEE Transactions on, **3:1**, pp. 39–48.

Andress, D., S. Das, F. Joseck, and T. D. Nguyen (2012): "Status of advanced light-duty transportation technologies in the US." Energy Policy, **41:0**, pp. 348–364. Modeling Transport (Energy) Demand and Policies.

References

Aoyama, T., Y. Hattori, J. Mizuta, and Y. Sato (1996): "An experimental study on premixed-charge compression ignition gasoline engine." In SAE Technical Paper 960081.

Åström, K. J. (2006): Introduction to Stochastic Control Theory. Dover Publications, Mineola, New York.

Åström, K. J. and B. Wittenmark (1997): Computer-Controlled Systems, 3rd edition. Prentice Hall, Upper Saddle River, New Jersey.

Atkinson, C., M. Allain, Y. Kalish, and H. Zhang (2009): "Model-based control of diesel engines for fuel efficiency optimization." In SAE Technical Paper 2009-01-0727.

Atkinson, C., M. Allain, and H. Zhang (2008): "Using model-based rapid transient calibration to reduce fuel consumption and emissions in diesel engines." In SAE Technical Paper 2008-01-1365.

Bengtsson, J. (2004): Closed-Loop Control of HCCI Engine Dynamics. PhD thesis, TFRT–1070-SE, Department of Automatic Control, Lund University, Lund, Sweden.

Bengtsson, J., M. Gäfvert, and P. Strandh (2004): "Modeling of HCCI engine combustion for control analysis." In Proceedings of the 43rd IEEE Conference on Decision and Control (CDC 2004), vol. 2, pp. 1682–1687.

Bengtsson, J., P. Strandh, R. Johansson, P. Tunestål, and B. Johansson (2006): "Multi-output control of a heavy duty HCCI engine using variable valve actuation and model predictive control." In SAE Technical Paper 2006-01-0873.

Beru AG (2008): "Mass-produced cleanliness: BERU Pressure Sensor Glow Plug reduces the emission of pollutants in the new VW 2.0 liter TDI. press release 284_en." www.beru.com.

Billings, S. (1980): "Identification of nonlinear systems—a survey." Control Theory and Applications, IEE Proceedings D, **127:6**, pp. 272–285.

Birch, S. (2008): "Audi diesel targets Bin 5, Euro 6." SAE Automotive Engineering International Online.

Bishop, C. M. (2006): Pattern Recognition and Machine Learning. Springer.

Bosch GmbH (2011a): "Diesel Systems. Sensors for Exhaust-Gas Treatment Systems." www.bosch-kraftfahrzeugtechnik.de/media Document nbr 292000P0PG-C/CCA-201108-En.

Bosch GmbH (2011b): "Glow Combustion Sensor." http://rb-kwin.bosch.com /en/powerconsumptionemissions/dieselsysteme/dieselsystem/ commercialvehiclesystems/startersystems/glow_plugs/ glowcombustionsensor.html Retrieved Feb 1 2012.

Boyd, S. and L. Vandenberghe (2004): Convex Optimization. Cambridge University Press, Cambridge, UK.

Canova, M., F. Chiara, M. Flory, S. Midlam-Mohler, Y. Guezennec, and G. Rizzoni (2007): "Dynamics and control of DI and HCCI combustion in a multi-cylinder diesel engine." In Proc. for the Fifth IFAC Symposium on Advances in Automotive Control, pp. 479–486. Aptos, CA.

Casella, G. and R. L. Berger (2002): Statistical Inference, 2nd edition. Duxbury, Pacific Grove, CA, USA.

Cassidy, J. F., M. Athans, and W.-H. Lee (1980): "On the design of electronic automotive engine controls using linear quadratic theory." IEEE Transactions on Automatic Control, **25(5)**, pp. 901–912.

Çebi, E. C., G. Rottenkolber, and E. Uyar (2011): "In-cylinder pressure based real-time estimation of engine-out particulate matter emissions of a diesel engine." In SAE Technical Paper 2011-01-1440.

Christensen, M., B. Johansson, and P. Einewall (1997): "Homogeneous charge compression ignition (HCCI) using isooctane, ethanol and natural gas—a comparison with spark ignition operation." In SAE Technical Paper 972874.

Citron, S. J. and J. E. O'Higgins (1989): "Cylinder-by-cylinder engine pressure and pressure torque waveform determination utilizing crankshaft speed fluctuations. United States Patent 4,843,870."

Curran, S., V. Prikhodkho, K. Cho, C. Sluder, J. Parks, R. Wagner, S. Kokjohn, and R. Reitz (2010): "In-cylinder fuel blending of gasoline/diesel for improved efficiency and lowest possible emissions on a multi-cylinder light-duty diesel engine." In SAE Technical Paper 2010-01-2206.

Darlington, A., K. Glover, and N. Collings (2006): "A simple diesel engine air-path model to predict the cylinder charge during transients: Strategies for reducing transient emissions spikes." In SAE Technical Paper 2006-01-3373.

Dec, J. E. (1997): "A conceptual model of DI diesel combustion based on laser-sheet imaging." In SAE Technical Paper 970873.

Delphi (2010): "Ammonia sensor: A breakthrough to prevent breakthroughs. feature story." http://delphi.com/news/featureStories/fs_2010_03_02_001/, Retrieved Jan 31 2012.

References

Delphi (2011): "Delphi particulate matter sensor." http://delphi.com/shared /pdf/ppd/sensors/particulate-matter-sensor.pdf Retrieved Feb 1 2012.

Delphi Technologies, Inc. (2011): "Bright spots newsletter winter 2011." http://delphi.com/pdf/dti/DTI-Winter-2011-Newsletter.pdf Retrieved Feb 1 2012.

Diesel, R. (1895): "Method of and apparatus for converting heat into work. United States Patent 542,846."

Dohner, A. R. (1981): "Optimal control solution of the automotive emission-constrained minimum fuel problem." Automatica, **17(3)**, pp. 441–458.

Eastwood, P. (2009): "Gas composition sensors." In Turner, Ed., Combustion Sensors, pp. 115–158. Momentum Press, New York, NY, USA.

Egler, W., R. J. Giersch, F. Boecking, J. Hammer, J. Hlousek, P. Mattes, U. Projahn, W. Urner, and B. Janetzky (2010): "Fuel injection systems." In Mollenhauer and Tschöke, Eds., Handbook of Diesel Engines, pp. 127–174. Springer Berlin Heidelberg.

Ekholm, K., M. Karlsson, P. Tunestål, R. Johansson, B. Johansson, and P. Strandh (2008): "Ethanol-diesel fumigation in a multi-cylinder engine." In SAE Technical Paper 2008-01-0033.

Energy Information Administration, U.S. Department of Energy (2009): "International energy outlook." DOE/EIA-0484(2009).

Enkvist, P., T. Nauclér, and J. Rosander (2007): "A cost curve for greenhouse gas reduction." The McKinsey Quarterly, **2007:1**, pp. 35–45.

European Union (2007): "Cleaner trucks and buses: Tighter limits for nitrogen oxides and particulate matter (Euro VI)." Press release, IP/07/1989.

Ferreau, H., G. Lorini, and M. Diehl (2006): "Fast nonlinear model predictive control of gasoline engines." In IEEE International Conference on Control Applications (CCA06), pp. 2754–2759.

Fleming, W. J. (2008): "New automotive sensors—a review." IEEE Sensors Journal, **8:11**, pp. 1900–1921.

García-Nieto, S., M. Martínez, X. Blasco, and J. Sanchis (2008): "Nonlinear predictive control based on local model networks for air management in diesel engines." Control Engineering Practice, **16:12**, pp. 1399–1413.

Gatowski, J. A., E. N. Balles, K. M. Chun, F. E. Nelson, J. A. Ekchian, and J. B. Heywood (1984): "Heat release analysis of engine pressure data." In SAE Technical Paper 84135.

Geladi, P. and B. R. Kowalski (1986): "Partial least-squares regression: A tutorial." Analytica Chimica Acta, **185**, pp. 1–17.

General Motors (2007): "GM takes new combustion technology out of the lab and on to the road, Press release 2007-08-24, archives.media.gm.com."

Glavmo, M., P. Spadafora, and R. Bosch (1999): "Closed loop start of combustion control utilizing ionization sensing in a diesel engine." In SAE Technical Paper 1999-01-0549.

Grondin, O., J. Chauvin, F. Guillemin, E. Nguyen, and G. Corde (2008): "Combustion parameters estimation and control using vibration signal : Application to the diesel HCCI engine." In Decision and Control, 2008. CDC 2008. 47th IEEE Conference on, pp. 5621–5627.

Grondin, O., P. Moulin, and J. Chauvin (2009): "Control of a turbocharged diesel engine fitted with high pressure and low pressure exhaust gas recirculation systems." In Proceedings of the 48th IEEE Conference on Decision and Control, held jointly with the 28th Chinese Control Conference (CDC/CCC 2009), Dec 16-18, Shanghai, China, pp. 6582–6589.

Guzzella, L. and C. H. Onder (2004): Introduction to Modeling and Control of Internal Combustion Engine Systems. Springer-Verlag, Berlin.

Haddad, W. M. and R. Moser (1994): "Optimal dynamic output feedback for nonzero set point regulation: The discrete-time case." IEEE Transactions on Automatic Control, **39(9)**, pp. 1921–1925.

Hafner, M., M. Schüler, O. Nelles, and R. Isermann (2000): "Fast neural networks for diesel engine control design." Control Engineering Practice, **8(11)**, pp. 1211–1221.

Hametner, C. and M. Nebel (2012): "Operating regime based dynamic engine modelling." Control Engineering Practice, **20**, pp. 397–407.

Hamming, R. W. (1998): Digital Filters, 3rd Edition. Courier Dover Publications, Mineola, NY.

Haraldsson, G., J. Hyvonen, P. Tunestål, and B. Johansson (2002): "HCCI combustion phasing in a multi-cylinder engine using variable compression ratio." In SAE Technical Paper 2002-01-2858.

Hardy, Q. (2011): "The big business of 'big data'." New York Times, Bits blog, bits.blogs.nytimes.com/2011/10/24/big-data.

Hastie, T., R. Tibshirani, and J. Friedman (2009): The Elements of Statistical Learning. Springer, New York.

References

Haugwitz, S., M. Karlsson, S. Velut, and P. Hagander (2005): "Anti-windup in mid-ranging control." In Proceedings of the 44th IEEE Conference on Decision and Control and European Control Conference ECC 2005. Seville, Spain.

Hayes, M. H. (1996): Statistical Digital Signal Processing and Modeling. John Wiley & Sons, Inc.

Heck, R. M., R. J. Farrauto, and S. T. Gulati (2009): Catalytic Air Pollution Control—Commercial Technology. Wiley, Hoboken, New Jersey.

Helden, R. v., R. Verbeek, and F. Willems (2004): "Optimization of urea SCR deNOx systems for HD diesel engines." In SAE Technical Paper 2004-01-0154.

Henningsson, M., B. Bernhardsson, P. Tunestål, and R. Johansson (2012a): "A machine-learning approach to information extraction from cylinder pressure sensors." In SAE Technical Paper 2012-01-0440.

Henningsson, M., P. Tunestål, and R. Johansson (2012b): "A virtual sensor for predicting diesel engine emissions from cylinder pressure data." In Submitted to the 2012 IFAC Workshop on Engine and Powertrain Control, Simulation and Modeling (E-COSM'12).

Heywood, J. B. (1988): Internal Combustion Engine Fundamentals. McGraw-Hill, New York.

Hiereth, H. and P. Prenninger (2007): "Charger control intervention and control philosophies for fixed-geometry and VTG chargers." In List, Ed., Charging the Internal Combustion Engine, Powertrain, pp. 162–183. Springer Vienna. 10.1007/978-3-211-47113-5_9.

Hillion, M., J. Chauvin, and N. Petit (2008): "Controlling the start of combustion on an HCCI diesel engine." In Proc. American Control Conference (ACC 2008), Jun 11-13, Seattle, WA, USA, pp. 2084–2091.

Hillion, M., J. Chauvin, and N. Petit (2011): "Control of highly diluted combustion in diesel engines." Control Engineering Practice, **19:11**, pp. 1274–1286.

Hirsch, M., D. Alberer, and L. del Re (2008): "Grey-box control oriented emissions models." In Proceedings of the 17th IFAC World Congress, Jul 6-11, Seoul, Korea, pp. 8514–8519.

Hotelling, H. (1933): "Analysis of a complex of statstical variables into principal components." Journal of Educational Psychology, **24**, pp. 417–441.

Hsieh, M.-F. and J. Wang (2011): "Development and experimental studies of a control-oriented SCR model for a two-catalyst urea-SCR system." Control Engineering Practice, **19:4**, pp. 409–422.

International Organization of Motor Vehicle Manufacturers (2011): "2009 production statistics." www.oica.net/category/production-statistics/2009-statistics/ Retrieved Nov 23 2011.

Iwabuchi, Y., K. Kawai, T. Shoji, and Y. Takeda (1999): "Trial of new concept diesel combustion system—premixed compression-ignited combustion." In SAE Technical Paper 1999-01-0185.

Jankovic, M., M. Jankovic, and I. Kolmanovsky (2000): "Constructive Lyapunov control design for turbocharged diesel engines." Control Systems Technology, IEEE Transactions on, **8:2**, pp. 288–299.

Johansson, R. (1993): System Modeling and Identification. Prentice Hall, Englewood Cliffs, NJ, USA.

Jung, M. and K. Glover (2006): "Calibratable linear parameter-varying control of a turbocharged diesel engine." Control Systems Technology, IEEE Transactions on, **14:1**, pp. 45–62.

Kalman, R. E. (1960): "A new approach to linear filtering and prediction problems." Journal Of Basic Engineering, **82:Series D**, pp. 35–45.

Karlsson, M., K. Ekholm, P. Strandh, R. Johansson, and P. Tunestål (2008): "LQG control for minimization of emissions in a diesel engine." In Proc. of the IEEE Multi-conference on Systems and Control (MSC 2008) Sep 3–5, pp. 245–250. San Antonio, TX, USA.

Karlsson, M., K. Ekholm, P. Strandh, R. Johansson, and P. Tunestål (2010a): "Dynamic mapping of diesel engine through system identification." In Proc. of the 2010 American Control Conference (ACC 2010) Jun 30–Jul 2, Baltimore, MD, USA.

Karlsson, M., K. Ekholm, P. Strandh, R. Johansson, and P. Tunestål (2010b): "Multiple-input multiple-output model predictive control of a diesel engine." In Proc. for the Sixth IFAC Symposium on Advances in Automotive Control (AAC 2010) Jul 12-14. Munich, Germany.

Karlsson, M., K. Ekholm, P. Strandh, R. Johansson, P. Tunestål, and B. Johansson (2007): "Closed-loop control of combustion phasing in an HCCI engine using VVA and variable EGR." In Proc. for the Fifth IFAC Symposium on Advances in Automotive Control (AAC 2007) Aug 20–22, pp. 517–524. Aptos, CA, USA.

References

Katayama, T. (2005): Subspace Methods for System Identification. Springer, London, UK.

Killingsworth, N., S. Aceves, D. Flowers, F. Espinosa-Loza, and M. Krstic (2009): "Hcci engine combustion-timing control: Optimizing gains and fuel consumption via extremum seeking." Control Systems Technology, IEEE Transactions on, **17:6**, pp. 1350–1361.

Kim, D., M. Y. Kim, and C. S. Lee (2004): "Effect of premixed gasoline fuel on the combustion characteristics of compression ignition engine." Energy & Fuels, **18**, pp. 1213–1219.

Kimura, S., O. Aoki, H. Ogawa, and S. Muranaka (1999): "New combustion concept for ultra-clean and high-efficiency small DI diesel engines." In SAE Technical Paper 1999-01-3681.

Kokjohn, S., R. Hanson, D. Splitter, J. Kaddatz, and R. Reitz (2011): "Fuel reactivity controlled compression ignition (RCCI) combustion in light- and heavy-duty engines." In SAE Technical Paper 2011-01-0357.

Kokjohn, S., R. Hanson, D. Splitter, and R. Reitz (2009): "Experiments and modeling of dual-fuel HCCI and PCCI combustion using in-cylinder fuel blending." In SAE Technical Paper 2009-01-2647.

Larimore, W. E. (1990): "Canonical variate analysis in identification, filtering, and adaptive control." In Proceedings of the 29th IEEE Conference on Decision and Control (CDC90), Dec 5–7, Honolulu, HI, USA., pp. 596–604.

Larsson, M. (2009): "Combustion sensing methods—in theory and practice." In Licentiate Thesis, Dept. of Applied Mechanics, Chalmers University of Technology, Göteborg, Sweden. Report no 2007:07.

Larsson, S. and I. Andersson (2008): "Self-optimising control of an SI-engine using a torque sensor." Control Engineering Practice, **16:5**, pp. 505–514.

Leermakers, C. A. J., B. Van den Berge, C. C. M. Luijten, L. M. T. Somers, and L. P. H. de Goey (2011): "Gasoline-diesel dual fuel: Effect of injection timing and fuel balance." In SAE Technical Paper 2011-01-2437.

Lewander, M., K. Ekholm, B. Johansson, P. Tunestål, N. Milovanovic, N. Keeler, and T. Harcombe (2008): "Investigation of the combustion characteristics with focus on partially premixed combustion in a heavy duty engine." In SAE Technical Paper 2008-01-1658.

Lewander, M., A. Widd, B. Johansson, and P. Tunestål (2012): "Steady-state fuel consumption optimization through feedback control of estimated cylinder individual efficiency." In Accepted to the 2012 American Control Conference (ACC 2012), Jun 27-29, Montreal, Canada.

Ljung, L. (1999): System Identification: Theory for the User. Prentice-Hall, Upper Saddle River, NJ, USA.

Maaß, B., R. Stobart, and J. Deng (2009): "Diesel engine emissions prediction using parallel neural networks." In Proc. American Control Conference (ACC 2009), Jun 10-12, St. Louis, MO, USA, pp. 1122–1127.

Maciejowski, J. M. (2002): Predictive Control with Constraints. Pearson Education Limited, Harlow, England.

Malaczynski, G. W. and M. E. Baker (2003): "Real-time digital signal processing of ionization current for engine diagnostic and control." In SAE Technical Paper 2003-01-1119.

Manente, V., B. Johansson, and P. Tunestål (2009): "Partially premixed combustion at high load using gasoline and ethanol, a comparison with diesel." In SAE Technical Paper 2009-01-0944.

Manning, C. D., P. Raghavan, and H. Schütze (2008): Introduction to Information Retrieval. Cambridge University Press, Cambridge, England.

Martinez-Frias, J., S. Aceves, D. Flowers, J. Smith, and R. Dibble (2000): "HCCI control by thermal management." In SAE Technical Paper 2000-01-2869.

Martinez-Frias, J., S. Aceves, D. Flowers, J. Smith, and R. Dibble (2001): "Equivalence ratio-EGR control of HCCI engine operation and the potential for transition to spark-ignited operation." In SAE Technical Paper 2001-01-3613.

Martyr, A. J. and M. A. Plint (2007): Engine Testing, 3rd edition. Butterworth-Heinemann.

Mathworks (2008): "Matlab R2008-b." www.mathworks.com.

Mathworks (2009): "Matlab R2009-a." www.mathworks.com.

McKelvey, T., I. Andersson, and M. Thor (2007): "Estimation of combustion information by crankshaft torque sensing in an internal combustion engine." In Computational Advances in Multi-Sensor Adaptive Processing, 2007. CAMPSAP 2007. 2nd IEEE International Workshop on, pp. 117–120.

Meyer, J. (2011): Calibration reduction in internal combustion engine fueling control: modeling, estimation and stability robustness. PhD thesis, Ohio State University.

Mock, R. and K. Lubitz (2008): "Piezoelectric injection systems." In Piezo-electricity, vol. 114 of Springer Series in Materials Science, pp. 299–310. Springer Berlin Heidelberg. 10.1007/978-3-540-68683-5_13.

Moulin, P., O. Grondin, and L. Fontvieille (2009): "Control of a two-stage turbocharger on a diesel engine." In Proceedings of the 48th IEEE Conference on Decision and Control, held jointly with the 28th Chinese Control Conference (CDC/CCC 2009), Dec 16-18, Shanghai, China, pp. 5200–5206.

Mrosek, M., H. Sequenz, and R. Isermann (2010): "Control oriented NO_x and soot models for diesel engines." In Proc. for the Sixth IFAC Symposium on Advances in Automotive Control, pp. 234–239. Munich, Germany.

Musculus, M. P. B. (2006): "Multiple simultaneous optical diagnostic imaging of early-injection low-temperature combustion in a heavy-duty diesel engine." In SAE Technical Paper 2006-01-0079.

Najt, P. M. and D. E. Foster (1983): "Compression-ignited homogeneous charge combustion." In SAE Technical Paper 830264.

Naone, E. (2011): "The new big data." Technology Review Online, www.technologyreview.com/computing/38397/.

Narendra, K. S. and P. G. Gallman (1966): "An iterative method for the identification of nonlinear systems using a Hammerstein model." IEEE Transactions on Automatic Control, **11(3)**, pp. 546–550.

Noehre, C., M. Andersson, B. Johansson, and A. Hultqvist (2006): "Characterization of partially premixed combustion." In SAE Technical Paper 2006-01-3412.

Noguchi, M., Y. Tanaka, T. Tanaka, and Y. Takeuchi (1979): "A study on gasoline engine combustion by observation of intermediate reactive products during combustion." In SAE Technical Paper 790840.

Odaka, M., H. Suzuki, N. Koike, and H. Ishii (1999): "Search for optimizing control method of homogeneous charge diesel combustion." In SAE Technical Paper 1999-01-0184.

Olsson, J., P. Tunestål, and B. Johansson (2001): "Closed-loop control of an HCCI engine." In SAE Technical Paper 2001-01-1031.

Olsson, J., P. Tunestål, B. Johansson, S. Fiveland, R. Agama, M. Willi, and D. Assanis (2002): "Compression ratio influence on maximum load of a natural gas fueled HCCI engine." In SAE Technical Paper 2002-01-0111.

Olsson, J., P. Tunestål, J. Ulfvik, and B. Johansson (2003): "The effect of cooled EGR on emissions and performance of a turbocharged HCCI engine." In SAE Technical Paper 2003-01-0743.

Omran, R., R. Younes, and J. C. Champoussin (2009): "Optimal control of a variable geometry turbocharged diesel engine using neural networks: Applications on the ETC test cycle." IEEE Transactions on Control Systems Technology, **17(2)**, pp. 380–393.

Onishi, S., S. H. Jo, K. Shoda, P. D. Jo, and S. Kato (1979): "Active thermo-atmosphere combustion (ATAC)—a new combustion process for internal combustion engines." In SAE Technical Paper 790501.

Optrand (2011): "Optrand incorporated. Fiber optic sensors for extreme environments." www.optrand.com Retrieved Feb 1 2012.

Ortner, P. and L. d. Re (2007): "Predictive control of a diesel engine air path." IEEE Transactions on Control Systems Technology, **15(3)**, pp. 449–456.

Ostman, F. and H. Toivonen (2011): "Adaptive cylinder balancing of internal combustion engines." Control Systems Technology, IEEE Transactions on, **19:4**, pp. 782–791.

Ouladsine, M., G. Bloch, and X. Dovifaaz (2004): "Neural modelling and control of a diesel engine with pollution constraints." Journal of Intelligent and Robotic Systems, **41**, pp. 157–171.

Pearson, K. (1901): "On lines and planes of closest fit to systems of points in space." Philosophical Magazine, **2:6**, pp. 559–572.

Projahn, U., H. Randoll, E. Biermann, J. Brückner, K. Funk, T. Küttner, W. Lehle, and J. Zuern (2010): "Fuel injection system control systems." In Mollenhauer and Tschöke, Eds., Handbook of Diesel Engines, pp. 175–191. Springer Berlin Heidelberg.

Pucher, H. (2010): "Gas exchange and supercharging." In Mollenhauer and Tschöke, Eds., Handbook of Diesel Engines, pp. 31–60. Springer Berlin Heidelberg.

Pudenz, K. (2007): "Audi sportback concept with combustion chamber sensors for lower emissions." ATZ online.

Ravi, N., M. Roelle, H.-H. Liao, A. Jungkunz, C.-F. Chang, S. Park, and J. Gerdes (2010): "Model-based control of HCCI engines using exhaust recompression." Control Systems Technology, IEEE Transactions on, **18:6**, pp. 1289–1302.

References

Ribbens, W. B., N. P. Mansour, G. Luecke, C. W. Battle, E. C. Jones, and L. E. Mansir (2003): *Understanding Automotive Electronics*, 6th Edition. Elsevier.

Risvik, H. (2008): "PCA Module 1.1.01." www.folk.uio.no/henninri/pca_module.

Robert Bosch GmbH (2011): *Bosch Automotive Handbook*, 8th Edition. Wiley.

Rolle, S. and A. Wiesmann (2011): "Combustion control and monitoring of two-stroke engines." Wärtsilä Technical Journal, **2011:02**, pp. 52–57.

Ryan, T. and T. J. Callahan (1996): "Homogeneous charge compression ignition of diesel fuel." In SAE Technical Paper 961160.

S. Simon, H. K. (2001): "Fuel injection valve and pressure sensor combination. United States Patent 6,318,342."

Sequenz, H. and R. Isermann (2011): "Emission model structures for an implementation on engine control units." In Proceedings of the 18th IFAC World Congress, Aug 28–Sep 2, Milan, Italy, pp. 11851–11856.

Seykens, X. L. J., R. S. G. Baert, L. M. T. Somers, and F. P. T. Willems (2009): "Experimental validation of extended NO and soot model for advanced HD diesel engine combustion." In SAE Technical Paper 2009-01-0683.

Shahroudi, K. E. (2008): "Robust design evolution and impact of in-cylinder pressure sensors to combustion control and optimization: A systems and strategy perspective." Master's Thesis, Massachussetts Institute of Technology, Cambridge, MA, USA.

Shaver, G. M., J. C. Gerdes, and M. Roelle (2004): "Physics-based closed-loop control of phasing, peak pressure and work output in HCCI engines utilizing variable valve actuation." In Proc. American Control Conference (ACC 2004), Jun 30–Jul 2, Boston, MA, USA, pp. 150–155.

Shaver, G. M., M. Roelle, and J. C. Gerdes (2006): "A two-input two-output control model of HCCI engines." In Proc. American Control Conference, pp. 472–477. Minneapolis, MN.

Shi, Y., R. D. Reitz, and H.-W. Ge (2011): *Computational Optimization of Internal Combustion Engines*. Springer, London.

Siemens VDO (2005): "Smart NOx sensor." www.siemensvdo.com.

Siemens VDO Automotive (2006): "Diesel gets greener with Siemens VDO's two-in-one glow plug pressure sensor. Press release." press.siemens.us.

Solyom, S. and S. Eriksson (2006): "Mid-ranging scheme for idle speed control of SI engines." In SAE Technical Paper 2006-01-0608.

Splitter, D., R. Hanson, S. Kokjohn, and R. Reitz (2011): "Reactivity controlled compression ignition (RCCI) heavy-duty engine operation at mid- and high-loads with conventional and alternative fuels." In SAE Technical Paper 2011-01-0363.

Stefanopoulou, A., I. Kolmanovsky, and J. Freudenberg (2000): "Control of variable geometry turbocharged diesel engines for reduced emissions." Control Systems Technology, IEEE Transactions on, **8:4**, pp. 733–745.

Steinparzer, F., K. Blumensaat, G. Paehr, W. Held, and C. Teetz (2010): "Vehicle diesel engines." In Mollenhauer and Tschöke, Eds., Handbook of Diesel Engines, pp. 507–557. Springer Berlin Heidelberg.

Strandh, P. (2006): HCCI Operation—Closed Loop Combustion Control Using VVA or Dual Fuel. PhD thesis, ISRN LUTMDN/TMHP–06/1039-SE, Department of Energy Sciences, Lund University.

Strandh, P., J. Bengtsson, R. Johansson, P. Tunestål, and B. Johansson (2004): "Cycle-to-cycle control of a dual-fuel HCCI engine." In SAE Technical Paper 2004-01-0941.

Strandh, P., J. Bengtsson, R. Johansson, P. Tunestål, and B. Johansson (2005): "Variable valve actuation for timing control of a homogeneous charge compression ignition engine." In SAE Technical Paper 2005-01-0147.

Strandh, P., M. Christensen, J. Bengtsson, R. Johansson, A. Vressner, P. Tunestål, and B. Johansson (2003): "Ion current sensing for HCCI combustion feedback." In SAE Technical Paper 2003-01-3216.

Sullivan, J. L., R. E. Baker, B. A. Boyer, R. H. Hammerle, T. E. Kenney, L. Muniz, and T. J. Wallington (2004): "CO2 emission benefit of diesel (versus gasoline) powered vehicles." Environmental Science & Technology, **38:12**, pp. 3217–3223.

Swift, S., K. Glover, and N. Collings (2008): "Safe operation and control of diesel particulate filters using level set methods." In Blondel et al., Eds., Recent Advances in Learning and Control, vol. 371 of Lecture Notes in Control and Information Sciences, pp. 233–247. Springer Berlin / Heidelberg.

Swingler, J. (2009): "Gas composition sensors." In Turner, Ed., Automotive Sensors, pp. 231–257. Momentum Press, New York, NY, USA.

Takeda, Y., N. Keiichi, and N. Keiichi (1996): "Emission characteristics of premixed lean diesel combustion with extremely early staged fuel injection." In SAE Technical Paper 961163.

References

Tennant, J. A., H. S. Rao, and J. D. Powell (1979): "Engine characterization and optimal control." In Proceedings of the 18th IEEE Conference on Decision and Control (CDC79), Dec 12–14, Fort Lauderdale, FL, USA., pp. 114–119.

Thring, R. H. (1989): "Homogeneous-charge compression-ignition (HCCI) engines." In SAE Technical Paper 892068.

Trajkovic, S., A. Milosavljevic, P. Tunestål, and B. Johansson (2006): "FPGA controlled pneumatic variable valve actuation." In SAE Technical Paper 2006-01-0041.

Traver, M. L., R. J. Atkinson, and C. M. Atkinson (1999): "Neural-network-based diesel engine emissions prediction using in-cylinder combustion pressure." In SAE Technical Paper 1999-01-1532.

Tschanz, F., A. Amstutz, C. H. Onder, and L. Guzzella (2010): "A real-time soot model for emission control of a diesel engine." In Proc. for the Sixth IFAC Symposium on Advances in Automotive Control, pp. 222–227. Munich, Germany.

Tschöke, H., A. Graf, J. Stein, M. Krüger, J. Schaller, N. Breuer, K. Engeljehringer, and W. Schindler (2010): "Diesel engine exhaust emissions." In Mollenhauer and Tschöke, Eds., Handbook of Diesel Engines, pp. 417–485. Springer Berlin Heidelberg.

Tunestål, P. (2009): "Self-tuning gross heat release computation for internal combustion engines." Control Engineering Practice, **17**, pp. 518–524.

U.S. Environmental Protection Agency (2001): "Control of air pollution from new motor vehicles: Heavy-duty engine and vehicle standards and highway diesel fuel sulfur control requirements; final rule. Federal Register / Vol. 66, Nr. 12."

U.S. Environmental Protection Agency (2008): "Regulatory announcement. EPA finalizes regulations requiring onboard diagnostic systems on 2010 and later heavy-duty engines used in highway applications over 14,000 pounds; revisions to onboard diagnostic requirements for diesel highway heavy-duty applications under 14,000 pounds." EPA-420-F-08-032.

U.S. Environmental Protection Agency (2011a): "Heavy-duty highway compression-ignition engines and urban buses—exhaust emission standards." http://www.epa.gov/otaq/standards/heavy-duty/hdci-exhaust.htm. Retrieved Jan 29 2012.

U.S. Environmental Protection Agency (2011b): "Inventory of U.S. greenhouse gas emissions and sinks: 1990-2009." EPA 430-R-11-005.

U.S. Environmental Protection Agency (2011c): "Regulatory announcement. EPA and NHTSA adopt first-ever program to reduce greenhouse gas emissions and improve fuel efficiency of medium- and heavy- duty vehicles." EPA-420-F-11-031.

van Overschee, P. and B. de Moor (1994): "N4SID: Subspace algorithms for the stochastic identificaiton problem." Automatica, **30(1)**, pp. 75–93.

van Overschee, P. and B. de Moor (1996): Subspace Identification for Linear Systems: Theory, Implementation, Applications. Kluwer, Boston, MA, USA.

Verhaegen, M. (1994): "Identification of the deterministic part of MIMO state space models given in innovations form from input-output data." Automatica, **30(1)**, pp. 61–74.

Vermillion, C., K. Butts, and K. Reidy (2010): "Model predictive engine torque control with real-time driver-in-the-loop simulation results." In Proc. of the 2010 American Control Conference (ACC 2010), Jun 30–Jul 2, Baltimore, MD, USA., pp. 1459–1464.

Vinot, S. and P. Coussy (2009): "Greenhouse gas emissions and the transport sector." Panorama 2009, www.ifpenergiesnouvelles.com.

Volvo Group (2007): "Volvo displays carbon-dioxide-free trucks, press release, www.volvo.com/group/global/en-gb/newsmedia/ pressreleases/2007/."

Wahlström, J., L. Eriksson, and L. Nielsen (2010): "EGR-VGT control and tuning for pumping work minimization and emission control." Control Systems Technology, IEEE Transactions on, **18:4**, pp. 993–1003.

Walker, A. (2004): "Controlling particulate emissions from diesel vehicles." Topics in Catalysis, **28**, pp. 165–170. 10.1023/B:TOCA.0000024346.29600.0e.

Wang, D. Y., S. Yao, M. Shost, J.-H. Yoo, D. Cabush, D. Racine, R. Cloudt, and F. Willems (2008): "Ammonia sensor for closed-loop SCR control." In SAE Technical Paper 2008-01-919.

Wang, J. (2008): "Hybrid robust air-path control for diesel engines operating conventional and low temperature combustion modes." Control Systems Technology, IEEE Transactions on, **16:6**, pp. 1138–1151.

Wang, Y.-Y., I. Haskara, and O. Yaniv (2011): "Quantitative feedback design of air and boost pressure control system for turbocharged diesel engines." Control Engineering Practice, **19:6**, pp. 626–637.

References

Wei, X. and L. del Re (2007): "Gain scheduled H_∞ control for air path systems of diesel engines using LPV techniques." Control Systems Technology, IEEE Transactions on, **15:3**, pp. 406–415.

Westerlund, C., B. Westerberg, I. Odenbrand, and R. Egnell (2010): "Model predictive control of a combined EGR/SCR HD diesel engine." In SAE Technical Paper 2010-01-1175.

Westlund, A. and H.-E. Ångström (2009): "Fast physical prediction of NO and soot in diesel engines." In SAE Technical Paper 2009-01-1121.

Widd, A., P. Tunestål, and R. Johansson (2008): "Physical modeling and control of homogeneous charge compression ignition (HCCI) engines." In Proc. of the 47th IEEE Conference on Decision and Control (CDC 2008), Dec 9-11, Cancún, Mexico., pp. 5615–5620.

Wiebe, I. I. (1970): Brennverlauf und Kreisprozessrechnung. VEB Verlag Technik, Berlin.

Wilhelmsson, C., P. Tunestål, B. Johansson, A. Widd, and R. Johansson (2009): "A physical two-zone no_x model intended for embedded implementation." In SAE Technical Paper 2009-01-1509.

Willems, F., E. Doosje, F. Engels, and X. Seykens (2010): "Cylinder pressure-based control in heavy-duty egr diesel engines using a virtual heat release and emission sensor." In SAE Technical Paper 2010-01-0564.

Wlodarczyk, M. (2006): "High accuracy glow plug-integrated cylinder pressure sensor for closed loop engine control." In SAE Technical Paper 2006-01-0184.

Zaidi, K., G. E. Andrews, and J. H. Greenhough (1998): "Diesel fumigation partial premixing for reducing ignition delay and amplitude of pressure fluctuations." In SAE Technical Paper 980535.

Zhao, F. and T. Asmus (2003): "HCCI control and operating range extension." In Zhao et al., Eds., Homogeneous Charge Compression Ignition (HCCI) Engines—Key Research and Development Issues. SAE.

Zöls, W., G. Bachmaier, M. Gerlich, F. Antritter, and C. Hillermeier (2010): "In-cylinder pressure measurement with a gasoline injector." In Proc. for the Sixth IFAC Symposium on Advances in Automotive Control, pp. 803–808. Munich, Germany.

Nomenclature

Symbols

α	Crank angle
α_{10}	Crank angle degree of 10% heat released
α_{50}	Crank angle degree of 50% heat released
α_{ID}	Ignition delay
β	Signal-to-noise ratio (optimal Wiener filter)
γ	Ratio of specific heats (thermodynamics)
γ	Weight of regularizaiton term (neural network training)
η_{be}	Brake efficiency
κ	Polytropic exponent for heat release computations
λ	Ratio of actual air-fuel ratio to stoichiometric air-fuel ratio
χ_{EGR}	EGR rate
χ_{NOx}	NO_x concentration
ζ	Target output variable
c_p	Specific heat at constant pressure
c_v	Specific heat at constant volume
d_p	Maximum pressure derivative
$\dot{m}_{air}$	Compressor mass flow
p	Pressure
p_{in}	Inlet manifold pressure
r_c	Compression ratio

u	Control variable
u_{EBP}	Exhaust back pressure valve position
u_{FD}	Duration of diesel fuel injection
u_{IVC}	Crank angle degree of inlet valve closing
u_{VGT}	VGT actuator position
x	State of state-space model
y	Measured output variable
y_{IMEP}	Measured net indicated mean effective pressure
H_c	MPC control horizon
H_p	MPC prediction horizon
N_{engine}	Engine speed
Q	Heat
R^2	Statistic for model validation
T	Temperature
V	Volume
V_D	Displaced volume
X_{op}	Exhaust gas opacity

Acronyms

ATDC	After top dead center
BMEP	Brake mean effective pressure
BTDC	Before top dead center
CAD	Crank angle degrees
CI	Compression ignition
CO	Carbon monoxide
CO_2	Carbon dioxide
DoE	Design of experiments
EBP	Exhaust back pressure (valve)
ECU	Electronic control unit
EGR	Exhaust gas recirculation (valve or rate)
FSN	Filter smoke number

HC	Hydrocarbons
HCCI	Homogeneous charge compression ignition
IMEPn	Indicated mean effective pressure
IVC	Inlet valve closing
LPV	Linear parameter varying
LQG	Linear quadratic Gaussian
LTC	Low-temperature combustion
MBT	Maximum brake torque
MIMO	Multiple-input multiple-output
MPC	Model predictive control
NN	Neural network
NO	Nitrogen oxide
NO_2	Nitrogen dioxide
NO_x	$NO + NO_2$
NVO	Negative valve overlap
OBD	On-board diagnostics
pc	Principal component
PCA	Principal component analysis
PI	Proportional-integral (controller)
PIC	Peripheral interface controller
PID	Proportional-integral-derivative (controller)
PM	Particulate matter
PPC	Partially premixed combustion
PRBS	Pseudo-random binary sequence
QP	Quadratic program
RCCI	Reactivity-controlled compression ignition
RMSE	Root mean square error
rpm	Revolutions per minute
SCR	Selective catalytic reduction
SI	Spark ignition
SOI	Start of injection
TDC	Top dead center
VAF	Variance accounted for

VGT	Variable geometry turbo
VVA	Variable valve actuation
VVT	Variable valve timing

Cylinder Color Codes

Cyl. 1	blue
Cyl. 2	green
Cyl. 3	red
Cyl. 4	cyan
Cyl. 5	magenta
Cyl. 6	yellow